Systems Biology Study of Breast Cancer Endocrine Response and Resistance

Chun Chen

Dissertation submitted to the faculty of the Virginia Polytechnic Institute and State University in partial fulfillment of the requirements for the degree

of

Doctor of Philosophy

In

Genetics, Bioinformatics and Computational Biology

John J. Tyson, Chair
William T. Baumann
Liwu Li
Jianhua Xing

Oct 29, 2013
Blacksburg, VA

Keywords: Mathematical modeling, breast cancer,
endocrine resistance, signaling switch, breast cancer landscape

Systems Biology Study of Breast Cancer Endocrine Response and Resistance

Chun CHEN

Abstract

As a robust system, cell can switch between different signaling programs according to their differentiation stages and external environments. Cancer cells hijack this plasticity to develop drug resistance. For example, breast cancers that are initially responsive to endocrine therapy often develop resistance robustly. This process is dynamically controlled by interactions of genes, proteins, RNAs and environmental factors at multiple scales. A systems biology study of this process focuses on the interactions of basic components, so as to uncover the molecular mechanism of drug resistance from a systemic and dynamical point of view.

In Chapter 2, I focused on the experimental observations that breast cancer cells can switch between estrogen receptor α (ERα) regulated and growth factor receptor (GFR) regulated signaling pathways for survival and proliferation. A mathematical model based on the signaling crosstalk between ERα and GFR was constructed. The model successfully explains several intriguing experimental findings related to bimodal distributions of GFR proteins in breast cancer cells, which had been lacking reasonable justifications for almost two decades. The model also explains how transient overexpression of ERα promotes resistance of breast cancer cells to estrogen withdrawal.

Understanding the non-genetic heterogeneity associated with this survival-signaling switch can shed light on the design of more efficient breast cancer therapies.

In Chapter 3, I utilized a novel strategy to model the transitions between the endocrine response and resistance states in breast cancer cells. Using the experimentally observed estrogen sensitivity phenotypes in breast cancer (sensitive, hypersensitive, and supersensitive) as example, I proposed a useful framework of modeling cell state transitions on the energy landscape of breast cancer as a dynamical system. Grounded on the most possible routes of transitions on the breast cancer landscape, a state transition model was developed. By analyzing this model, I investigated the optimum settings of two intuitive strategies, sequential and intermittent treatments, to overcome endocrine resistance in breast cancer. The method used in this study can be generalized to study treatment strategies and improve treatment efficiencies in breast cancer as well as other types of cancer.

Dedication

To my loved family.

Acknowledgements

I would like to take this great opportunity to thank a few of the many people who have helped me a lot during my PhD studies.

First I must express my heartfelt thanks to my advisor, Prof. John Tyson. The longer I've stayed in my academic career, the more I realize how lucky I've been as a student of John. He is a great scientist and mentor. He not only inspires us with immense knowledge but also guides us through difficulties with patience and enthusiasm. I greatly appreciate his continuous support and guidance for all these years.

I sincerely thank Prof. William Baumann for his intensive help with my projects. His bright ideas, positive attitude and masterful skills helped drive the projects forward when I faced project-ending difficulties. His understanding and generous support will be always appreciated.

I would also thank the rest of my committee, Prof. Jianhua Xing and Prof. Liwu Li. They always had insightful ideas and infectious enthusiasm that motivated me a lot. They not only provided valuable comments on my research but also helped tremendously in my career development.

I want to express my thanks to Prof. Robert Clarke and his experimental group on breast cancer at Georgetown University. Thanks to Anni, Rebecca, Ayesha, Rong, Harrini, Katherine and Jessica. The experience of collaborating and work with them is very precious to me.

I need to thank all the members in Tyson's lab and Xing's lab: Kathy, Tongli, Debashis,

Sandip, Baris, Janani, Rajat, Oak, Iman, Kartic, Tian, Anael, Cihan, Alida, Jignesh, Pavel, Thomas, Zhanghan, Yan, Xiaoshan, Ping, Hang, Jingyu, Abhishek, Debasish and Xiaojun. I am especially grateful to the encouragement from Kathy Chen, whose nice organization also made the lab a delightful home to stay.

Many thanks to the GBCB program. Special thank to Dennie Munson, who spent a lot of time to help me fix troubles of various kinds.

Lastly, I must thank my wife Lingling and our parents for the invaluable support they have given me. Also, I have to thank my son Eason for the joy he has brought and his cooperation when I had to work beside him.

Attribution

Several colleges and collaborators made contributions in this research and preparing the materials presented in this dissertation.

In Chapter 1, I presented an experimental result to show short-term responses of MCF7 breast cancer cells to estrogen withdrawal. This unpublished data is from our collaborators at Georgetown University School of Medicine. Dr. Rong Hu, a postdoctoral research at Prof. Robert Clarke's group, generously provided this and many other important results.

In Chapter 2, I presented my published work 'Modeling the estrogen receptor to growth factor receptor signaling switch in human breast cancer cells', which is shown in FEBS Letters (2013) at http://dx.doi.org/10.1016/j.febslet.2013.08.022. Prof. William Baumann from Department of Electrical & Computer Engineering at Virginia Tech co-authored this paper. He designed the study from initial, helped in analyzing the data during the study, and significantly improved the writing of the manuscript in the end. Prof. Robert Clarke from Lombardi Comprehensive Cancer Center at Georgetown University School of Medicine co-authored this paper for his extensive and helpful suggestions and supports on the biological side. Prof. John Tyson, university distinguished professor in the Department of Biological Sciences at Virginia Tech, advised me throughout the entire project. And he is the corresponding author on this paper.

Chapter 3 included my manuscript 'Transitions between endocrine therapy response and resistance on the breast cancer landscape', which is ready for submission. Prof. William

Baumann helped in improving a lot of details of this manuscript. Prof Jianhua Xing from Department of Biological Sciences at Virginia Tech made helpful suggestions over the methods used in this study. Lingling Xu, a PhD candidate from Department of Physics at Virginia Tech, helped significantly to provide theoretical/mathematical analysis on this project. Prof. Robert Clarke provided extensive and helpful suggestions and supports on the biological side. Prof. John Tyson advised me throughout the entire project and he will be the corresponding author on this paper.

Table of Contents

List of Figures

List of Tables

Chapter 1. Biological Background and Research Overview

1.1 Biological Background

1.1.1 Endocrine therapy in breast cancer and endocrine resistance

Breast cancer is the most common invasive cancer in women. One in eight women will be diagnosed with breast cancer in their lifetime. In the United States, it was estimated that about 232,340 new cases of invasive breast cancer will be diagnosed in women in 2013. Currently, there are more than 2.9 million breast cancer survivors in the United States [1].

In order to detect and treat breast cancer, people have long been searching for effective molecular targets and biomarkers that are actively involved in breast cancer physiology. It was found that approximately 70% of breast cancers express estrogen receptor α (ERα) [2, 3]. Sustained activation of ERα by exposure to estrogen is a well-recognized driver for breast cancer [2-4]. In these ERα-positive breast cancer cells, evidences indicate a pivotal role of ERα pathway in regulating the survival and growth of breast cancer cells [2, 3]. Thus, interfering with ERα functions, such as manipulating hormones, has been widely used as endocrine therapies to treat breast cancer for more than 100 years. Practically, ERα functions can be inhibited in multiple ways (Fig.1.1) [2]: 1) by depriving cells of estrogen, e.g., by inhibiting estrogen biosynthesis with aromatase

inhibitors (AIs); 2) by antagonizing ERα ligand binding with selective estrogen receptor modulators (SERMs, e.g. tamoxifen); 3) by reducing ERα expression levels with selective estrogen receptor down-regulators (SERDs, e.g. faslodex). Endocrine therapies have been very successful in reducing breast cancer mortality, especially in the past two decades. Tamoxifen, as the most successful targeted cancer therapy, has reduced the annual breast cancer death rate by one-third since its clinical application [2].

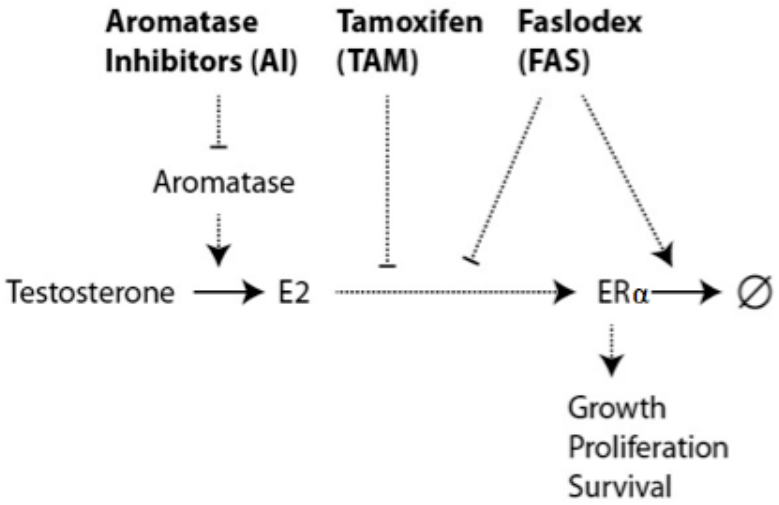

Figure 1.1 The molecular mechanisms of three major categories of endocrine therapies. Aromatase inhibitors (AIs) prevent the production of 17β-estradiol (E2, the primary estrogen present in breast tumors); SERMs category (exampled by tamoxifen) compete with E2 to bind ERα; SERDs category (exampled by faslodex) compete with E2 to bind ERα, and also promote the degradation of ERα.

However, not all breast cancers have satisfactory response to endocrine therapies [2]. About 30% breast cancers are ERα-negative, and they fail to respond to any anti-estrogens targeting ERα pathway [2]. Even in the ERα-positive category, about 35~40% breast cancers show intrinsic resistance to anti-estrogens [2]. Moreover, acquired resistance is also a major problem. Despite initial response to endocrine therapies, many ERα-positive breast cancers ultimately develop resistance to endocrine therapies slowly [2]. The molecular mechanism of endocrine resistance has been intensively studied based on ERα positive breast cancer cell lines that were selected for adaptation to a specific endocrine treatment [2, 3, 5]. For example, E2 (17β-estradiol, the primary estrogen present in breast tumors) independent breast cancer cell line LCC1 was developed after a combination of *in vitro*/*in vivo* E2 removal in MCF7 breast cancer cells [6]; faslodex resistant LCC9 cell line was further developed after long-term treatment of LCC1 with faslodex [7]. Substantial studies were performed to uncover the molecular basis for diverse endocrine responsiveness of these different cell lines. Experimental evidence suggests quite different expression/activation patterns of a few key molecules/processes were observed in MCF7, LCC1 and LCC9 cell lines [8-10]. Another interesting example is the long-term E2 deprived (LTED) MCF-7 cell line [11-13]. Both E2-hypersensitivity and E2-supersensitivity (or E2-independence) have been observed in the process of long-term E2 deprivation in MCF-7 cells. Diverse ERα activation modes were reported to associate with these different E2 sensitivities [14]. In all, there have been many gene candidates/events postulated as key players in eliciting acquired endocrine resistance in breast cancer cells, both *in vitro* and *in vivo* [2, 3, 5].

Notwithstanding our increasing knowledge on the roles of individual key genes in de-sensitizing the anti-tumor effects of endocrine treatments, little is known about how these gene candidates are mechanistically activated and further fixed during the development of acquired endocrine resistance. Traditionally, it was thought that mutations are the reason for the dysregulation of these genes in endocrine resistant breast cancers. For example, gene copy number variations in a lot of key genes, such as ERα and HER2, have been widely reported in endocrine resistant breast cancer cells [15-17]. Recently, growing evidence indicate that adaptive endocrine responses such as the compensatory activation of growth factor receptor (GFR) pathway and the reprograming of ERα activation modes also play pivotal roles in developing endocrine resistance [14, 18]. Understanding the molecular mechanism and the signaling pathway that are utilized by breast cancer cells to adapt to endocrine treatment will be critical for designing new strategies to prevent, delay and reverse endocrine resistance in breast cancer.

1.1.2 Adaptive endocrine response: Growth factor receptor pathway activation

The GFR pathway comprises the majority of the key players identified in breast cancer cells that have acquired endocrine resistance [2, 3, 5, 14, 19-21]. Increased epidermal growth factor receptor (EGFR) signaling is reported as a common feature in established cell lines that have become resistant to antiestrogen treatment [22-27]. MCF7-derived sub cell lines that have gained resistance to E2-deprivation, tamoxifen or faslodex in vitro clearly demonstrate EGFR and/or HER2 signaling dominance, accompanied by elevated activation of ERK1/2 MAP kinase and PI3K/AKT [25, 27, 28]. Obviously, these kinases are able to maintain cell survival and growth despite compromised ERα signaling

pathway. It is important to understand how these components in the GFR pathway are compensatorily activated in breast cancer cells under endocrine treatment. As mentioned above, gene mutations and Darwinian selection are able to contribute. This is evidenced by the fact that the HER2 gene is amplified in 30% of resistant breast cancers [29]. However, it is also well known that there exist bidirectional crosstalk links between ERα and GFR pathways [30-32], implying that adaptive responses can also occur without mutations.

Recent studies have shown activation of the GFR pathway activation in response to endocrine treatment [33], supporting the scenario of cellular adaptation rather than genetic selection. Evidences show that estrogen can suppress the expression and activity of HER2 and EGFR, two major members in the epidermal growth factor receptor family, in a number of different ERα-positive cell lines such as ZR-75-1, T47D and MCF7 [34-36]. A 409 bp region located in the first intron of the HER2 gene mediates the inhibition of HER2 expression by estrogen [37]. ERα is necessary for estrogen to mediate HER2 repression and anti-estrogens such as faslodex can reverse this process [34, 38]. Further mutational analysis on ERα revealed that the AF2 domain in ERα is required for estrogen mediated HER2 repression [39]. Since the AF2 domain in ERα is necessary for estrogen binding, it is suggested that the repression of HER2 expression is mediated by the E2 liganded ERα, which acts as a gene repressor upon binding with the promoter region of HER2 gene. Newman et al proposed a similar model, whereby E2-liganded ERα can compete with HER2 enhancer for binding p160 co-activators, thus resulting in inhibition of HER2 expression [39]. Similar mechanisms have also been studied in estrogen mediated EGFR repression [40].

Thus, anti-estrogens can effectively de-repress the estrogen-mediated inhibition of HER2 and EGFR expression, resulting in compensatory expression and activation of these GFRs. In experiments, increase in HER2 and EGFR expression occurs within 1 week after tamoxifen treatment [41]. And tamoxifen somehow induced the breast cancer cells to 'switch' to HER2 and EGFR signaling to maintain downstream activity of MAPK and AKT, supporting cell survival and resistance to tamoxifen [41]. Co-treatment of these cells with both tamoxifen and gefitinib will effectively block the compensatory activation of GFR pathway, resulting in improved endocrine responsiveness and delayed endocrine resistance [41]. Comparable results have also been reported in studies using both faslodex and gefitinib [25, 41, 42]. Currently, co-targeting of the GFR pathway in addition to endocrine therapy is under active evaluation as a promising therapeutic strategy to cure breast cancer [18, 43].

Intriguingly, however, not all growth factors are equally utilized to develop endocrine resistance in breast cancer cells. It is established that insulin-like growth factor type 1 receptor (IGF-1R) has positive cooperation with ERα [44]. As such, it has been recognized that anti-estrogens can sometimes release the inhibition of ERα on GFR pathway to elicit compensatory responses, and sometimes abolish the positive cooperation between ERα and GFR (e.g., IGF-1R) to exert its anti-proliferation effects. In addition, the GFR pathway is involved in an auto-regulation loop by activating ERα in an estrogen-independent manner [20, 45]. It becomes clear that how ERα is activated determines whether ERα has positive or negative correlation with the GFR pathway. Thus, exploring the different activation modes of ERα associated with the GFR pathway is of great important to understand the mechanism of acquired endocrine resistance.

1.1.3 Adaptive endocrine response: Estrogen receptor pathway reprogramming

Variation in status of ERα is an important adaptive response in anti-estrogen treated breast cancer cells. Endocrine treatment can change ERα status significantly. For example, loss of ERα expression (without mutations of the ERα gene) is quite common in long-term faslodex treated, or GFR overexpressed breast cancer cells [20, 46]. And this process is fully reversible [20, 47], suggesting that the 'on-off' switch of ERα expression is regulated at the epigenetic level but not genetic level. Adding more complexity to the adaptive response to endocrine treatment, ERα has three different activation modes under different conditions (Fig.1.2). These three activation modes of ERα include:

1) Ligand-dependent genomic activation (LDGA). Estrogen-liganded ERα can activate target gene expression either through direct binding of ERα dimers to estrogen response elements (EREs) in DNA, or with the help of other transcription factors (AP1 or SP1) to bind indirectly to serum response elements (SREs), so as to activate transcription [2, 3]. Notice that, ERα under this activation mode inhibits the expression and activity of HER2 and EGFR [37, 40].

2) Ligand-independent genomic activation (LIGA). Even without estrogen binding, ERα can be phosphorylated and activated by certain kinases (ERK, AKT, p90RSK, IKK, S6K etc.) at multiple sites (Ser118/104/106/167 etc.), thus promoting target gene transcription in a ligand-independent way [48]. It has been reported that Cyclin D and XBP1 binding can also facilitate the LIGA of ERα [49, 50]. It is noted that ERα under LIGA mode has positive interaction with the GFR pathway. An auto-regulation loop established by ERα (LIGA) and the GFR pathway has been reported to play key roles in tamoxifen resistant

breast cancer cells [20, 45].

3) Ligand-dependent non-genomic activation (LDNA). ERα or ERα variants localized in the cell membrane or cytoplasm can cooperate with a few membrane or cytoplasmic proteins (e.g., PELP1, GPCR, HPIP, Shc, MNAR, p130Cas, AR, Integrins, IGF1R, HER2, EGFR) to recruit non-receptor tyrosine kinase SRC, which can activate downstream PI3K/AKT and MAPK kinase cascades, resulting in activation of transcription factors (NFκB, Fos, Jun, NcoA, Myc, CREB, Elk1, STAT1/3, etc.) [51, 52].

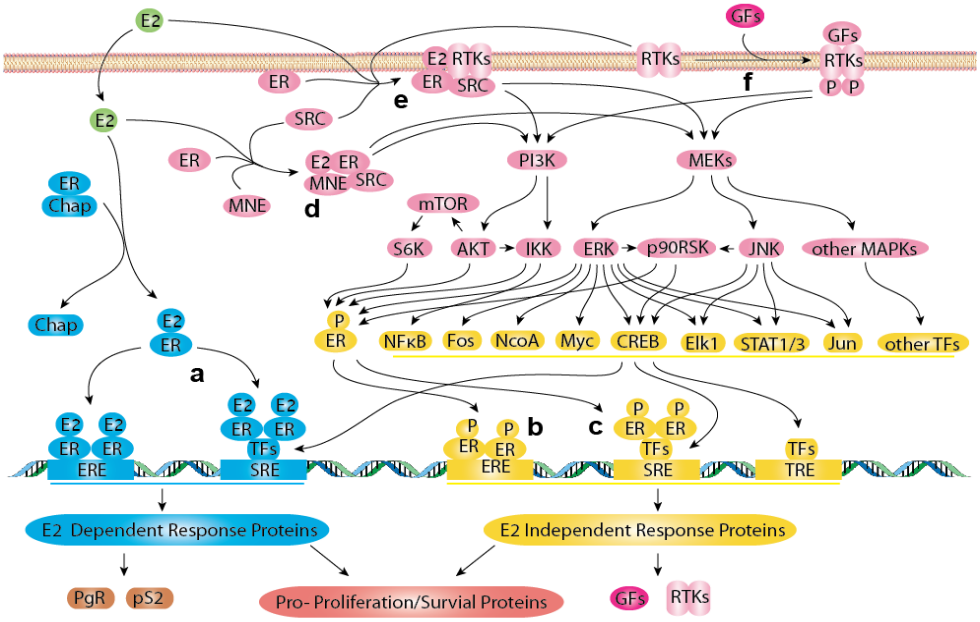

Figure 1.2 Different activation modes of ERα and growth factor receptor pathway in breast cancer cells. a. Ligand-dependent genomic activation (LDGA)**:** E2 liganded ERα activates target genes; b and c. Ligand-independent genomic activation (LIGA): PI3K/AKT and MAP Kinases activated by receptor tyrosine kinases (GFRs) or non-receptor tyrosine kinase (SRC) further phosphorylate and activate ERα in ligand independent way; d and e. Ligand-dependent non-genomic activation (LDNA): Non-genomic (membrane and cytoplasmic) ERα can facilitate kinase activation mediated by non-receptor tyrosine kinase SRC, and activation of the downstream transcription factors (TFs); f. Growth factor receptor pathway. Note that all three ERα activation modes contribute to the expression of pro-growth, pro-proliferation and pro-survival genes. Subtle functional differences of these ERα activation modes are not considered in this figure. Abbreviations in this figure: E2 (Estrogen); ER (Estrogen receptor α); ERE (Estrogen Response Elements); SRE (Serum Response Elements); PgR (Progesterone Receptor); Chap (Chaperones), MNE (modulator of non-genomic estrogen receptors);

GFs (Growth factors) RTK (Receptor Tyrosine Kinases); TRE (TF Response Elements).

These three ERα activation modes have been well recognized and widely discussed in the literature [2, 3, 5, 53]. Note that downstream events regulated by ERα under different activation modes should also be distinct. The physiology of breast cancer cells with ERα activated in different modes is also decided by varying context-dependent factors (the balance of co-activators/co-repressors, the competition of ERα with other transcription factors and posttranslational modifications of ERα). It has been observed that changes in ERα activation modes in breast cancer cells are associated with varying endocrine responsiveness [14]. Increased ERα phosphorylation (LIGA) and membrane ERα expression (LDNA) are common features in breast cancer with acquired endocrine resistance. And the predominance of LIGA/LDNA rather than LDGA mode of ERα is suggested as the molecular basis for the observed estrogen hypersensitivity and independence in LTED breast cancer cell lines, when compared to estrogen-sensitive MCF7 cells [14]. However, how ERα activation modes are regulated and associated with responsiveness to endocrine treatment is still poorly understood, and thus requires further investigation. Preliminary data from our experimental collaborators indicate that in MCF7 cells ERα can be activated by phosphorylation at Ser167 within hours in response to E2 withdrawal (Fig.1.4). At the same time, increase expression of HER2 and EGFR are also observed. Further studies are urgently required to understand the molecular mechanism of ERα activation mode reprogramming under endocrine treatment conditions.

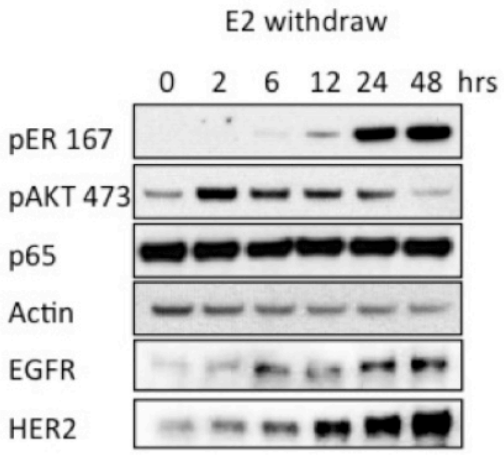

Figure 1.3 Increased expression of EGFR, HER2 and activation of AKT, ERα after E2 withdrawal in MCF7 cells. pER 167 refers to ERα phosphorylated on Ser 167. Data are used with permission of Rong Hu et al., unpublished.

1.2 Research Motivation

GFR pathway activation and ERα reprogramming are common compensatory events in ERα positive breast cancers under endocrine treatment. What are the physiological consequences of these adaptive endocrine responses? Most ERα positive breast cancers depend on the ERα pathway for survival and proliferation. And they are responsive to endocrine treatment. The initial anti-proliferation responses include the induction of apoptosis and cell cycle arrest [54]. However, GFR pathway activation and/or ERα reprogramming elicited by endocrine treatment can limit the anti-proliferative effects of endocrine treatment by providing 'escape' pathways. For example, according to Pratt et al.'s observation [55], an increase of NFκB activation induced by E2 depletion is usually not sufficient to prevent apoptosis in most MCF7 cells. Nonetheless, a sub-population of cells with high compensatory NFκB activity can escape apoptosis, even though they are cell-cycle compromised. These living but 'slow' cells can act as 'seed cells' to further accumulate intricate genetic or epigenetic modifications to resume fast proliferation and ultimately gain endocrine resistance. Thus, investigating how cells initially make decisions between 'anti-proliferative' and 'escape' pathways, and why 'escape' pathways are enhanced/fixed in cell lines with acquired endocrine resistance (such as in LCC1, LCC9 etc.), will be of great value to develop new strategies to delay, prevent and overcome endocrine resistance in the future.

Systems biology is a hybrid approach that utilizes computational techniques to interpret experimental data and make predictions [56, 57]. It focuses on the interactions of basic components in the cellular signaling transactions, so as to provide a systemic and

dynamical view of the molecular mechanism underlying cell physiology. Mathematical modeling is an integral part of systems biology. It provides a unique way to understand complex cellular behaviors, such as adaptation, switch and oscillation, in simple mathematical terms [58]. Successful examples in the past decades include mathematical models of the cell cycle, apoptosis and DNA damage responses [59-65]. In addition to explaining dynamical and complex cellular behaviors that are difficult to be understood by intuition alone, these models also exhibit strong predictive power to guide further experimental design. In terms of breast cancer modeling, a roadmap has been proposed to build quantitative and mathematical models of the basic modules (such as apoptosis, autophagy and cell cycle machinery) that will ultimately be combined together to determine susceptibility or resistance of breast cancer cells to endocrine therapy (Fig.1.4) [54].

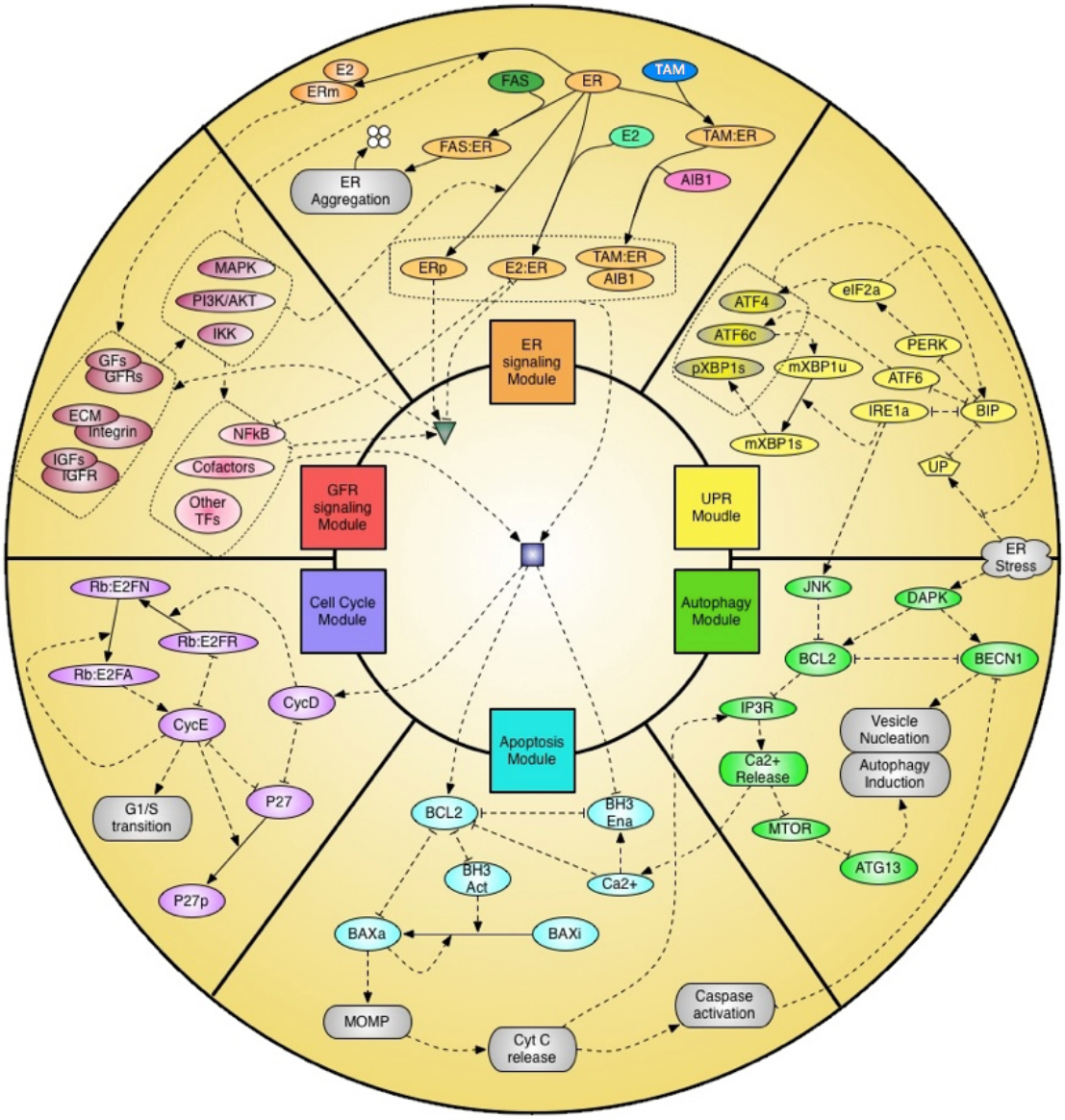

Figure 1.4 Schematic diagram of the signaling circuits and decision modules and their interactions in breast cancer cells. Following modules are included: Growth factor receptor pathway (GFR signaling Module), estrogen receptor pathway (ER signaling Module), unfolded protein response pathway (UPR Module), Autophagy Module, Apoptosis Module and Cell cycle Module. The triangle and square in the middle refers to intermediates that connect different modules at gene regulation level. For detailed discussion on these modules please refer to [54].

The motivation of this study is to use a systems biology strategy to specifically understand the mechanism of breast cancer endocrine response and resistance, focusing on the role of adaptive endocrine responses in developing endocrine resistance in breast cancer. The core of this study is the crosstalk mechanisms between the ERα and GFR pathways. Understanding the crosstalk as a dynamic system requires help from analytic tools, such as mathematical modeling. At this stage, detailed knowledge of the ERα-GFR crosstalk is still not yet available. So our first step is to apply systems biology strategy to study the roles of ERα-GFR crosstalk in terms of simplified models. Improved knowledge with more mechanistic details will help to refine the model in the future.

1.3 Research Overview

In Chapter 2, we proposed a model of the ERα to GFR survival-signaling switch in human breast cancer cells. It is widely accepted that breast cancer cells can shift between ERα and GFR signaling pathways for survival and proliferation under different conditions [18, 43]. Understanding this survival-signaling switch can shed light on drug resistance mechanisms and the design of more efficient breast cancer therapies.

The motivation led us to propose a mathematical model of the crosstalk between ERα and GFR pathways to study how this survival-signaling switch is organized and regulated. Ordinary differential equations were built to describe the dynamical behaviors of the ERα-GFR crosstalk. Compared to a similar model that was built by us previously [54], this model used a formalism that allows us to capture complex dependencies in a

simpler manner for simulation and analysis. In addition, epigenetic factors are considered to allow GFR pathway to exhibit slow activation.

Our model successfully explains the following experimental observations in GFR-transfected MCF7 cells [66, 67]: (1) there are three different distribution patterns of GFR in different sub-clones, (2) the bimodal GFR distribution pattern can be reversibly manipulated by the addition and withdrawal of estrogen, and (3) the asymmetry in the time it takes to switch from low to high GFR expression versus switching from high to low expression. Moreover, the model explains experiments showing that the GFR distribution cannot be changed by estrogen manipulation in normal MCF7 cells, and showing that transient ERα overexpression can up-regulate GFR expression and promote estrogen-independent growth in MCF7 cells [68]. The model improves our understanding of non-genetic heterogeneity and acquired endocrine resistance in breast cancer. This paper has been published in FEBS Letters in 2013 [69].

In Chapter 3, we utilize a novel strategy to model the transitions between endocrine therapy response and resistance in breast cancer cells. In the clinic, there are two common strategies used to overcome acquired endocrine resistance in breast cancer: 1) sequential treatment with different endocrine drugs [70], and 2) intermittent treatment by giving the patient a 'drug holiday' between endocrine treatments [71, 72]. It remains unclear why these two strategies are effective and how to optimize these two strategies.

In order to provide a theoretical tool to understand these questions, we present a mathematical model that captures the transitions among the three different experimentally observed estrogen sensitivity phenotypes in breast cancer (sensitive, hypersensitive, and

supersensitive) [14]. The model is again based on the signaling crosstalk between ERα and GFR pathways. We build a useful framework to understand the global properties of cell state transitions on the energy landscape of the breast cancer cell as a dynamical system. Grounded on the most probable routes of transitions on the breast cancer landscape, a state transition model was developed and evaluated.

As the results of this study, we show that population selection plays a crucial role in promoting acquired resistance in breast cancer. In addition, the simplified state transition model was computed from our biologically based model to investigate the population-scale effects of both sequential and intermittent treatment protocols and to enable the optimization of protocol parameters. The approach used in this study can be generalized to investigate treatment strategies and improve treatment efficiencies in breast cancer as well as other types of cancer. This study has been prepared for submission.

1.4 Reference

1. http://www.cancer.org/cancer/breastcancer/detailedguide/breast-cancer-key-statistics.
2. Musgrove, E.A. and R.L. Sutherland, *Biological determinants of endocrine resistance in breast cancer*. Nat Rev Cancer, 2009. **9**(9): p. 631-43.
3. Osborne, C.K. and R. Schiff, *Mechanisms of endocrine resistance in breast cancer*. Annu Rev Med, 2011. **62**: p. 233-47.

4. Harvey, J.M., et al., *Estrogen receptor status by immunohistochemistry is superior to the ligand-binding assay for predicting response to adjuvant endocrine therapy in breast cancer*. J Clin Oncol, 1999. **17**(5): p. 1474-81.

5. Massarweh, S. and R. Schiff, *Unraveling the mechanisms of endocrine resistance in breast cancer: new therapeutic opportunities*. Clin Cancer Res, 2007. **13**(7): p. 1950-4.

6. Brunner, N., et al., *Acquisition of hormone-independent growth in MCF-7 cells is accompanied by increased expression of estrogen-regulated genes but without detectable DNA amplifications*. Cancer Res, 1993. **53**(2): p. 283-90.

7. Brunner, N., et al., *MCF7/LCC9: an antiestrogen-resistant MCF-7 variant in which acquired resistance to the steroidal antiestrogen ICI 182,780 confers an early cross-resistance to the nonsteroidal antiestrogen tamoxifen*. Cancer Res, 1997. **57**(16): p. 3486-93.

8. Clarke, R., et al., *Antiestrogen resistance in breast cancer and the role of estrogen receptor signaling*. Oncogene, 2003. **22**(47): p. 7316-39.

9. Clarke, R., et al., *Gene network signaling in hormone responsiveness modifies apoptosis and autophagy in breast cancer cells*. J Steroid Biochem Mol Biol, 2009. **114**(1-2): p. 8-20.

10. Clarke, R., et al., *Endoplasmic reticulum stress, the unfolded protein response, and gene network modeling in antiestrogen resistant breast cancer*. Horm Mol Biol Clin Investig, 2011. **5**(1): p. 35-44.

11. Santen, R.J., et al., *Adaptation of estrogen-regulated genes in long-term estradiol deprived MCF-7 breast cancer cells*. Breast Cancer Res Treat, 2005. **94**(3): p. 213-23.

12. Santen, R.J., et al., *Adaptive hypersensitivity to estrogen: mechanism for sequential responses to hormonal therapy in breast cancer*. Clin Cancer Res, 2004. **10**(1 Pt 2): p. 337S-45S.

13. Johnston, S.R. and M. Dowsett, *Aromatase inhibitors for breast cancer: lessons from the laboratory*. Nat Rev Cancer, 2003. **3**(11): p. 821-31.

14. Nicholson, R.I., et al., *Growth factor-driven mechanisms associated with resistance to estrogen deprivation in breast cancer: new opportunities for therapy*. Endocr Relat Cancer, 2004. **11**(4): p. 623-41.

15. Aguilar, H., et al., *Biological reprogramming in acquired resistance to endocrine therapy of breast cancer*. Oncogene, 2010. **29**(45): p. 6071-83.

16. Bartlett, J.M., et al., *Evaluating HER2 amplification and overexpression in breast cancer*. J Pathol, 2001. **195**(4): p. 422-8.

17. Nugoli, M., et al., *Genetic variability in MCF-7 sublines: evidence of rapid genomic and RNA expression profile modifications*. BMC Cancer, 2003. **3**: p. 13.

18. Saji, S., F. Sato, and N.T. Ueno, *Fuel, electricity, ER and HER2--a hybrid-car model of breast cancer*. Nat Rev Clin Oncol, 2012. **9**(7).

19. Nicholson, R.I., et al., *Growth factor signalling in endocrine and anti-growth factor resistant breast cancer*. Rev Endocr Metab Disord, 2007. **8**(3): p. 241-53.

20. Nicholson, R.I., et al., *Growth factor signalling and resistance to selective oestrogen receptor modulators and pure anti-oestrogens: the use of anti-growth*

factor therapies to treat or delay endocrine resistance in breast cancer. Endocr Relat Cancer, 2005. **12 Suppl 1**: p. S29-36.

21. Gee, J.M., et al., *Deciphering antihormone-induced compensatory mechanisms in breast cancer and their therapeutic implications*. Endocr Relat Cancer, 2006. **13 Suppl 1**: p. S77-88.

22. Vickers, P.J., et al., *A multidrug-resistant MCF-7 human breast cancer cell line which exhibits cross-resistance to antiestrogens and hormone-independent tumor growth in vivo*. Mol Endocrinol, 1988. **2**(10): p. 886-92.

23. van den Berg, H.W., et al., *Expression of receptors for epidermal growth factor and insulin-like growth factor I by ZR-75-1 human breast cancer cell variants is inversely related: the effect of steroid hormones on insulin-like growth factor I receptor expression*. Br J Cancer, 1996. **73**(4): p. 477-81.

24. van Agthoven, T., et al., *Induction of estrogen independence of ZR-75-1 human breast cancer cells by epigenetic alterations*. Mol Endocrinol, 1994. **8**(11): p. 1474-83.

25. McClelland, R.A., et al., *Enhanced epidermal growth factor receptor signaling in MCF7 breast cancer cells after long-term culture in the presence of the pure antiestrogen ICI 182,780 (Faslodex)*. Endocrinology, 2001. **142**(7): p. 2776-88.

26. Long, B., et al., *Changes in epidermal growth factor receptor expression and response to ligand associated with acquired tamoxifen resistance or oestrogen independence in the ZR-75-1 human breast cancer cell line*. Br J Cancer, 1992. **65**(6): p. 865-9.

27. Knowlden, J.M., et al., *Elevated levels of epidermal growth factor receptor/c-erbB2 heterodimers mediate an autocrine growth regulatory pathway in tamoxifen-resistant MCF-7 cells*. Endocrinology, 2003. **144**(3): p. 1032-44.

28. Jordan, N.J., et al., *Increased constitutive activity of PKB/Akt in tamoxifen resistant breast cancer MCF-7 cells*. Breast Cancer Res Treat, 2004. **87**(2): p. 167-80.

29. Tsuda, H.H., *Prognostic and predictive value of c-erbB-2 (HER-2/neu) gene amplification in human breast cancer*. Breast Cancer, 2001. **8**(1): p. 38-44.

30. McClelland, R.A., et al., *Short-term effects of pure anti-oestrogen ICI 182780 treatment on oestrogen receptor, epidermal growth factor receptor and transforming growth factor-alpha protein expression in human breast cancer*. Eur J Cancer, 1996. **32A**(3): p. 413-6.

31. Massarweh, S. and R. Schiff, *Resistance to endocrine therapy in breast cancer: exploiting estrogen receptor/growth factor signaling crosstalk*. Endocr Relat Cancer, 2006. **13 Suppl 1**: p. S15-24.

32. Arpino, G., et al., *Crosstalk between the estrogen receptor and the HER tyrosine kinase receptor family: molecular mechanism and clinical implications for endocrine therapy resistance*. Endocr Rev, 2008. **29**(2): p. 217-33.

33. Hiscox, S., J. Gee, and R.I. Nicholson, *Therapeutic resistance to anti-hormonal drugs in breast cancer : new molecular aspects and their potential as targets*. 2009, Dordrecht: Springer. xi, 198 p.

34. Russell, K.S. and M.C. Hung, *Transcriptional repression of the neu protooncogene by estrogen stimulated estrogen receptor*. Cancer Res, 1992. **52**(23): p. 6624-9.

35. Read, L.D., et al., *Hormonal modulation of HER-2/neu protooncogene messenger ribonucleic acid and p185 protein expression in human breast cancer cell lines*. Cancer Res, 1990. **50**(13): p. 3947-51.

36. Dati, C., et al., *Inhibition of c-erbB-2 oncogene expression by estrogens in human breast cancer cells*. Oncogene, 1990. **5**(7): p. 1001-6.

37. Bates, N.P. and H.C. Hurst, *An intron 1 enhancer element mediates oestrogen-induced suppression of ERBB2 expression*. Oncogene, 1997. **15**(4): p. 473-81.

38. Taverna, D., et al., *erbB-2 expression in estrogen-receptor-positive breast-tumor cells is regulated by growth-modulatory reagents*. Int J Cancer, 1994. **56**(4): p. 522-8.

39. Newman, S.P., et al., *Cofactor competition between the ligand-bound oestrogen receptor and an intron 1 enhancer leads to oestrogen repression of ERBB2 expression in breast cancer*. Oncogene, 2000. **19**(4): p. 490-7.

40. Chrysogelos, S.A., et al., *Mechanisms of EGF receptor regulation in breast cancer cells*. Breast Cancer Res Treat, 1994. **31**(2-3): p. 227-36.

41. Gee, J.M., et al., *The antiepidermal growth factor receptor agent gefitinib (ZD1839/Iressa) improves antihormone response and prevents development of resistance in breast cancer in vitro*. Endocrinology, 2003. **144**(11): p. 5105-17.

42. Shou, J., et al., *Mechanisms of tamoxifen resistance: increased estrogen receptor-HER2/neu cross-talk in ER/HER2-positive breast cancer*. J Natl Cancer Inst, 2004. **96**(12): p. 926-35.

43. Rimawi, M.F. and C.K. Osborne, *Breast Cancer: Blocking both driver and escape pathways improves outcomes*. Nat Rev Clin Oncol, 2012. **9**(3): p. 133-4.

44. Nicholson, R.I. and J.M. Gee, *Oestrogen and growth factor cross-talk and endocrine insensitivity and acquired resistance in breast cancer*. Br J Cancer, 2000. **82**(3): p. 501-13.

45. Zilli, M., et al., *Molecular mechanisms of endocrine resistance and their implication in the therapy of breast cancer*. Biochim Biophys Acta, 2009. **1795**(1): p. 62-81.

46. Oh, A.S., et al., *Hyperactivation of MAPK induces loss of ERalpha expression in breast cancer cells*. Mol Endocrinol, 2001. **15**(8): p. 1344-59.

47. Lopez-Tarruella, S. and R. Schiff, *The dynamics of estrogen receptor status in breast cancer: re-shaping the paradigm*. Clin Cancer Res, 2007. **13**(23): p. 6921-5.

48. Lannigan, D.A., *Estrogen receptor phosphorylation*. Steroids, 2003. **68**(1): p. 1-9.

49. Zwijsen, R.M., et al., *CDK-independent activation of estrogen receptor by cyclin D1*. Cell, 1997. **88**(3): p. 405-15.

50. Ding, L., et al., *Ligand-independent activation of estrogen receptor alpha by XBP-1*. Nucleic Acids Res, 2003. **31**(18): p. 5266-74.

51. Bartella, V., et al., *New advances on the functional cross-talk between insulin-like growth factor-I and estrogen signaling in cancer*. Cell Signal, 2012. **24**(8): p. 1515-21.

52. Parsons, S.J., et al., *Cooperative Interactions Between c-Src, Estrogen Receptors and Receptor Tyrosine Kinases in Breast Cancer*. Advances in Rapid Sex-Steroid Action, 2012. **Part 1**: p. 31-59.

53. Heldring, N., et al., *Estrogen receptors: how do they signal and what are their targets*. Physiol Rev, 2007. **87**(3): p. 905-31.

54. Tyson, J.J., et al., *Dynamic modelling of oestrogen signalling and cell fate in breast cancer cells*. Nat Rev Cancer, 2011. **11**(7): p. 523-32.

55. Pratt, M.A., et al., *Estrogen withdrawal-induced NF-kappaB activity and bcl-3 expression in breast cancer cells: roles in growth and hormone independence*. Mol Cell Biol, 2003. **23**(19): p. 6887-900.

56. Kitano, H., *Systems biology: a brief overview*. Science, 2002. **295**(5560): p. 1662-4.

57. Kitano, H., *Computational systems biology*. Nature, 2002. **420**(6912): p. 206-10.

58. Tyson, J.J., K. Chen, and B. Novak, *Network dynamics and cell physiology*. Nat Rev Mol Cell Biol, 2001. **2**(12): p. 908-16.

59. Tyson, J.J., *Modeling the cell division cycle: cdc2 and cyclin interactions*. Proc Natl Acad Sci U S A, 1991. **88**(16): p. 7328-32.

60. Fussenegger, M., J.E. Bailey, and J. Varner, *A mathematical model of caspase function in apoptosis*. Nat Biotechnol, 2000. **18**(7): p. 768-74.

61. Chen, K.C., et al., *Integrative analysis of cell cycle control in budding yeast*. Mol Biol Cell, 2004. **15**(8): p. 3841-62.

62. Ma, L., et al., *A plausible model for the digital response of p53 to DNA damage*. Proc Natl Acad Sci U S A, 2005. **102**(40): p. 14266-71.

63. Chen, C., et al., *Modeling of the role of a Bax-activation switch in the mitochondrial apoptosis decision*. Biophys J, 2007. **92**(12): p. 4304-15.

64. Albeck, J.G., et al., *Modeling a snap-action, variable-delay switch controlling extrinsic cell death*. PLoS Biol, 2008. **6**(12): p. 2831-52.

65. Batchelor, E., et al., *Recurrent initiation: a mechanism for triggering p53 pulses in response to DNA damage*. Mol Cell, 2008. **30**(3): p. 277-89.

66. Miller, D.L., et al., *Emergence of MCF-7 cells overexpressing a transfected epidermal growth factor receptor (EGFR) under estrogen-depleted conditions: evidence for a role of EGFR in breast cancer growth and progression*. Cell Growth Differ, 1994. **5**(12): p. 1263-74.

67. Liu, Y., et al., *MCF-7 breast cancer cells overexpressing transfected c-erbB-2 have an in vitro growth advantage in estrogen-depleted conditions and reduced estrogen-dependence and tamoxifen-sensitivity in vivo*. Breast Cancer Res Treat, 1995. **34**(2): p. 97-117.

68. Tolhurst, R.S., et al., *Transient over-expression of estrogen receptor-alpha in breast cancer cells promotes cell survival and estrogen-independent growth*. Breast Cancer Res Treat, 2011. **128**(2): p. 357-68.

69. Chen, C., et al., *Modeling the estrogen receptor to growth factor receptor signaling switch in human breast cancer cells*. FEBS Lett, 2013.

70. Ali, S. and R.C. Coombes, *Endocrine-responsive breast cancer and strategies for combating resistance*. Nat Rev Cancer, 2002. **2**(2): p. 101-12.

71. Stoll, B.A., *Rechallenging breast cancer with tamoxifen therapy*. Clin Oncol, 1983. **9**(4): p. 347-51.

72. Sabnis, G., et al., *Sensitivity to the aromatase inhibitor letrozole is prolonged after a "break" in treatment*. Mol Cancer Ther, 2010. **9**(1): p. 46-56.

Chapter 2. Modeling the estrogen receptor to growth factor receptor signaling switch in human breast cancer cells

Chun Chen[‖], William T. Baumann[‡], Robert Clarke[§], John J. Tyson*

*Department of Biological Sciences, [‡]Department of Electrical & Computer Engineering, and [‖]Graduate Program in Genetics, Bioinformatics and Computational Biology, Virginia Polytechnic Institute & State University, Blacksburg VA 24061, USA

[§]Lombardi Comprehensive Cancer Center, Georgetown University School of Medicine, Washington DC 20057, USA

* Corresponding author. Fax: +1 540 231 9307.

E-mail address: tyson@vt.edu.

2.1 Abstract

Breast cancer cells develop resistance to endocrine therapies by shifting between estrogen receptor (ER)-regulated and growth factor receptor (GFR)-regulated survival signaling pathways. To study this switch, we propose a mathematical model of crosstalk between these pathways. The model explains why MCF7 sub-clones transfected with HER2 or EGFR show three GFR-distribution patterns, and why the bimodal distribution pattern can be reversibly modulated by estrogen. The model illustrates how transient overexpression of ER activates GFR signaling and promotes estrogen-independent

growth. Understanding this survival-signaling switch can help in the design of future therapies to overcome resistance in breast cancer.

Keywords: Mathematical modeling; estrogen receptor signaling; growth factor receptor signaling; breast cancer; endocrine resistance

Abbreviations

AKT, a serine/threonine-specific protein kinase, also known as Protein Kinase B (PKB);

CCS, Charcoal-stripped fetal-calf serum;

CSC, Cancer Stem Cell;

E2, 17β-estradiol;

E2:ER, E2-bound Estrogen Receptor;

EGFR, Epidermal Growth Factor Receptor;

ER, Estrogen Receptor;

ER-P, Phosphorylated Estrogen Receptor;

FCS, Fetal Calf Serum;

GFR, Growth Factor Receptor;

HER2, Human Epidermal Growth Factor Receptor-2;

MAPK, Mitogen Activated Protein Kinases;

mTOR, Mammalian Target Of Rapamycin;

NFκB, Nuclear Factor kappa-light-chain-enhancer of activated B cells.

PI3K, Phosphatidylinositide 3-Kinases;

Highlights

- We model a switch between estrogen receptor and growth factor receptor pathways.
- The model explains three patterns of HER2 or EGFR expression in MCF7 sub-clones.
- The model shows how estrogen modulates growth factor receptor expression patterns.
- The model suggests a novel switch mechanism for acquired resistance in breast cancer.

2.2 Introduction

Mammalian cells can switch between different signaling pathways to achieve distinct physiological goals in response to environmental stimuli, as exemplified by immune cell differentiation [1]. This plasticity is important for normal cells to differentiate properly and to survive in stressful environments. In cancer cells, this plasticity often results in drug resistance including acquired resistance to anti-estrogenic drugs.

The estrogen receptor (ER) and growth factor receptor (GFR) pathways are major drivers of survival and proliferation in 85% of breast tumors [2, 3]. In clinical practice, expression of ERα (the most prevalent of two ER genes) and HER2 (a major GFR and member of the EGFR superfamily) are validated biomarkers used to determine treatment strategies for individual patients [4]. Approximately 70% of breast cancers express ERα [5], and various endocrine therapies have been developed to interfere with ER action [5]. Antagonizing GFR pathways (*e.g.*, using trastuzumab) in HER2+ breast cancer also improves disease-free and overall survival for breast cancer patients [6]. However, the

ultimate efficacy of therapies targeting individual pathways is not satisfactory. For example, tamoxifen successfully reduces by one-third the annual death rate from breast cancer, but one-third of tamoxifen-treated women develop recurrent disease within 15 years [5]. Resistance to anti-estrogens or GFR pathway antagonists also develops in human breast cancer cell lines [7-9].

We have used mathematical modeling guided by experimental observations to explore the mechanism underlying acquired resistance to endocrine therapies as driven by the ER-GFR switch. Acquired resistance could arise by activation of a compensatory escape pathway when the normal driver pathway is inhibited [3], the so-called 'hybrid-car' model of breast cancer [10]. Since breast cancer cells can switch reversibly and robustly between ER and GFR pathways for proliferation and survival [3, 10], blocking either the ER or GFR pathway will usually result in activation of the other, allowing some cells to survive and eventually resume proliferation. Evidence for a close regulatory relationship between ER and GFR signaling includes the reciprocal expression of ER and GFR in most breast cancers [11], and activation of GFR pathway components (HER2, EGFR, MAPK, PI3K, AKT, mTOR, NFκB etc.) as compensatory responses to anti-estrogens [5, 12-14]. Interestingly, these compensatory processes are reversible after withdrawing the endocrine treatment [15]. Moreover, recent evidence indicates that ER negative (ER−) breast cancer cells may develop resistance to GFR pathway antagonists by restoring the ER pathway and hence becoming responsive to anti-estrogens [16, 17].

ER and GFR are sometimes positively associated in breast cancers [18, 19]. Whether ER and GFR are negatively or positively correlated depends on how ER is activated. ER can be activated either by binding to 17β-estradiol (E2, the primary estrogen present in breast

tumors) to form an active E2:ER complex, or by phosphorylation (ER-P) by various kinases (e.g. ERK and AKT) at multiple sites [5, 20, 21]. E2:ER has an inhibitory effect on GFR. E2 withdrawal can release the inhibition of ER on GFR expression and NFκB activity [22-26], consistent with the fact that E2:ER binds the promoter region of GFR genes (e.g., HER2 and EGFR) and acts as a repressor [27, 28]. However, E2-independent ER-P is positively associated with GFR, and it can up-regulate certain ligands (e.g., TGFα, EGF and amphiregulin) of the GFR signaling network, which in turn activate the kinases that phosphorylate more ER [29-31]. This auto-activation loop has been implicated in tamoxifen-resistance [31, 32]. NFκB, a major integrator of the GFR signaling network, is involved with E2:ER in a mutual-inhibition feedback loop [24, 33]. NFκB also controls the expression of a broad spectrum of genes regulating important cellular behaviors including cell differentiation [34, 35]. In particular, NFκB activates the transcription factor TWIST and represses the expression of E-cadherin, which in turn enhances the epithelial-mesenchymal transition (EMT) in breast cancer [36]. EMT is associated with a de-differentiation process whereby epithelial-like breast cancer cells increase their 'stemness' and undergo a phenotypic transition from HER2– to HER2+ [37]. EMT in breast cancer cells is likely due to genome-scale epigenetic reprogramming, including the promoter activity of HER2 [38]. Epigenetic changes such as methylation or acetylation can occur during differentiation or de-differentiation and are often reversible [36-38].

While the crosstalk between ER and GFR pathways in breast cancer, especially in MCF7 cells, has been widely studied [5, 13, 20, 22, 31, 39, 40], a comprehensive, dynamic view of ER-GFR crosstalk is still lacking. Previously, we proposed a simplified model that

could account for the effects of E2 withdrawal on the bimodal distribution of GFR (HER2 or EGFR) in MCF7 cells [41]. However, this model combined all components of the GFR pathway into one variable and required an unreasonably slow rate constant to fit the experimental data. A more realistic model would allow the GFR pathway to exhibit both rapid (e.g., post-translational modifications of GFR proteins) and slow modifications (e.g., epigenetic modifications of GFR promoters). Moreover, a recent report indicates that transient ER overexpression can robustly activate E2-independent growth of MCF7 cells [42], suggesting further modifications to achieve a more realistic model.

Here we present a new model to explore the mathematical characteristics of the ER-GFR switch that is a central determinant of breast cancer cell fate in response to endocrine therapies. The model explains many aspects of the available experimental data (Supplementary Documents, Figs. 2.7-2.10), for example: (1) in sub-clones of MCF7 cells transfected with GFR (HER2 or EGFR), there are three different distribution patterns of GFR [43, 44], (2) for sub-clones with a bimodal distribution of GFR, the distribution can be reversibly manipulated by varying E2 levels [43, 44], (3) whereas E2 withdrawal in GFR-transfected MCF7 cells switches on GFR expression within weeks, E2 addition takes months to switch off expression [43, 44], (4) E2 withdrawal can up-regulate GFR expression within 5 weeks in GFR-transfected MCF7 cells, but fails to do so in wild type MCF7 cells [43, 44], and (5) transient ER overexpression in MCF7 cells can switch on the GFR pathway and promote E2-independent growth [42]. The model provides a new tool to understand and evaluate these intriguing experimental observations, and it may help in finding new strategies to overcome anti-estrogen resistance in breast cancer.

2.3 Materials and Methods

We postulate a highly condensed model of the interaction between ER and GFR (Fig. 2.1A and Supplementary Documents). The protein level of GFR is down-regulated by E2:ER complex [27, 28]. After E2 withdrawal, GFR is released from inhibition and its downstream kinases phosphorylate ER to an E2-independent form, ER-P [5, 20, 21]. ER-P can activate and stabilize the GFR pathway, creating a positive feedback loop [29-31]. In addition, GFR further activates transcription factors such as NFκB, promoting a series of epigenetic changes contributing to increased GFR expression and establishing another positive feedback loop [34, 35]. For simplicity, we combine the epigenetic factors contributing to GFR expression into the quantity 'EPI'. 'E2ER' and 'ERP' are used to represent E2:ER and ER-P. The wiring diagram in Fig. 1A was translated into ordinary differential equations (ODEs) by a formalism that allows us to capture complex dependencies in a simple manner [45] for simulation and analysis. We used the program XPP-AUT, available freely at http://www.math.pitt.edu/~bard/xpp/xpp.html, to simulate the model and to draw bifurcation diagrams. The ensemble stochastic simulations were performed with Matlab Version 7.9.0. A detailed version of materials and methods is provided in the supplementary document in 2.8.

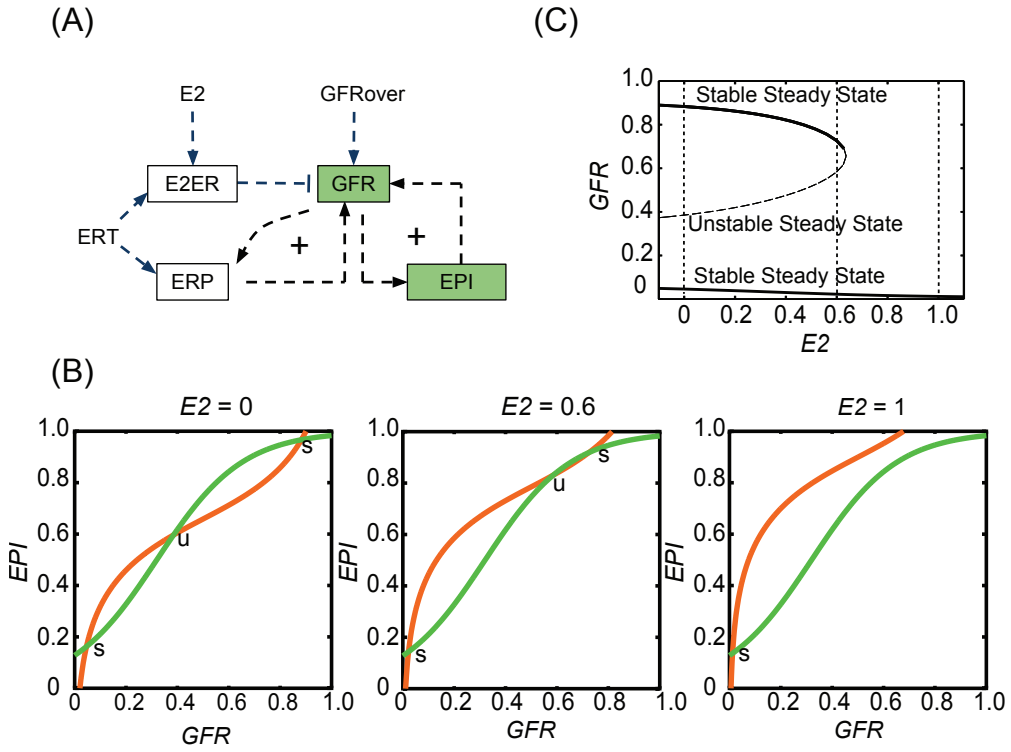

Figure 2.1 A model of the crosstalk between ER and GFR pathways exhibits bistable switching properties. (**A**) Influence diagram of the model. *E2*, estrogen level; *ERT*, total ERα level; *E2ER*, estrogen-dependent E2:ER complex; *ERP*, phosphorylated ER; *GFR*, growth factor receptor; *EPI*, epigenetic components in GFR pathway; *GFRover*, number of extra GFR gene copies. (**B**) Nullclines of the system at different E2 levels. s, stable steady state; u, unstable steady state. (**C**) Bifurcation diagram of *GFR*, with *E2* as the bifurcation parameter. The curves trace the steady state level of GFR as a function of E2 level. For a given value of *E2*, a cell may express a low or high value of *GFR* (upper and lower solid lines; the middle dashed line indicates a branch of unstable steady states).

2.4 Results

2.4.1 Bifurcation analysis of the survival-signaling switch

The nullclines of our system of equations (EQ.2.S1-S2 in Section 2.8) are plotted in Fig. 2.1B. The intersections of these two curves correspond to steady states of the model. The number of steady states is controlled by the E2 level. When $E2 = 1$, there is one stable steady state corresponding to low *GFR* and low *EPI* (GFR–/EPI–). When *E2* is reduced below 0.65, there are three steady states, two of which are stable and a third which is unstable. The stable steady states have GFR and EPI levels that are either both low (GFR–/EPI–) or both high (GFR+/EPI+). Figure 2.1C illustrates how the steady states of the system change with the E2 level. The system has three steady states in the range of $0 < E2 < 0.65$ and only one stable steady state when $E2 > 0.65$. However, *E2* is not the only parameter that influences the system's bistability. *GFRover*, which represents the influence of additional GFR genes transfected into MCF7 cells, can also be used as a bifurcation parameter. Figure 2.2A shows that when *E2* is held constant at $E2 = 1$ the system is bistable only when $3.2 < GFRover < 12.8$. We will show how this bistable survival-signaling switch can explain the results of several important experiments that are difficult to understand without a model.

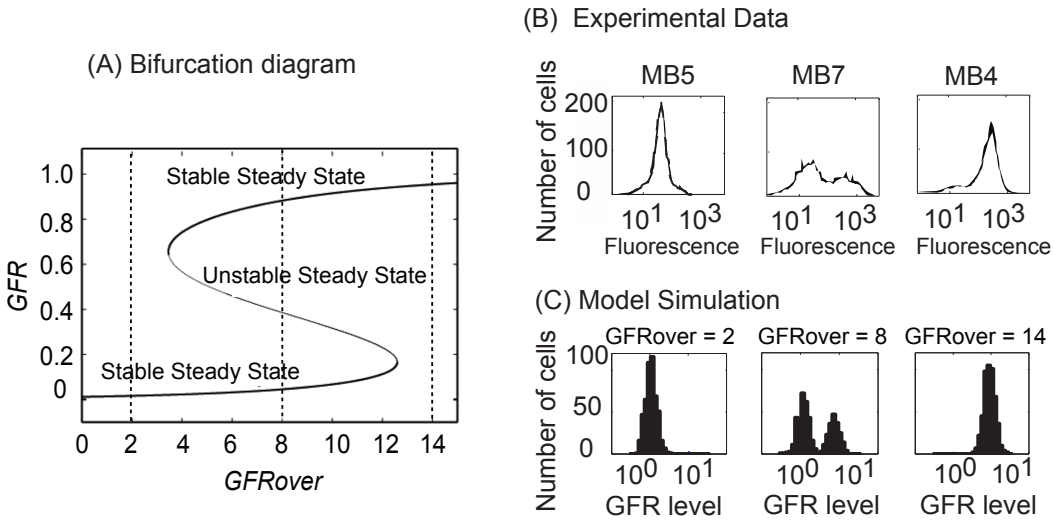

Figure 2.2 Three distribution patterns of GFR are exhibited in GFR-transfected MCF7. (**A**) Signal–response curve for *GFR* as a function of *GFRover*. The steady-state value of *GFR* is plotted as a function of *GFRover* (from 0 to 14). For intermediate values of *GFRover*, a cell may express either a low or high level of GFR (upper and lower solid lines; the middle dashed line indicates a branch of unstable steady states). (**B**) Different HER2 distribution patterns in HER2-overexpressed MCF7 sub-clones. Sub-clones MB5, MB7 and MB4 represent three typical distribution patterns of HER2 observed in experiment. Experimental data are adapted from [43]. (**C**) Distribution of GFR in 500 cells that are stochastically simulated at different values of *GFRover* (2, 8, and 14) for four months by starting from random initial conditions. GFR level = 10^{GFR} in these histograms.

2.4.2 Three distribution patterns of GFR

Liu *et al*. transfected HER2 cDNA into MCF7 cells and created multiple stable sub-clones, which were further screened for HER2 protein expression levels using flow cytometry. Interestingly, three HER2 distribution patterns were observed in the sub-clones they selected [43]: (1) a single peak of cells with elevated HER2 protein (MB4 in Fig. 2.2B), (2) a single peak of cells with low HER2 protein, identical to control MCF7 cells (MB5 in Fig. 2.2B), and (3) a bimodal (two-peaked) distribution of HER2 (MB7 in Fig. 2.2B). Southern blotting was used to confirm that, within a sub-clone, all cells had the same number of integrated HER2 copies; hence, the bimodal distribution did not result from varying genetic conditions. Similar results in MCF7 cells transfected with EGFR have been reported [44], but a satisfactory explanation for these observations is lacking.

The major difference between these sub-clones could be that during transfection different numbers of HER2 or EGFR genes were integrated into the individual cells that formed the sub-clones. In our model, we use *GFRover* to denote the amount of transfected GFR and have shown that the system is bistable only when *GFRover* is within a specific range (Fig. 2.2A). When very few GFR gene copies are integrated into the cell (e.g., *GFRover* = 2), the system has only one stable steady state at low GFR expression, while integration of a high number of copies (e.g., *GFRover* = 14) results in only one stable steady state at high GFR expression. However, integration of an intermediate number of copies (e.g., *GFRover* = 8) creates a system with two stable steady states (either high or low GFR expression). To model distribution patterns of GFR in a population of cells, we

performed 500 stochastic simulations (see Fig. 2.2C), starting from random initial conditions, of four month duration for each of three different cases (*GFRover* = 2, 8 and 14). The results of these simulations clearly replicate the experimental observations. When *GFRover* = 2, there is only one peak of cells at a low GFR level, corresponding to MB5 in Fig. 2.2B. When *GFRover* = 14, there is only one peak of cells at a high GFR level, corresponding to MB4 in Fig. 2.2B. And when *GFRover* = 8, two peaks of cells (bimodal distribution) coexist, corresponding to MB7 in Fig. 2.2B. (We note that the number of GFR gene copies actually transfected in the experiments is unknown and so the values used here for GFRover are arbitrary and can be rescaled if copy number data becomes available.)

2.4.3 GFR bimodal distribution manipulated by E2

By using a sub-clone of MCF7 cells with a bimodal HER2 distribution, Liu et al. further showed the sensitivity of HER2 expression to culture conditions [43]. Growing the cells for 5 weeks in charcoal-stripped fetal calf serum (CCS), which is depleted of E2, resulted in a single peak of cells expressing high levels of HER2. Similarly, Miller et al. reported that MCF7 cells transfected with EGFR and cultured in CCS create a population consisting predominantly of cells with high EGFR levels [44]. However, wild type MCF7 cells cultured in CCS for one year still show a population consisting predominantly of cells with low EGFR levels [44].

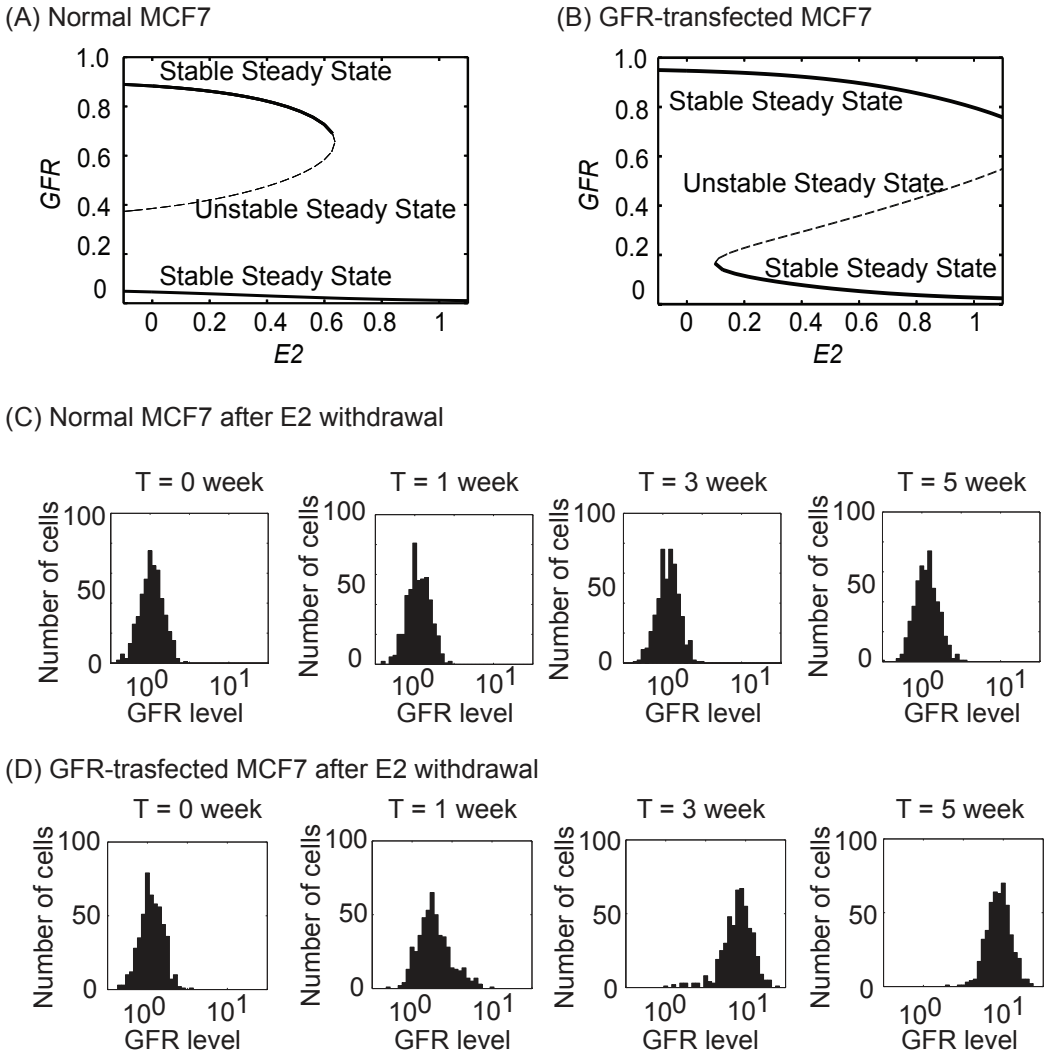

Figure 2.3 E2 withdrawal turns on GFR in GFR-transfected but not in normal MCF7 cells. (**A**, **B**) Bifurcation diagrams of *GFR* with *E2* as bifurcation parameter in normal MCF7 cells (*GFRover* = 0) and in GFR-transfected MCF7 cells (*GFRover* = 5). (**C**, **D**) Temporal evolutions of GFR distribution under E2-withdrawal conditions for normal MCF7 cells (*GFRover* = 0) and for GFR-transfected MCF7 cells (*GFRover* = 5). In each case, 500 cells were simulated over the course of five weeks. GFR level = 10^{GFR} in these histograms.

Figure 2.3 provides an explanation for these results. In normal MCF7 cells cultured with E2, the cells are on the lower branch (low GFR) of Fig. 2.3A. When E2 is depleted, the cells will stay on this branch unless stochastic variations are strong enough to occasionally push a cell to the upper branch (high GFR, Fig. 2.3A). Note that there is a significant barrier separating the lower steady state from the unstable steady state (middle branch). We simulated a population of 500 MCF7 cells starting from low GFR in the E2-withdrawal condition for five weeks. No cell jumped to the high-GFR state, and there was no change in the GFR distribution pattern at the population level (Fig. 2.3C). However, when GFR is transfected into MCF7 cells ($GFRover = 5$), the barrier at $E2 = 0$ disappears (Fig. 2.3B) and the system only has one stable steady state at high GFR. Thus, when starting from the low-GFR initial condition, all cells will move to the high-GFR state. A simulation of 500 GFR-transfected MCF7 cells for five weeks produced a change in the GFR distribution pattern similar to that reported by Liu et al. and Miller et al. (Fig. 2.3D).

Experiments also show that the distribution pattern of GFR can be reversibly controlled by E2 [43, 44]. Growing the MB8 sub-clone MCF7 cells (with bimodal HER2 distribution) in CCS for five weeks resulted in a single peak at high HER2 (Fig. 2.4, top left). Continuing to grow these cells in fetal calf serum (FCS), which contains E2, gradually leads to the rise of a peak at low HER2 (Fig. 2.4, left panel) [43]. Similar dynamics have also been reported in MCF7 cells with EGFR overexpression [44]. Southern blots confirmed that there was no variation in transfected HER2 gene copy number during E2 manipulation; Northern blots showed that HER2 mRNA expression is

consistent with the protein level [43]. These data imply that genetic mutations are not the cause of HER2 heterogeneity in these MCF7 cells.

The bifurcation diagram in Fig. 2.3B provides an explanation for these experimental results. Consider a population of GFR-transfected MCF7 cells depleted of E2 ($E2 = 0$) and having high GFR expression. If E2 is now provided to the cells ($E2 = 1$), they will stay in the high-GFR state, but the barrier to transitioning to the low-GFR state will be diminished. Given adequate time, stochastic variations may induce some cells to transition to the low-GFR branch. We simulated a population of 5000 cells under these conditions, and the GFR distributions from the model compared well with the experimental observations (Fig. 2.4, right panel). Note that after E2 withdrawal, GFR-transfected MCF7 cells can switch on GFR within weeks, but cells need months to turn off GFR after E2 addition. Our simulation also replicates this asymmetry in response time (Figs. 2.3 and 2.4).

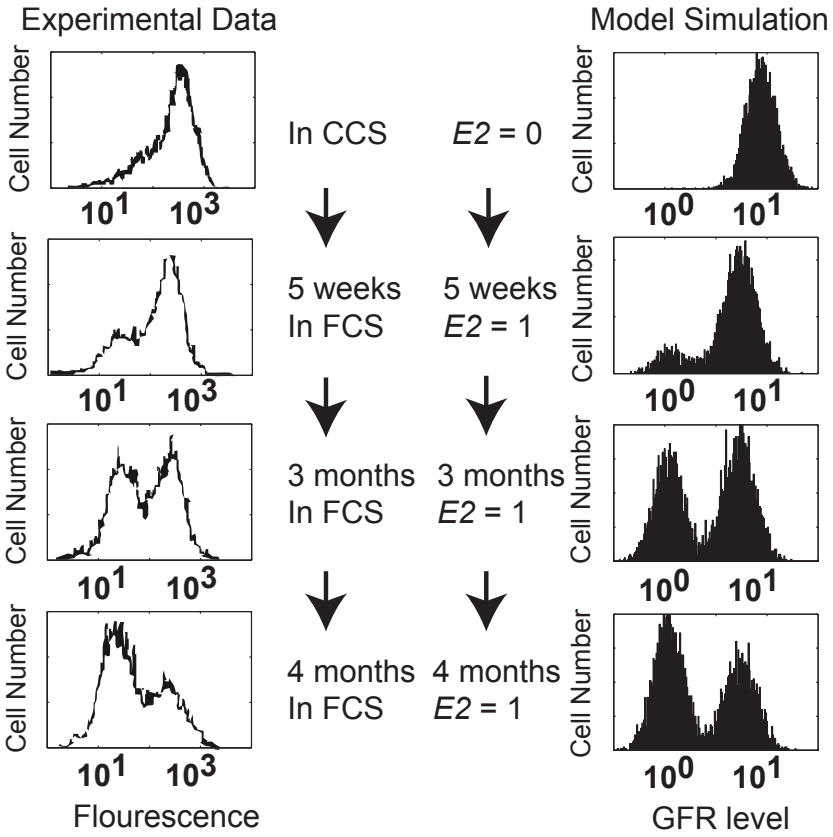

Figure 2.4 GFR bimodal distribution is reversibly controlled by different E2 levels. Left panel, experimental data adapted from [43]. The MB8 sub-clone of GFR-transfected MCF7 cells showing a bimodal HER2 distribution was treated with a series of E2 conditions: CCS, without E2, for 5 weeks; FCS, with E2, for 5 weeks, 3 months and 4 months. Right panel, model simulations, showing the distribution of GFR level in 5000 GFR-transfected MCF7 cells (*GFRover* = 5) under the same conditions as the experiments. GFR level = 10^{GFR} in these histograms.

2.4.4 Role of ER overexpression

A recent study observed that ER overexpression in MCF7 cells activates the ER-regulated genes pS2 and PR in the absence of E2 [42]. Prolonged culturing of these cells leads to proliferation in E2-depleted conditions. However, this proliferation can still be inhibited by faslodex (a pure ER antagonist), indicating the role of E2-independent ER-P activation in maintaining cell proliferation. By contrast, long term culturing of wild type MCF7 cells in the absence of E2 failed to cause resumed cell growth. More interesting, the overexpression of ER by adenovirus gene transfection in their study was only transient, as evidenced by the complete loss of co-transfected GFP protein after culturing the cells for 12 weeks.

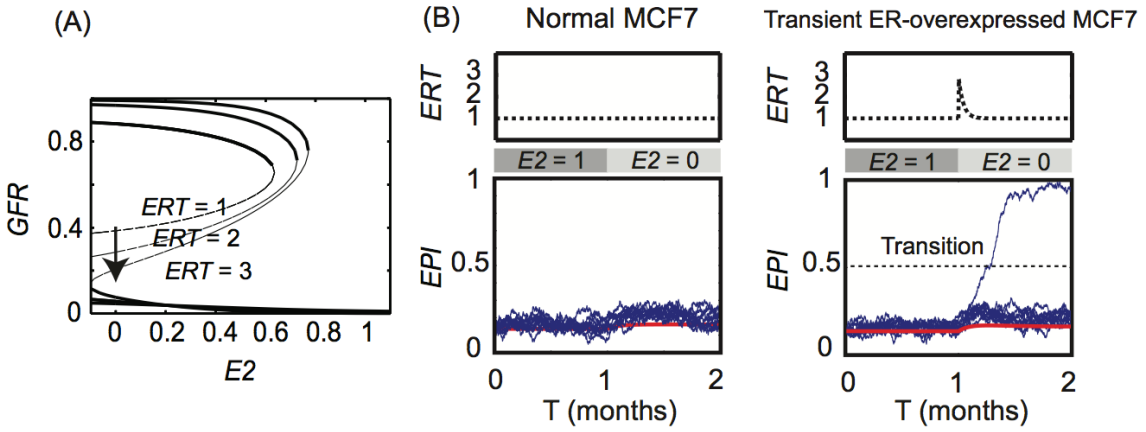

Figure 2.5 ER overexpression increases the probability of a survival-signaling switch. (**A**) Bifurcation diagram of *GFR* with *E2* as bifurcation parameter at different ER levels (*ERT* = 1, 2 and 3). (**B**) Transient ER overexpression opens a time window for transitions frm low to high GFR levels. Left panel, normal MCF7 cells show no transitions in stochastic simulations of 10000 cells (20 cells are plotted for illustration). Right panel, 80 transitions are observed within a short time window during transient ER overexpression in MCF7 cells (20 cells and one example of a transition are plotted for illustration). The pulse of ER overexpression is simulated by Eq. (1) in the manuscript. Red line, trace of a deterministic simulation; blue lines, traces of 20 stochastic simulations; the horizontal dotted line shows the threshold we set to score transitions (*EPI* = 0.5).

To understand these experimental results using our model, we first evaluated the role of ER overexpression. Figure 2.5A shows bifurcation diagrams of GFR level, with *E2* as the bifurcation parameter, at different ER levels (*ERT* = 1, 2 and 3). This figure shows that increasing ER levels decrease the barrier for cells to switch from the GFR–/ERP–/EPI– state to the GFR+/ERP+/EPI+ state when E2 is deprived. Consequently, a transient increase of ER will also result in a transient decrease of the barrier, opening a temporary window to an increased probability of state transitions under noise. To demonstrate this outcome, we stochastically simulated a population of 10,000 cells and evaluated how transient ER overexpression influences the frequency of transitions in E2-depleted MCF7 cells. No transition was observed during one month of E2 depletion in normal MCF7 cells (*ERT* = 1, Fig. 2.5B, left panel). However, in MCF7 cells with transiently over-expressed ER there were 80 transitions during a similar time window (Fig. 2.5B, right panel). Cells that transition will have high levels of GFR, EPI, and ER, implying the capability of E2-independent cell growth. The number of transitions is influenced by the strength of the *ERT* pulse, which was simulated with the following equation:

$$ERT = ER_0 + ERover \cdot e^{-t \cdot \frac{\ln 2}{T_{1/2}}} \tag{2.1}$$

where ER_0 = 1, $ERover$ = 1.8, $T_{1/2}$ = 0.25 month, t starts from the time of ER overexpression.

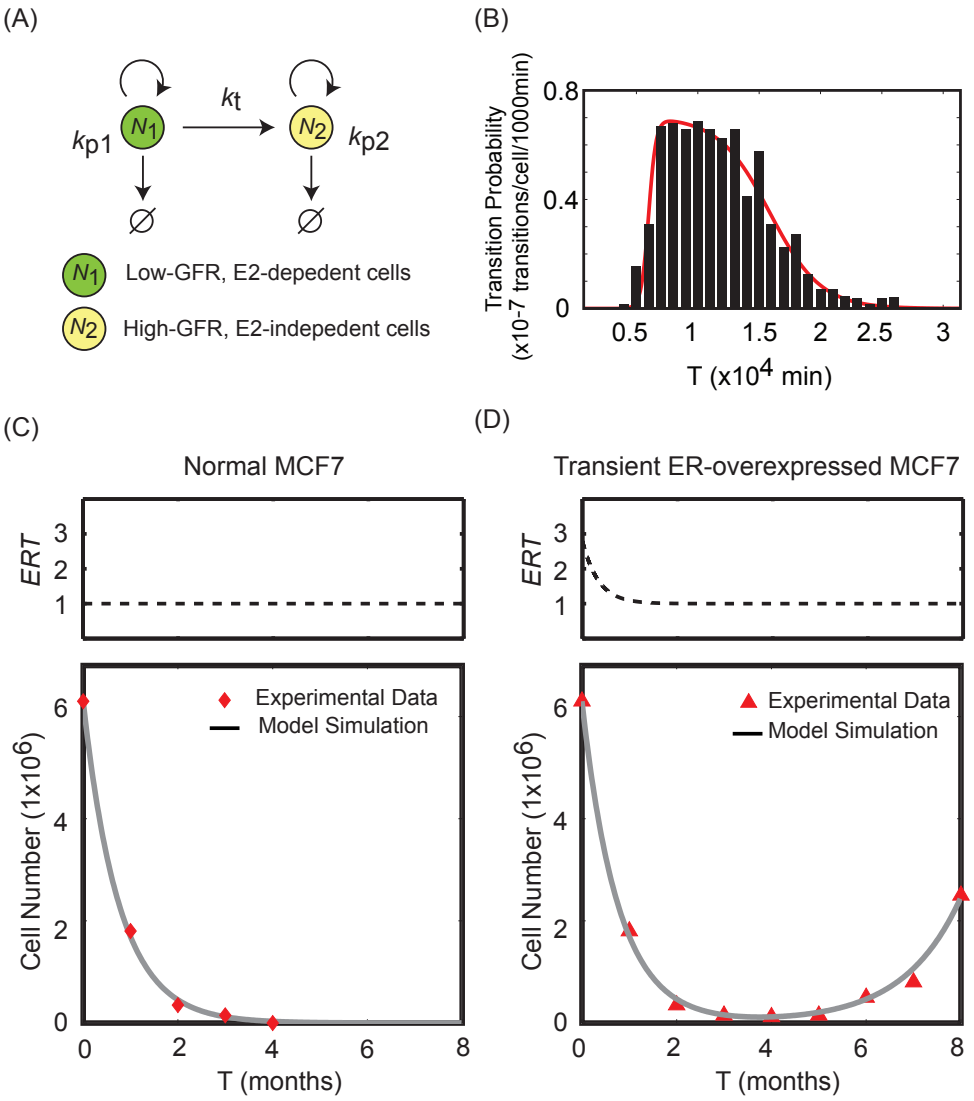

Figure 2.6 A population growth model shows the effects of transient ER overexpression. (**A**) Schematic representation of the population growth model. k_{p1}, k_{p2} = (specific birth rate – specific death rate) for cell populations N_1 and N_2, respectively. k_t = rate at which low-GFR cells switch to high-GFR cells. (**B**) Transition probability of MCF7 cells that transiently overexpress ER according to the survival-signaling switch model described in Fig. 2.5. Black bars, percentages of cells having transitions in given time intervals (1000 min); Red line, fitted curve showing how k_t varies with time in ER-overexpressed MCF7 cells. (**C**) Experimental data (red diamonds) and simulation results

(grey line) for the dynamics of total cell number in normal MCF7 cells after E2 depletion. (**D**) Experimental data (red triangles) and simulation results (grey line) for the dynamics of total cell number in transient ER-overexpressed MCF7 cells after E2 depletion. The pulse of ER overexpression is simulated by Eq. (2.1). Experimental data are adapted from [42].

To capture the experimental proliferation data in E2-depleted conditions, we created a simple population growth model (Fig. 2.6A) given by the equations:

$$\frac{dN_1}{dt} = k_{p1} \cdot N_1 - k_t \cdot N_1 \tag{2.2}$$

$$\frac{dN_2}{dt} = k_t \cdot N_1 + k_{p2} \cdot N_2 \tag{2.3}$$

In these equations, N_1 denotes the number of low-GFR, E2-dependent MCF7 cells and N_2 denotes the number of high-GFR, E2-independent MCF7 cells. The two cell types have different proliferation rates (k_{p1}, k_{p2}), and there is a transition rate, k_t, which describes how fast a low-GFR cell can switch to a high-GFR cell under E2-depleted conditions. Notice that $k_t = 0$ in normal MCF7 cells, since no transition is observed in Fig. 2.5B. Furthermore, k_t is not a constant in MCF7 cells with transient ER overexpression. To determine the dynamics of k_t we stochastically simulated a population of 6×10^6 cells with transiently overexpressed ER. The percentage of cells having transitions within independent time intervals is plotted in Fig. 2.6B (black bars), and the histogram was fit by a function of the form:

$$k_t(t) = \frac{1}{1+e^{-a\cdot(t-b)}} \cdot \frac{1}{1+e^{c\cdot(t-d)}} \cdot h \tag{2.4}$$

where fitting parameters a, b, c, d and h are all positive values. The red curve in Fig. 2.6B is the result of the fit and describes how k_t varies with time in MCF7 cells with the transient ER overexpression we consider. Using a standard curve fitting method (Matlab

Version 7.9.0, Curve Fitting Toolbox), we determined the best fitting parameter values to be $a = 3.322\times10^{-3}$, $b = 6\times10^{3}$, $c = 4.802\times10^{-4}$, $d = 1.587\times10^{4}$ and $h = 7.029\times10^{-8}$.

Choosing the parameters $ERover = 1.8$, $k_{p1} = -3\times10^{-5}$, and $k_{p2} = 2\times10^{-5}$, our simulation results for total cell number ($N_1 + N_2$) in Fig. 2.6 C-D match the experimental results (red diamonds and triangles) for both the normal and ER-overexpressed cells. Thus, by combining models at two different scales (molecular and population), we provide a plausible explanation for how transient ER overexpression can promote E2-independent growth in MCF7 breast cancer cells.

2.5 Discussion

Breast cancer is the most common invasive cancer in women. Endocrine therapy, as the most successful targeted cancer therapy, has been very effective in reducing breast cancer mortality. However, resistance often develops and the recurrence rate of breast cancer after targeted therapies remains unacceptably high. The molecular mechanisms of acquired endocrine resistance have been intensively studied both *in vivo* and in breast cancer cell lines, such as ER+ MCF7 cells. Many genes have been postulated as key players in acquired endocrine resistance [5, 20, 22, 39], but despite knowledge of their roles in cell survival and growth, little is known about how the 'escape' paths are mechanistically activated, dynamically regulated, and epigenetically maintained during the development of endocrine resistance. Understanding the molecular mechanisms used

by breast cancer cells to acquire resistance to endocrine treatment is critical for designing new therapies for breast cancer.

Emergence of resistance is closely associated with cellular heterogeneity. It has been widely recognized that breast cancer cells, including the well-studied MCF7 cells, are inherently heterogeneous. Distinct cell phenotypes in the same MCF7 cell population can be observed. Upon treatment, individual MCF7 cells can have diverse responses: while some cells die through apoptosis, others remain alive [23]. MCF7 cells also exhibit heterogeneous expression of a few key proteins. For example, although the MCF7 cell line is generally classified as ER+, a minority of these cells express low levels of ER [46]. The bimodal experimental data considered in the present work also supports the heterogeneity of cancer cells [43, 44].

What is the source of this heterogeneity? A population comprised of cancer cells with distinct phenotypes is usually attributed to mutations resulting from the genomic instability of cancer cells. However, this emphasis on genetic causes for heterogeneity has been challenged, as summarized by Huang et al. [47]. Recent studies indicate that viability within a population of cancer cells can also result from noisy gene expression and the fact that gene networks have multiple stable states, providing a non-genetic source of heterogeneity [47]. The presence of cancer stem cells (CSCs) in breast cancer strongly supports a non-genetic basis for tumor heterogeneity. There should be no genetic difference between CSCs and differentiated 'bulk' cells unless they acquire new mutations. CSCs, unlike bulk cells, are usually ER– and dependent on the GFR pathway to survive [48, 49]. For example, evidence shows that NFκB inhibitors can preferentially inhibit CSCs in MCF7 cells, but not MCF7 bulk cells [50]. Moreover, CSCs have the

potential to develop into bulk cells, and *vice versa*. These reversible transitions between stem cells and bulk cells are implicated in the well-documented cellular mesenchymal-epithelial transition and epithelial-mesenchymal transition. During either of these transitions, cells are reported to have an increased or decreased 'stemness' associated with changes in expression of specific stem cell surface markers [37].

In this work, a mathematical model based on a bistable switch with an epigenetic component successfully explains five intriguing experimental observations in MCF7 cells [42-44] (Fig. 2.7-10). (1) The bifurcation analysis in Fig. 2.2A shows that GFR-transfected MCF-7 cells have three distinct possibilities for GFR expression (low, both low and high, and high) depending on the number of GFR copies that were transfected, explaining why different experimental subclones exhibited these three different GFR profiles. (2) For a subclone with a bimodal GFR expression, the model analysis in Fig. 2.3B shows that E2 deprivation will force the cells into a high GFR state, as the low GFR state disappears, and re-adding E2 will return the cells to the bimodal state, in accord with experiment, Fig. 2.4. (3) Figure 2.3B also shows why the transition of a bimodal subclone to a high GFR state upon E2 deprivation is fast, as there is only one stable state and no barrier to cross to get there, while reversing the transition by re-adding E2 is slow, as cells must transition across a barrier to regain the low GFR state. (4) For non-transfected MCF-7 cells, the model analysis in Fig. 2.3A shows that E2 deprivation will not result in a high GFR state, since there is a large barrier preventing state switching, even though such deprivation does result in a high GFR state for the bimodal subclones, Fig. 2.3B, as they have no barrier to cross. (5) The analysis in Fig. 2.5 shows that transient ER overexpression lowers the barrier to the high GFR state during a small time

window and allows a few E2-deprived MCF-7 cells to cross the barrier. This explains why a population of E2 deprived MCF-7 cells will die out, but a similar population with a transient ER overexpression will eventually regrow, Fig. 2.6.

It should be emphasized that the model we present here, because it is an abstract and simplified version of reality, has some limitations. While a bistable switch is not unexpected, due to the presence of positive feedback loops in the ER-GFR crosstalk network, further experiments are required to confirm the exact mechanism. In particular, we emphasize epigenetic regulation of GFR promoters (EPI) in our current model, creating an epigenetic switch by assuming that EPI controls and is being controlled by GFR. The reality could be more complicated, since cell differentiation and de-differentiation processes are closely linked with both ER and GFR pathways. MicroRNAs, epigenetic regulation, and inter-cellular communications are implicated in differentiation/de-differentiation processes [1, 37, 51]; however, much is unknown at present. Moreover, cell-signaling networks may have as many steady states as there are physiological states, each steady state being represented in a subpopulation of cells within a cell culture or tissue. The low-GFR, E2-dependent and the high-GFR, E2-independent states are just two examples of many states that are possible.

Notwithstanding these limitations, the model of a survival-signaling switch presented here helps to understand certain dynamic behaviors of breast cancer cells that are difficult to comprehend by intuitive reasoning alone. Refining this model by obtaining data from primary breast cancers, as opposed to cell lines, will increase its clinical relevance and could aid in the search for new strategies to overcome breast cancer resistance.

2.6 Acknowledgements

This work was supported in part by the US National Institutes of Health grant U54-CA149147 (to R.C., J.J.T. and W.T.B.), and by fellowships to C.C. provided by the Virginia Polytechnic Institute and State University graduate program in Genetics, Bioinformatics and Computational Biology.

2.7 References

1. Alberts, B., *Molecular biology of the cell*. 4th ed. 2002, New York: Garland Science. xxxiv, 1548 p.
2. Dickson, R.B. and M.E. Lippman, *Growth factors in breast cancer*. Endocr Rev, 1995. **16**(5): p. 559-89.
3. Rimawi, M.F. and C.K. Osborne, *BREAST CANCER Blocking both driver and escape pathways improves outcomes*. Nature Reviews: Clinical Oncology, 2012. **9**(3): p. 133-134.
4. Patani, N., L.A. Martin, and M. Dowsett, *Biomarkers for the clinical management of breast cancer: International perspective*. Int J Cancer, 2013. **133**(1): p. 1-13.
5. Musgrove, E.A. and R.L. Sutherland, *Biological determinants of endocrine resistance in breast cancer*. Nat Rev Cancer, 2009. **9**(9): p. 631-43.
6. Arteaga, C.L., et al., *Treatment of HER2-positive breast cancer: current status and future perspectives*. Nat Rev Clin Oncol, 2012. **9**(1): p. 16-32.

7. Clarke, R., et al., *Progression of human breast cancer cells from hormone-dependent to hormone-independent growth both in vitro and in vivo*. Proc Natl Acad Sci U S A, 1989. **86**(10): p. 3649-53.

8. Clarke, R., et al., *Hormonal carcinogenesis in breast cancer: cellular and molecular studies of malignant progression*. Breast Cancer Res Treat, 1994. **31**(2-3): p. 237-48.

9. Santen, R.J., et al., *Adaptive hypersensitivity to estrogen: mechanism for sequential responses to hormonal therapy in breast cancer*. Clin Cancer Res, 2004. **10**(1 Pt 2): p. 337S-45S.

10. Saji, S., F. Sato, and N.T. Ueno, *Fuel, electricity, ER and HER2--a hybrid-car model of breast cancer*. Nat Rev Clin Oncol, 2012. **9**(7).

11. Sainsbury, J.R., et al., *Epidermal-growth-factor receptors and oestrogen receptors in human breast cancer*. Lancet, 1985. **1**(8425): p. 364-6.

12. Clarke, R., et al., *Antiestrogen resistance in breast cancer and the role of estrogen receptor signaling*. Oncogene, 2003. **22**(47): p. 7316-39.

13. Nicholson, R.I., et al., *Growth factor signalling in endocrine and anti-growth factor resistant breast cancer*. Rev Endocr Metab Disord, 2007. **8**(3): p. 241-53.

14. Gee, J.M.W., et al., *Antihormone induced compensatory signalling in breast cancer: an adverse event in the development of endocrine resistance*. Hormone Molecular Biology and Clinical Investigation, 2011. **5**(2): p. 2.

15. Hiscox, S., J. Gee, and R.I. Nicholson, *Therapeutic resistance to anti-hormonal drugs in breast cancer : new molecular aspects and their potential as targets*. 2009, Dordrecht: Springer. xi, 198 p.

16. Bayliss, J., et al., *Reversal of the estrogen receptor negative phenotype in breast cancer and restoration of antiestrogen response*. Clin Cancer Res, 2007. **13**(23): p. 7029-36.

17. Xia, W., et al., *A model of acquired autoresistance to a potent ErbB2 tyrosine kinase inhibitor and a therapeutic strategy to prevent its onset in breast cancer*. Proc Natl Acad Sci U S A, 2006. **103**(20): p. 7795-800.

18. Curtis, C., et al., *The genomic and transcriptomic architecture of 2,000 breast tumours reveals novel subgroups*. Nature, 2012. **486**(7403): p. 346-52.

19. Koboldt, D.C., et al., *Comprehensive molecular portraits of human breast tumours*. Nature, 2012. **490**(7418): p. 61-70.

20. Osborne, C.K. and R. Schiff, *Mechanisms of endocrine resistance in breast cancer*. Annu Rev Med, 2011. **62**: p. 233-47.

21. Lannigan, D.A., *Estrogen receptor phosphorylation*. Steroids, 2003. **68**(1): p. 1-9.

22. Nicholson, R.I., et al., *Growth factor-driven mechanisms associated with resistance to estrogen deprivation in breast cancer: new opportunities for therapy*. Endocrine-Related Cancer, 2004. **11**(4): p. 623-641.

23. Pratt, M.A.C., et al., *Estrogen withdrawal-induced NF-kappa B activity and Bcl-3 expression in breast cancer cells: Roles in growth and hormone independence*. Molecular and Cellular Biology, 2003. **23**(19): p. 6887-6900.

24. Kalaitzidis, D. and T.D. Gilmore, *Transcription factor cross-talk: the estrogen receptor and NF-kappaB*. Trends Endocrinol Metab, 2005. **16**(2): p. 46-52.

25. Gionet, N., et al., *NF-kappaB and estrogen receptor alpha interactions: Differential function in estrogen receptor-negative and -positive hormone-independent breast cancer cells*. J Cell Biochem, 2009. **107**(3): p. 448-59.

26. Zhou, Y., et al., *The NFkappaB pathway and endocrine-resistant breast cancer*. Endocr Relat Cancer, 2005. **12 Suppl 1**: p. S37-46.

27. Bates, N.P. and H.C. Hurst, *An intron 1 enhancer element mediates oestrogen-induced suppression of ERBB2 expression*. Oncogene, 1997. **15**(4): p. 473-81.

28. Chrysogelos, S.A., et al., *Mechanisms of EGF receptor regulation in breast cancer cells*. Breast Cancer Res Treat, 1994. **31**(2-3): p. 227-36.

29. Hutcheson, I.R., et al., *Oestrogen receptor-mediated modulation of the EGFR/MAPK pathway in tamoxifen-resistant MCF-7 cells*. Breast Cancer Res Treat, 2003. **81**(1): p. 81-93.

30. Nicholson, R.I., et al., *Nonendocrine pathways and endocrine resistance: observations with antiestrogens and signal transduction inhibitors in combination*. Clin Cancer Res, 2004. **10**(1 Pt 2): p. 346S-54S.

31. Nicholson, R.I., et al., *Growth factor signalling and resistance to selective oestrogen receptor modulators and pure anti-oestrogens: the use of anti-growth factor therapies to treat or delay endocrine resistance in breast cancer*. Endocr Relat Cancer, 2005. **12 Suppl 1**: p. S29-36.

32. Zilli, M., et al., *Molecular mechanisms of endocrine resistance and their implication in the therapy of breast cancer*. Biochimica Et Biophysica Acta-Reviews on Cancer, 2009. **1795**(1): p. 62-81.

33. Biswas, D.K., et al., *Crossroads of estrogen receptor and NF-kappaB signaling*. Sci STKE, 2005. **2005**(288): p. pe27.

34. Shostak, K. and A. Chariot, *NF-kappaB, stem cells and breast cancer: the links get stronger*. Breast Cancer Res, 2011. **13**(4): p. 214.

35. Baud, V. and M. Karin, *Is NF-kappaB a good target for cancer therapy? Hopes and pitfalls*. Nat Rev Drug Discov, 2009. **8**(1): p. 33-40.

36. De Craene, B. and G. Berx, *Regulatory networks defining EMT during cancer initiation and progression*. Nat Rev Cancer, 2013. **13**(2): p. 97-110.

37. Singh, A. and J. Settleman, *EMT, cancer stem cells and drug resistance: an emerging axis of evil in the war on cancer*. Oncogene, 2010. **29**(34): p. 4741-51.

38. Mishra, S.K., et al., *Dynamic chromatin remodeling on the HER2 promoter in human breast cancer cells*. FEBS Lett, 2001. **507**(1): p. 88-94.

39. Massarweh, S. and R. Schiff, *Unraveling the mechanisms of endocrine resistance in breast cancer: new therapeutic opportunities*. Clin Cancer Res, 2007. **13**(7): p. 1950-4.

40. Gee, J.M.W., et al., *Deciphering antihormone-induced compensatory mechanisms in breast cancer and their therapeutic implications*. Endocrine-Related Cancer, 2006. **13**: p. S77-S88.

41. Tyson, J.J., et al., *Dynamic modelling of oestrogen signalling and cell fate in breast cancer cells*. Nat Rev Cancer, 2011. **11**(7): p. 523-32.

42. Tolhurst, R.S., et al., *Transient over-expression of estrogen receptor-alpha in breast cancer cells promotes cell survival and estrogen-independent growth*. Breast Cancer Res Treat, 2011. **128**(2): p. 357-68.

43. Liu, Y., et al., *MCF-7 breast cancer cells overexpressing transfected c-erbB-2 have an in vitro growth advantage in estrogen-depleted conditions and reduced estrogen-dependence and tamoxifen-sensitivity in vivo*. Breast Cancer Res Treat, 1995. **34**(2): p. 97-117.

44. Miller, D.L., et al., *Emergence of MCF-7 cells overexpressing a transfected epidermal growth factor receptor (EGFR) under estrogen-depleted conditions: evidence for a role of EGFR in breast cancer growth and progression*. Cell Growth Differ, 1994. **5**(12): p. 1263-74.

45. Tyson, J.J. and B. Novak, *Functional motifs in biochemical reaction networks*. Annu Rev Phys Chem, 2010. **61**: p. 219-40.

46. Palmari, J., et al., *Distribution of estrogen receptor heterogeneity in growing MCF-7 cells measured by quantitative microscopy*. Cytometry, 1997. **27**(1): p. 26-35.

47. Brock, A., H. Chang, and S. Huang, *OPINION Non-genetic heterogeneity - a mutation-independent driving force for the somatic evolution of tumours*. Nature Reviews: Genetics, 2009. **10**(5): p. 336-342.

48. O'Brien, C.S., et al., *Resistance to Endocrine Therapy in Breast Cancer: Are It Breast Cancer Stem Cells Implicated?* Cancer Stem Cells in Solid Tumors, 2011: p. 381-402.

49. Shipitsin, M., et al., *Molecular definition of breast tumor heterogeneity*. Cancer Cell, 2007. **11**(3): p. 259-273.

50. Zhou, J., et al., *NF-kappaB pathway inhibitors preferentially inhibit breast cancer stem-like cells*. Breast Cancer Res Treat, 2008. **111**(3): p. 419-27.

51. Melo, S.A. and M. Esteller, *Dysregulation of microRNAs in cancer: playing with fire*. FEBS Lett, 2011. **585**(13): p. 2087-99.

2.8 Supporting materials

Modeling the estrogen receptor to growth factor receptor signaling switch in human breast cancer cells

Chun Chen[‖], William T. Baumann[‡], Robert Clarke[§], John J. Tyson*

*Department of Biological Sciences, [‡]Department of Electrical & Computer Engineering, and [‖]Graduate Program in Genetics, Bioinformatics and Computational Biology, Virginia Polytechnic Institute & State University, Blacksburg VA 24061, USA

[§]Lombardi Comprehensive Cancer Center, Georgetown University School of Medicine, Washington DC 20057, USA

* Corresponding author. Fax: +1 540 231 9307.

E-mail address: tyson@vt.edu.

2.8.1 Schematic illustrations of the experimental observations

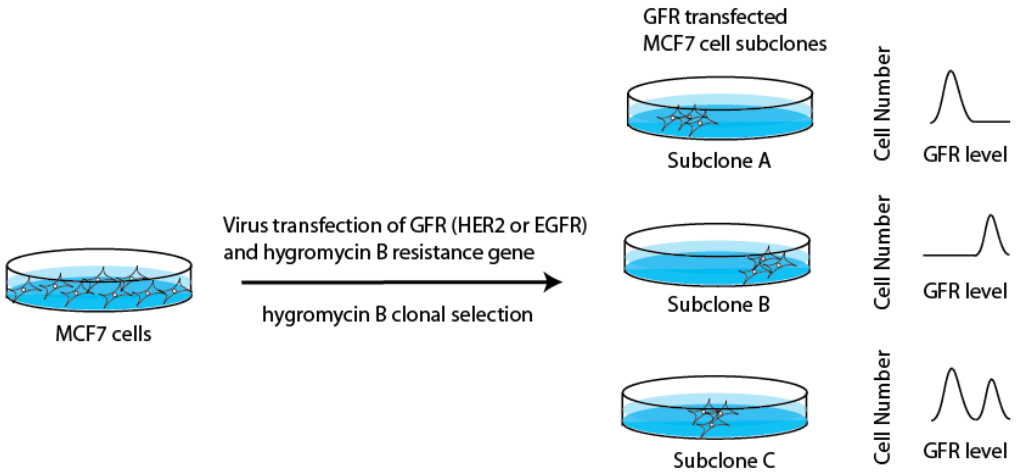

Figure 2.7 Three different distribution patterns of GFR in sub-clones of MCF7 cells transfected with GFR (HER2 or EGFR) [1, 2].

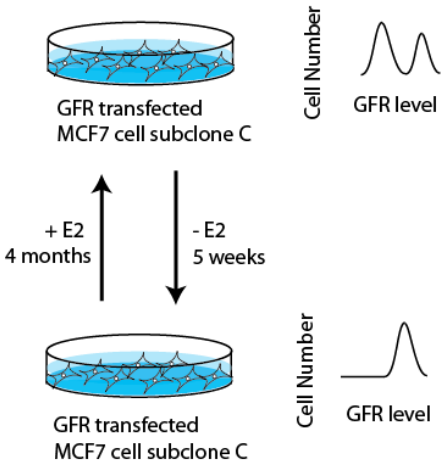

Figure 2.8 E2 reversibly modifies the bimodal distribution of GFR in a GFR-transfected MCF7 subclone [1, 2]. E2 withdrawal switches on GFR expression within weeks, whereas E2 addition takes months to switch off GFR expression [1, 2].

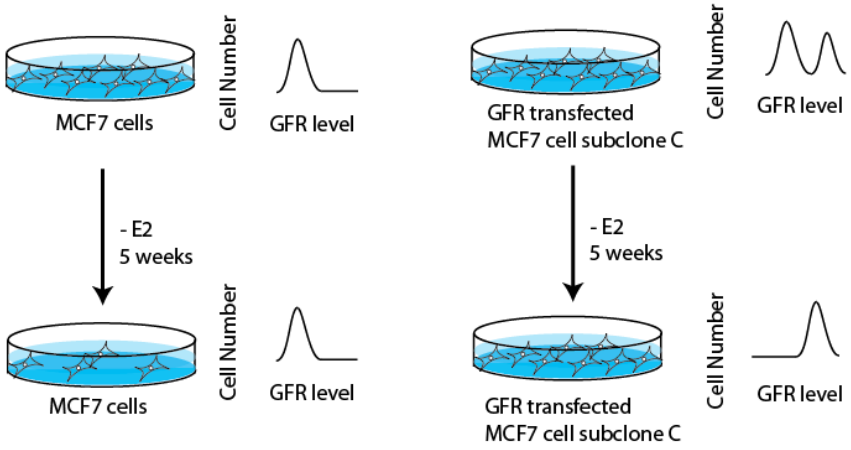

Figure 2.9 E2 withdrawal can up-regulate GFR expression within 5 weeks in GFR-transfected MCF7 cells, but fails to do so in wild type MCF7 cells [1, 2]**.**

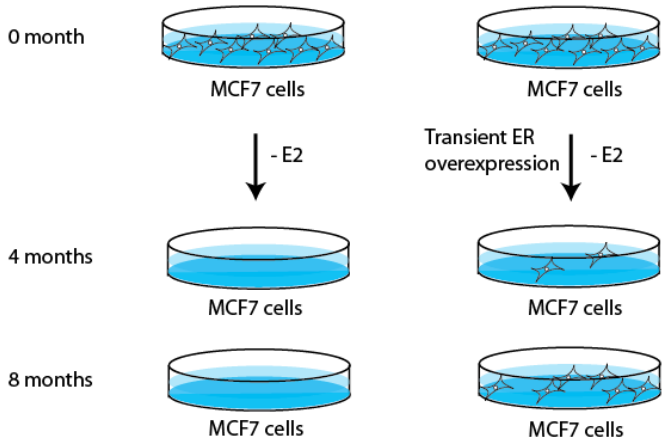

Figure 2.10 Transient ER overexpression in MCF7 cells can switch on the GFR pathway and promote E2-independent growth [3].

2.8.2 Full Materials and Methods

2.8.2.1 Model Implementation

We postulate a highly condensed model of the interaction between ER and GFR (Fig. 2.1A in manuscript). The protein level of GFR is down-regulated by E2:ER complex. After E2 withdrawal, GFR expression is released from inhibition, and its downstream kinases activate E2-independent ER-P. ER-P can activate and stabilize the GFR pathway, creating a positive feedback loop. In addition, GFR further activates transcription factors such as NFκB, promoting a series of epigenetic changes contributing to increased GFR expression and establishing another positive feedback loop. For simplicity, we combine the epigenetic factors contributing to GFR expression into the quantity 'EPI'. 'E2ER' and 'ERP' are used to represent E2:ER and ER-P.

The wiring diagram in Fig. 2.1A was translated into ordinary differential equations (ODEs) to enable simulation and analysis. In these equations, the levels of GFR, EPI, E2ER and ERP are represented by italicized variables: *GFR*, *EPI*, *E2ER* and *ERP*. The rates of change for *E2ER* and *ERP* are considered fast compared to the rates for *GFR* and *EPI*, so for simplicity only *GFR* and *EPI* are described by differential equations. E2ER and ERP are assumed to be proportional to *ERT,* a parameter we use to vary the total level of ER in the cell. Note that E2-binding and phosphorylation of ER are not necessarily mutually exclusive. Moreover, we assume that *GFR* and *EPI* have a dynamical range of about 10-fold, so on a log10 scale they vary between 0 and 1. Since our model is phenomenological in nature, we do not use standard reaction rate equations.

Rather, we apply a formalism that allows us to capture complex dependencies in a simple manner [4]. The model equations are:

$$\frac{dEPI}{dt} = \gamma_{\mathrm{EPI}} \cdot \left(H\left(W_{\mathrm{EPI}}\right) - EPI \right) \tag{2.S1}$$

$$\frac{dGFR}{dt} = \gamma_{\mathrm{GFR}} \cdot \left(H\left(W_{\mathrm{GFR}}\right) - GFR \right) \tag{2.S2}$$

$$E2ER = H\left(W_{\mathrm{E2ER}}\right) \cdot ERT \tag{2.S3}$$

$$ERP = H\left(W_{\mathrm{ERP}}\right) \cdot ERT \tag{2.S4}$$

where

$$H(W) = \frac{1}{1 + e^{-W}} \tag{2.S5}$$

$$W_{\mathrm{EPI}} = \omega_{\mathrm{EPI}} + \omega_{\mathrm{EPI,GFR}} \cdot GFR \tag{2.S6}$$

$$W_{\mathrm{GFR}} = \omega_{\mathrm{GFR}} + \omega_{\mathrm{GFR,EPI}} \cdot EPI + \omega_{\mathrm{GFR,E2ER}} \cdot E2ER + \omega_{\mathrm{GFR,ERP}} \cdot ERP + \omega_{\mathrm{GFR,GFRover}} \cdot GFRover \tag{2.S7}$$

$$W_{\mathrm{E2ER}} = \omega_{\mathrm{E2ER}} + \omega_{\mathrm{E2ER,E2}} \cdot E2 \tag{2.S8}$$

$$W_{\mathrm{ERP}} = \omega_{\mathrm{ERP}} + \omega_{\mathrm{ERP,GFR}} \cdot GFR \tag{2.S9}$$

The parameters γ_{EPI} and γ_{GFR} determine the rate at which *EPI* and *GFR* approach their steady state values. $H(W)$ is a sigmoidal function. W_i is the net activation or inhibition of species i (i = EPI, GFR, E2ER and ERP), and ω_i determines whether species i is 'on' or 'off' when there is no other factor regulating i. $\omega_{i,j}$ indicates the influence of species or stimulus j (j = EPI, GFR, E2ER, ERP, GFRover, E2) on species i. A description of the

variables used in our model is given in Table 2.1. The parameter values, listed in Table 2.2, were obtained by manually choosing values to fit the experimental observations. Initially, the parameters for the deterministic part of the model where chosen to obtain a bifurcation diagram as a function of *GFRover* that exhibited three distinct patterns of expression and simultaneously a bifurcation diagram as a function of *E2* that allowed GFRs to switch on when E2 was withdrawn. Then the noise parameters where chosen to capture the experimentally observed timing of the on and off transitions of GFR. The noise and deterministic parameters are not independent and so ultimately all the parameters were adjusted in concert to match the experiments. Since we are modeling this system at a high level of abstraction, none of our parameters are directly related to measurable physical rate constants of the system, but rather are phenomenological parameters that match the phenotypic performance of the system. We used the program XPP-AUT, available freely at http://www.math.pitt.edu/~bard/xpp/xpp.html, to simulate the model and draw bifurcation diagrams.

Table 2.1 Model variables and their descriptions.

Variables	Range	Description
EPI	[0,1]	Epigenetic factors contributing to GFR expression
GFR	[0,1]	GFR expression level
E2ER	[0, *ERT*]	E2-dependent E2:ER activity
ERP	[0, *ERT*]	E2-independent ER-P activity

Table 2.2 Model parameters, descriptions, and numerical values.

Parameters	Description	Value
γ_{EPI}	Rate of EPI reaching its steady state	3×10^{-4} min^{-1}
γ_{GFR}	Rate of GFR reaching its steady state	5×10^{-2} min^{-1}
ω_{EPI}	Basal inhibition of EPI	–1.92
ω_{GFR}	Basal inhibition of GFR	–4
ω_{E2ER}	Basal inhibition of E2ER	–2.1
ω_{ERP}	Basal inhibition of ERP	–1.5
$\omega_{EPI,GFR}$	EPI activation by GFR	6
$\omega_{GFR,EPI}$	GFR activation by EPI	5
$\omega_{GFR,E2ER}$	GFR inhibition by E2ER	–2
$\omega_{GFR,ERP}$	GFR activation by ERP	1.85
$\omega_{GFR,GFRover}$	GFR activation by GFRover	0.15
$\omega_{E2ER,E2}$	E2ER activation by E2	3
$\omega_{ERP,GFR}$	GFR activation by ERP	3
E2	E2 level	1 (normal); 0 (E2-depleted)
ERT	Total ER level	1 (normal); >1 (ER-overexpressed)
GFRover	Excess GFR in transfected cells	0 (normal); >0 (GFR-transfected)

2.8.2.2 Stochastic simulation

To account for stochastic effects in the model, noise terms are added to the differential equations for *EPI* and *GFR*, while the algebraic equations are left unchanged, for simplicity. The Langevin equation for variables i (i = *EPI* or *GFR*) takes the form:

$$\frac{di}{dt} = \gamma_i \cdot (s_i - i) + F_i(t) \tag{2.S10}$$

where s_i defines the steady state level of i and $F_i(t)$ is a Gaussian white noise process. The equilibrium second moment of the variable i, $<(s_i - i)^2>_{eq} = \theta_i$, is related to γ_i and the second moment of the noise by a fluctuation-dissipation theorem [5, 6]:

$$< F_i(t) F_i(t') >_{eq} = 2 \cdot \gamma_i \cdot \theta_i \cdot \delta(t - t') \tag{2.S11}$$

We choose a suitable value for θ_i and rewrite Eq. 2.S10 as:

$$\frac{di}{dt} = \gamma_i \cdot (s_i - i) + \sqrt{2 \cdot \gamma_i \cdot \theta_i} \cdot \zeta_i(t) \tag{2.S12}$$

where $\zeta_i(t)$ is a temporally uncorrelated, statistically independent, Gaussian white noise process formally defined by $\zeta_i(t) \equiv \lim_{dt \to 0} N(0, 1/dt)$ with $< \zeta_i(t) \zeta_i(t') >= \delta(t - t')$.

The Langevin equations are integrated and propagated by the explicit method:

$$i(t + \Delta t) = i(t) + \gamma_i \cdot (s_i - i) \cdot \Delta t + \sqrt{2 \cdot \gamma_i \cdot \theta_i \cdot \Delta t} \cdot \eta_i(t) \tag{2.S13}$$

where the $\eta_i(t)$ are independent normal random variables. We used $\theta_{EPI} = 0.0008$ and $\theta_{GFR} = 0.01$ to fit the experimental data. The stochastic simulations were performed in Matlab Version 7.9.0.

2.8.3 References of supporting materials

1. Liu, Y., et al., *MCF-7 breast cancer cells overexpressing transfected c-erbB-2 have an in vitro growth advantage in estrogen-depleted conditions and reduced estrogen-dependence and tamoxifen-sensitivity in vivo*. Breast Cancer Res Treat, 1995. **34**(2): p. 97-117.
2. Miller, D.L., et al., *Emergence of MCF-7 cells overexpressing a transfected epidermal growth factor receptor (EGFR) under estrogen-depleted conditions: evidence for a role of EGFR in breast cancer growth and progression*. Cell Growth Differ, 1994. **5**(12): p. 1263-74.
3. Tolhurst, R.S., et al., *Transient over-expression of estrogen receptor-alpha in breast cancer cells promotes cell survival and estrogen-independent growth*. Breast Cancer Res Treat, 2011. **128**(2): p. 357-68.
4. Tyson, J.J. and B. Novak, *Functional motifs in biochemical reaction networks*. Annu Rev Phys Chem, 2010. **61**: p. 219-40.
5. Kubo, R., *The fluctuation-dissipation theorem*. Reports on Progress in Physics, 1966. **29**: p. 30.
6. Zwanzig, R., *Dynamic Disorder - Passage through a Fluctuating Bottleneck*. Journal of Chemical Physics, 1992. **97**(5): p. 3587-3589.

Chapter 3. Transitions between endocrine therapy response and resistance on the breast cancer landscape

Chun Chen[1], William T. Baumann[2], Jianhua Xing[3], Lingling Xu[4], Robert Clarke[5], John J. Tyson[3*]

[1]Graduate Program in Genetics, Bioinformatics and Computational Biology, [2]Department of Electrical & Computer Engineering, [3]Department of Biological Sciences, and [4]Department of Physics, Virginia Polytechnic Institute & State University, Blacksburg VA 24061, USA

[5]Lombardi Comprehensive Cancer Center, Georgetown University School of Medicine, Washington DC 20057, USA

[*] Corresponding author. Fax: +1 540 231 9307.

E-mail address: tyson@vt.edu.

3.1 Abstract

Endocrine therapy, targeting the estrogen receptor pathway, is the most common adjuvant treatment for estrogen receptor-positive breast cancer. Unfortunately, breast cancers frequently develop resistance to these therapies. Two intuitive strategies have been employed to fight acquired endocrine resistance: sequential treatment, in which second-

line endocrine drugs are used to gain additional responses, and intermittent treatment, in which a 'drug holiday' is imposed between endocrine treatments. To gain a more rigorous understanding of the molecular mechanisms underlying these strategies, we present a mathematical model that captures the transitions among three different, experimentally observed, estrogen-sensitivity phenotypes in breast cancer (sensitive, hypersensitive, and supersensitive). To provide a global view of the transitions between these phenotypes, we compute the potential landscape associated with the model. We show how this breast cancer landscape can be reshaped by population selection, which is a crucial force in promoting acquired resistance. In addition, a simplified state-transition model was computed from our molecular signaling-based model to investigate the population-scale effects of both sequential and intermittent treatment protocols for breast cancer and to enable the optimization of protocol parameters. The approach used in this study can be generalized to investigate treatment strategies and to improve treatment efficiencies for other types of cancer as well.

Keywords: Breast Cancer, Endocrine Resistance, Potential Landscape, Sequential Treatment, and Intermittent Treatment.

Running title: Modeling the breast cancer landscape

3.2 Introduction

Breast cancer remains one of the most common cancers in women. Approximately 70% of breast cancers express estrogen receptor-α (ERα), which is a major driver of survival and proliferation in breast cancer cells [1]. Endocrine therapies, targeting the ERα pathway, have become routine and effective treatments for breast cancer [2]. Three types of endocrine therapy are commonly used: 1) aromatase inhibitors (AIs), to deprive cells of estrogen (E2), the ligand of ERα, by reducing E2 biosynthesis, (2) selective estrogen receptor modulators (SERMs, e.g., tamoxifen), to inhibit ERα binding with E2, and (3) selective estrogen receptor down-regulators (SERDs, e.g., faslodex), to reduce ERα expression. Despite their success in reducing the annual death rate from breast cancer by one-third over the past decades, resistance to endocrine therapies often develops, creating a fundamental problem in breast cancer treatment [2].

Pre-clinical and clinical observations suggest that breast cancer with acquired resistance may respond to second-line or third-line endocrine treatment (Fig. 3.1A). For example, growth of breast cancer with acquired resistance to tamoxifen can be inhibited by AIs, which provide a more pronounced deprivation of E2 [3]. An AI-resistant patient can still benefit from faslodex, which destabilizes ERα [3]. However, AIs or faslodex are not more effective than tamoxifen as a first-line therapy. And AI-resistant breast cancers are usually cross-resistant to tamoxifen, whereas faslodex-resistant breast cancers are cross-resistant to both AIs and tamoxifen [3]. Thus, consecutive treatment with different anti-estrogens has been widely studied in clinical trials in order to maximize the response window for breast cancer patients [4]. The development of resistance to endocrine

therapy has long been recognized as a progressive, step-wise phenomenon where cancer cells can gradually shift from an estrogen-dependent, responsive phenotype to a less-responsive phenotype, and ultimately to an estrogen-independent phenotype [3].

Giving breast cancer patients a 'drug holiday' is a well-accepted strategy to deal with acquired endocrine resistance [5-7] (Fig. 3.1A). Breast cancers that have become resistant to tamoxifen may give a second or third response when re-challenged by the drug [5]. Similarly, faslodex withdrawal is reported to partially reverse acquired faslodex-resistant phenotype in breast cancer [6]. The duration of treatment and the interval between treatments appear to be critical parameters for the effectiveness of intermittent treatment. However, a rigorous understanding of how breast cancer patients can benefit from intermittent treatment is still lacking, preventing us from optimizing treatment strategies. Optimization of sequential treatment faces a similar problem [8].

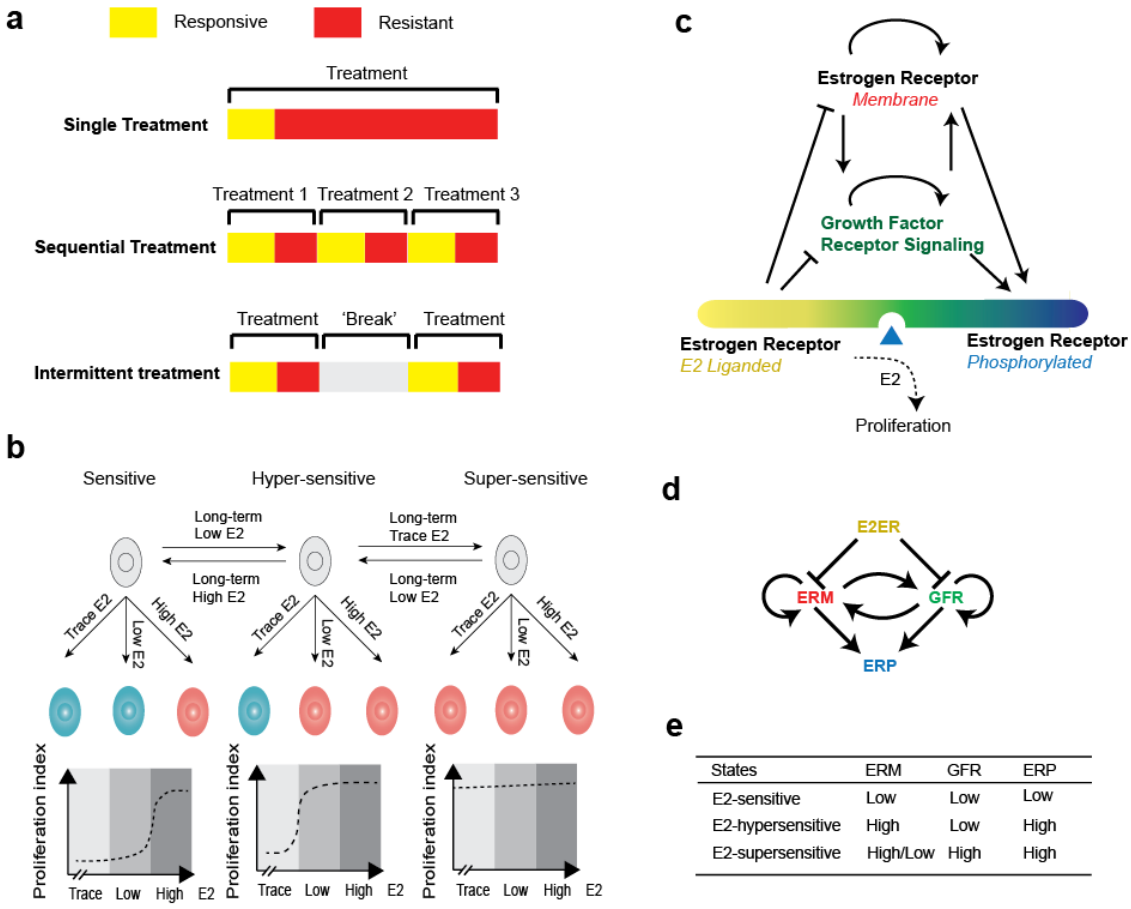

Figure 3.1 Breast cancer shifts between endocrine responsive and resistant states. (**A**) Schematic summary of the consequences of single, sequential, and intermittent endocrine treatments in breast cancer. Yellow denotes responsive, red resistant, and gray the treatment-withdrawn states. (**B**) Schematic illustration of the transitions between different E2 sensitivity phenotypes in breast cancer. Left, E2-sensitive state; middle, E2-hypersensitive state; right, E2-supersensitive state. Blue cells in the middle panel indicate a low proliferation index, while red cells indicate a high proliferation index. The bottom panel shows the dose-response curves of the proliferation index to E2 levels (from TRACE to LOW to HIGH) for the corresponding E2 sensitivity states. The transitions are reversible when the conditions on the arrows are applied. (**C**) The three activation modes

of ERα and their crosstalk with GFR signaling. Barbed arrows, activation; blunt arrows, inhibition. (**D**) Wiring diagram based on panel C. E2ER, E2-liganded ERα; ERM, membrane ERα; ERP, phosphorylated ERα; GFR, growth factor receptors. (**E**) The levels of ERM, GFR and ERP for the three different E2 sensitivity states, as summarized in [3, 9].

The aim of this study is to build a mathematical model to account for the different estrogen- responsiveness phenotypes observed in breast cancer cells and to use this model to explore the transitions between endocrine responsiveness to endocrine resistance under sequential and intermittent treatment. It is widely reported that there are three phenotypes (states) of breast cancer cells related to E2 sensitivity [3, 9] (Fig. 3.1B). Both clinical observations [10] and cell line studies [11] suggest that breast cancer cells, which are E2 sensitive initially (Fig. 3.1B, left), can adapt to E2 deprivation by entering an E2 hypersensitive state, for which the non-physiologically low concentration of E2 remaining after E2 withdrawal is sufficient to support cell proliferation (Fig. 3.1B, middle). Prolonged and profound E2 deprivation can lead to an E2-independent (or E2-supersensitive) state [3, 9] (Fig. 3.1B, right). Not all cells make the state transitions necessary for proliferation. Rather, the progression described above represents somatic evolution, whereby cells that switch to the hypersensitive or supersensitive states outgrow their disadvantaged peers. The diversity of cell phenotypes that is necessary for somatic evolution can be caused by genomic and/or non-genomic heterogeneity [12]. The dominant role of non-genomic heterogeneity assumed in our study is supported by experiments that demonstrate the reversibility of hypersensitive and supersensitive phenotypes in breast cancer cells during two years of E2 manipulation [13]. From a dynamical perspective, these experiments suggest the existence of at least three stable steady states, corresponding to the different E2-sensitivity states, and the tendency of the cell-fate control system to flip from one steady state to another and back again.

In physics, an intuitively appealing way to visualize the dynamics of a system is to view the system as a particle moving on a surface defined by a ‘potential energy’. In two

dimensions, this surface can be plotted as a landscape where the particle moves downhill and falls into basins. When the landscape contains multiple basins of attraction, there are multiple stable states where the particle can remain indefinitely. If the system is subject to random external forces, it is possible for the system to be kicked from one basin of attraction to another. Inspired by this idea, C. Waddington proposed in the 1940s to describe cell fate decisions by the dynamics of a control system on an 'epigenetic landscape' [14]. The basins of attraction were (in Waddington's view) stable cell fates, and the paths that cells take across the landscape corresponded to the differentiation events of cells in a developing organism. In recent years, the ability to compute a potential landscape from an underlying mathematical model has been used to visualize a variety of cell fate decisions [15-21]. While the imagery of Waddington's landscape has been used to discuss the fate of cancer cells during the development of resistance to therapy [17, 20], little has been done to quantitatively map this landscape from a mathematical model of the underlying signaling network of cancer cells.

In this study we first construct a cellular-level model, based on experimental evidence, that accounts for the three E2 sensitivity states observed in breast cancer cells. By computing the potential landscape associated with this model, which we refer to as the breast cancer landscape, we provide a visual picture of how breast cancer cells change phenotypes in response to variations in protein expression (noise) and varying environmental conditions (therapy). We also evaluate the effects of population selection in reshaping the breast cancer landscape. In addition, we use the minimum action path (MAP) between basins (attractors) on the breast cancer landscape to estimate the transition probabilities in a simple state-transition model [18, 22]. Based on this state-

transition model, we investigate the population dynamics of breast cancer cells under both sequential and intermittent treatment. In accord with clinical evidence, the model shows that a proper treatment sequence is important to achieve maximum response and avoid cross-resistance. The quantitative model also allows us to search for an optimal protocol for intermittent treatment to overcome endocrine resistance. Thus, our study provides a novel and useful exploration of breast cancer treatment strategies grounded in a cellular-level, biologically-based mathematical model.

3.3 Materials and Methods

3.3.1 Three ERα Activation modes and crosstalk with GFR

The ERα pathway in breast cancer cells has three distinct branches [2, 23, 24], see Fig. 3.1C: (1) the E2 branch, where ERα bound to E2 becomes an active transcription factor of genes supporting cell survival and proliferation, (2) the phosphorylation branch, where ERα becomes an active transcription factor subsequent to phosphorylation at multiple sites (including Ser118, 104, 106, and 167) in its AF1 domain, and (3) the membrane branch, where membrane-bound ERα mediates the activation of the MAPK and PI3K/AKT pathways (the 'non-genomic' role of ERα). These three branches of the ERα pathway, encompassing both the genomic and non-genomic roles of ERα, crosstalk with each other and with the growth factor receptor signaling network (GFR in Fig. 3.1D) [25, 26]. We consider the following four crosstalk mechanisms: (1) E2-liganded ERα (E2ER in Fig. 3.1D) inhibits expression of both GFR [27, 28] and membrane ERα [29] (ERM in

Fig. 3.1D); (2) both GFR and ERM activate downstream kinases that phosphorylate ERα [2, 23] (ERP in Fig. 3.1D); (3) ERM has positive interactions with GFR signaling at different levels [2, 23]; (4) both ERM and GFR are involved in positive feedback loops at the signaling and/or epigenetic levels [9, 29-31]. Although detailed mechanisms are still lacking, experimental data indicate that the different E2 sensitivities in breast cancer cells are determined by the balance of the three ERα signaling branches (E2ER, ERP, and ERM) and GFR signaling [3, 9].

3.3.2 Model Implementation

Our mathematical model of the influence diagram in Fig. 3.1D uses stochastic differential equations (SDEs) to capture both the deterministic effects of species' interactions in a signaling network and the random effects of intrinsic and extrinsic sources of noise [32-35]. Let X_i be the name of the *i*th species in our interaction diagram (ERE2, ERM, and GFR). (Although ERP is an output of the network in Fig. 3.1D, its activity does not feedback on production or destruction of the other species in the model, so ERP is not a dynamical variable in our model.) Letting $[X_i]$ = activity of X_i and $x_i = \log_{10}[X_i]$, we write the SDEs for our model as

$$\frac{dx_i}{dt} = F_i + \zeta_i(t),\ i = 1, 2, 3; \quad (1)$$

where

$$F_i = \gamma_i \cdot [H(W_i) - x_i],\ \ H(W_i) = 1/(1 + e^{-W_i}),\ \text{ and }\ \ W_i = \omega_i + \sum_{j=1}^{3} \omega_{ij} \cdot x_j \quad (2)$$

We assume that all concentrations in our model have a dynamical range of about 10-fold, so, on a $\log_{10}$ scale, the x_i's vary between 0 and 1. The parameters γ_i determine the rates at which the variables x_i approach their time-varying 'target' values, $x_i = H(W_i)$. Note that $H(W_i)$ is a sigmoidal function that varies between 0 and 1, with a value of ½ when $W_i = 0$. W_i is the net activation or inhibition on species X_i, and the leading term, ω_i, determines whether X_i is activated or inhibited when there are no regulatory signals impinging on X_i from any species in the network. In the summation, ω_{ij} is the strength of the interaction from X_j to X_i ($\omega_{ij} > 0$ for activation and < 0 for inhibition). $\zeta_i(t)$ is a temporally uncorrelated, statistically independent Gaussian white noise process with

$$\langle \zeta_i(t)\zeta_i(t') \rangle = 2 \cdot D_i \cdot \delta(t - t') \tag{3}$$

where D_i characterizes the magnitude of the random fluctuations on each species.

The details of our model are provided in Supplementary Tables. Table 3.1 defines the variables of our model, Table 3.2 lists the precise equations of the model, and Table 3.3 records the parameter values we used for our simulations. In deriving the model equations, we applied a quasi-equilibrium approximation to ERE2, because the binding of E2 to ER occurs on a much faster time scale than variations in ERM and GFR, which have epigenetic regulations. Hence, only ERM and GFR are described by SDEs. We also assumed that ERM and GFR are subject to similar random fluctuations, so $D_1 = D_2 = D$ in Eq. (3). We used Matlab (Version 7.9.0) to perform simulations.

Since our modeling is done at a phenomenological level, none of our parameters are directly related to measurable physical rate constants of the system; rather, they are

assigned to match the phenotypic properties of the ERα-GFR control system. Initially, the parameters for the deterministic part of the model were chosen to ensure that the system has attractors corresponding to E2-sensitive, E2-hypersensitive and E2-supersensitive states. Then, for the stochastic simulations, we chose the noise parameter, D = 0.005, to ensure that the system's landscape changes in a manner similar to experimental observations (Fig. 3.2A). To model selection pressures, we chose the shape of the Proliferation Index curves for cells in each state (Fig. 3.2C) to capture qualitatively the experimentally observed properties of E2-sensitive, -hypersensitive, and -supersensitive cells.

3.3.3 Mapping the Breast Cancer Landscape

A dynamical system whose state moves in the direction of the negative gradient of a potential function can be conveniently visualized by plotting the potential energy landscape and viewing the system state as a particle that moves downhill on this landscape, coming to rest at a local minimum. While open biological systems, such as the one we consider here, are not governed by the gradient of a potential function, the ideas in [16-19, 36] can be used to compute a potential landscape useful for visualization. The basins of this landscape are regions of high probability for finding the system, and the hills are regions that the system rarely visits.

We write the governing equations (1) of our breast cancer model in vector form as

$$\frac{d\mathbf{x}}{dt} = \mathbf{F}(\mathbf{x}) + \boldsymbol{\zeta}(t) \ , \qquad (4)$$

where $\mathbf{x} = \begin{pmatrix} x_1 \\ x_2 \end{pmatrix}$, with similar definitions of $\mathbf{F}$ and $\boldsymbol{\zeta}$. Let $P(\mathbf{x},t)$ be the probability distribution function for state $\mathbf{x}$ and time t, i.e., $P(\mathbf{x},t)\mathrm{d}x_1\mathrm{d}x_2$ = probability of finding the system in the small area $(x_1, x_1+\mathrm{d}x_1)\times(x_2, x_2+\mathrm{d}x_2)$ at time t. The equation governing $P(\mathbf{x},t)$ is

$$\frac{\partial P(\mathbf{x},t)}{\partial t} = -\boldsymbol{\nabla} \cdot \mathbf{J}(\mathbf{x}, t) \tag{5}$$

where $\boldsymbol{\nabla} \cdot \mathbf{J} = \frac{\partial J_1}{\partial x_1} + \frac{\partial J_2}{\partial x_2}$ and

$$\mathrm{J}(\mathrm{x}, \mathrm{t}) = \mathrm{F}(\mathrm{x})\mathrm{P}(\mathrm{x}, \mathrm{t}) - \mathrm{D}\nabla\mathrm{P}(\mathrm{x}, \mathrm{t}) \tag{6}$$

is the probability flux for our system.

Let us wait long enough for the probability density function, and hence the flux, to reach a steady state, and then solve Eq. (6) for $\mathbf{F}(\mathbf{x})$ in terms of $P_{ss}(\mathbf{x})$ and $\mathbf{J}_{ss}(\mathbf{x})$:

$$\mathbf{F}(\mathbf{x}) = -D\boldsymbol{\nabla}U(\mathbf{x}) + \frac{\mathrm{J_{ss}}(\mathbf{x})}{P_{\mathrm{ss}}(\boldsymbol{x})} \tag{7}$$

where $U(\mathbf{x}) = -\ln(P_{ss}(\mathbf{x}))$. Thus, $\mathbf{F}$ can be expressed as the gradient of a potential function $U(\mathbf{x})$ plus a flux field. Although the system's dynamics is not governed solely by the gradient of $U(\mathbf{x})$ but includes as well a 'spiraling' motion due to the flux field [15], the generalized potential $U = -\ln(P_{ss})$ still provides a useful visualization of the dynamics of the system, and we refer to $U(\mathbf{x})$ as the breast cancer landscape in this study. Because of the way U is related to $P_{ss}(\mathbf{x})$, basins of U correspond to high probability states and hills to low probability states. For details of solving the diffusion equations, refer to Supplementary Text 1.

3.3.4 Cell State Transition Model

In the small noise case, the system spends most of its time fluctuating around one of its m steady states ($m = 4$ in this study) with occasional transitions between states. Hence, it is inefficient to track the states of cells in a large population by simulating each cell individually. To study state switching within large population of cells, we transform the cellular-level, multiple steady-state model into a Markov state-transition model by using the cellular model to compute the Markov state transition rates. To this end, we divided the two-dimensional state space of the cellular-level model into four blocks, representing the four discrete phenotypes, which we refer to as 'states' R_1, R_2, R_3 and R_4 in Fig. 3.2A and Fig. 3.3B. Similar to [37, 38], we describe a population of cells by a state vector, **v,** of length $m = 4$. The i^{th} entry of the vector is the number of cells in state R_i, and the total number of cells in the population at time t is $N(t) = \sum_{i=1}^{4} v_i(t)$. The state vector evolves according to the equation $\frac{d\mathbf{v}}{dt} = \mathbf{A} \cdot \mathbf{v}$ where $\mathbf{A}$ is an $m \times m$ transition rate matrix. The off-diagonal elements of $\mathbf{A}$, $A_{ij} = k_{ij}$, are the transition rates from state j to state i, and the diagonal elements are $A_{ii} = u_i - \sum_{j \neq i} k_{ji}$, where u_i is the proliferation rate of cells in state i. Thus, starting from a vector reflecting the initial populations of R_1, …, R_4 at time 0, we can easily compute the temporal evolution of the population (For details see Supplementary Text 2). The average Proliferation Index (PI) of the population at each time step is then calculated by $PI(t) = \frac{N(t+\Delta t) - N(t)}{\Delta t \cdot N(t)}$. PI is the specific reproduction rate of the population: $PI > 0$ signifies an expanding population, and $PI < 0$ signifies a diminishing population.

3.3.5 Minimum Action Path

To estimate the transition rates k_{ij} among the different states in the dynamical system, which we need for the population-level model, we followed the approach in [18, 22, 39] based on applying the Wentzell-Freidlin theory [40] to Eq. (4) for the 'small noise' case. The key idea of this theory is that the most probable transition path from state j at time 0 to state i at time T, $\boldsymbol{\varphi}_{ij}^{*}(t)$ for $t \in [0, T]$, minimizes the action functional (Eq. 8) over all possible paths:

$$S_T\left[\boldsymbol{\varphi}_{ij}\right] = \frac{1}{2}\int_0^T \left|\dot{\boldsymbol{\varphi}}_{ij} - \mathbf{F}(\boldsymbol{\varphi}_{ij})\right|^2 \mathrm{d}t \tag{8}$$

This optimal path is referred to as the minimum action path (MAP). We are interested in MAPs between fixed-point attractors (stable steady states) in the system. The MAPs connecting each pair of attractors were computed numerically by applying the minimum action method used in [22, 39]. For T large enough to allow a transition from state j to state i, $S_T\left[\boldsymbol{\varphi}_{ij}^{*}\right]$ becomes independent of T, which is what we desire. In our case, $T = 40$ is a reasonable choice: large enough but not too large (see Fig. 3.7 in the Supplementary Material).

The MAP $\boldsymbol{\varphi}_{ij}^{*}$ is useful for our purposes because we find that k_{ij}, the transition rate from state j to state i, is related to $S_T\left[\boldsymbol{\varphi}_{ij}^{*}\right]$ by the empirical equation

$$k_{ji} = \beta \cdot \exp\left\{-\alpha \cdot \left(S_T\left[\boldsymbol{\varphi}_{ij}^{*}\right]\right)^n\right\} \tag{9}$$

where the parameters α, β and n are estimated by fitting Eq. (9) to the results of direct Monte Carlo simulations of the dynamic model, where the Langevin Eq. (4) is integrated by the explicit method:

$$x_i(t + \Delta t) = x_i(t) + \gamma_i \cdot \big(H(W_i) - x_i(t)\big) \cdot \Delta t + \sqrt{2 \cdot D_i \cdot \Delta t} \cdot \eta_i(t) \qquad (10)$$

Here the η_i are independent, normal, random deviates with mean 0 and variance 1.

3.4 Results

3.4.1 The breast cancer landscape

Both clinical observations and cell line studies suggest that breast cancer cells can shift between three different E2 sensitivity states [3, 9] (Fig. 3.1B): E2-sensitive, E2-hypersensitive and E2-supersensitive (independent). In E2-sensitive cells, E2-liganded ERα (E2ER) is the major driver of pro-survival and pro-proliferation signaling, whereas ERα in the cell membrane (ERM), phosphorylated ERα (ERP), and GFRs are kept at low levels of activity. As summarized in [3, 9], E2-hypersensitive cells are closely associated with elevated ERα in the cell membrane (ERM), where ERα plays a non-genomic role to mediate the activation of the MAPK and PI3K/AKT pathways. GFRs, such as IGF1R and HER2, are not necessarily overexpressed in E2- hypersensitive cells. A possible explanation for hypersensitivity is that ERα, phosphorylated by kinases in the upregulated pathway, may have increased affinity for E2. In E2-supersensitive cells, however, increased IGF1R and HER2 signaling play pivotal roles in activating MAPK

and PI3K/AKT, resulting in further phosphorylation of ERα (ERP) and E2-independent growth of breast cancer cells. These observations are summarized in Fig. 3.1E. The activity levels of ERM and GFR determine the E2-sensitivity state of our model. Thus, of the four states in Fig. 3.2A, R_1 corresponds to E2-senstivity (GFR low, ERM low), R_2 corresponds to E2-hypersensitivity (GFR low, ERM high), and R_3 and R_4 corresponds to E2-supersensitivity (GFR high, ERM high or low).

The breast cancer landscape computed from our model is plotted in Fig. 3.2C for three different E2 conditions ([E2] = 10^2, 10^0 and 10^{-2}) corresponding to HIGH, LOW and TRACE amounts of E2. Varying the level of E2 reshapes the landscape and can induce cells to transition from one state to another. When E2 level is HIGH, the potential landscape has only one dominant basin at state block R_1, where both ERM and GFR are low (Fig. 3.2C, left), indicating an E2-sensitive state. Most cells will stay in this state. Reducing E2 to LOW level (Fig. 3.2C, middle) reshapes the landscape, deepening the basin at R_2 and causing some cells to shift from the E2-sensitive state to the E2-hypersensitive state. Further decreasing E2 to TRACE amounts creates a dominant basin at R_4, the E2-supersensitive state (Fig. 3.2C, right), and the E2-sensitive basin at R_1 becomes very shallow. Both E2-hypersensitive and E2-supersensitive cells will coexist in this condition, with a preference for the supersensitive state.

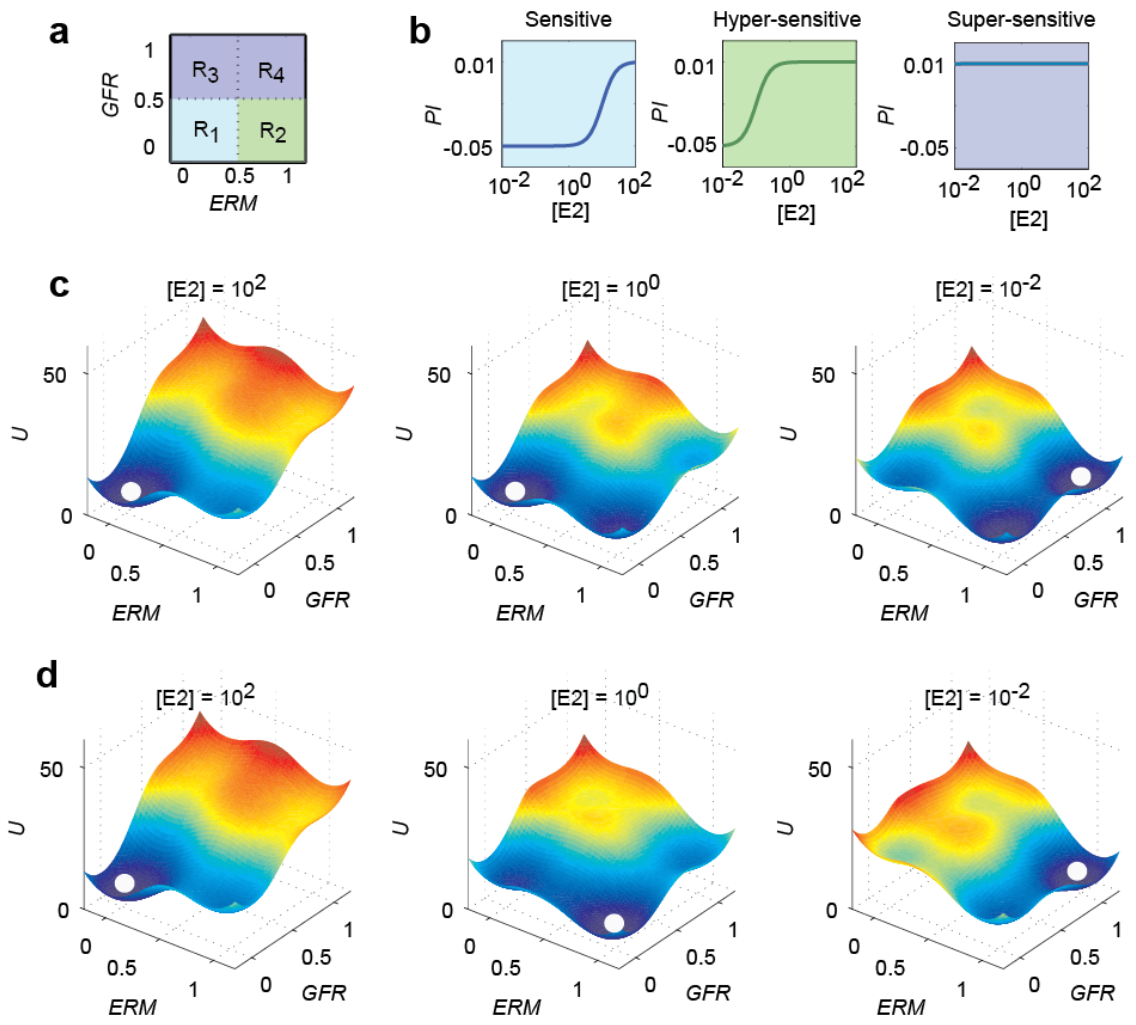

Figure 3.2 E2 levels and selection pressure manipulate the breast cancer landscape. (**A**) The state space of the system is divided into four blocks (R_1-R_4). Cells within the same block are assumed to have the same dose-response curve of proliferation index (PI) to E2 level (**B**). The breast cancer landscapes at different E2 levels ([E2] = 10^2, 10^0 and 10^{-2}, corresponding to HIGH, LOW and TRACE levels of E2 in Fig. 3.1B) are computed using $U = -\ln P_{ss}$, either without (**C**) or with (**D**) selection pressure. The elevation decreases from red to blue. White balls are put in the basins with lowest U in each plot. The selection pressures used in (**D**) are described in (**B**). In (**C**) cells in all states are assumed to have the same proliferation index ($PI = 0$ for all [E2]), thus cells are not under

selection pressure. $PI > 0$ means cell growth overwhelms cell death; $PI = 0$ means a balance of cell growth and death; $PI < 0$ means cell death overwhelms cell growth. *ERM*, activity of membrane ERα; *GFR*, activity of growth factor receptors.

In addition to cell state transitions (cellular adaptation) in response to a changing E2 environment, breast cancer cells are also under selection pressure due to the different proliferation rates that apply to each cell state in a given E2 environment. To model this selection pressure, the state space of the model was divided into four blocks (R_1, R_2, R_3 and R_4 as before), with each block assigned a specific proliferation index (*PI*) as a function of *E2* (Fig. 3.2B). Allowing cells in each block to proliferate at their assigned rates given the specified E2 concentration results in the landscapes in Fig. 3.2C (see Supplementary Text 1 for calculation details). Selection pressure deepens some basins and destroys others (Fig. 3.2D). In particular, for LOW values of E2, selection pressure causes the dominant basin to shift from the E2-sensitive state (R_1) to the E2-hypersensitive state (R_2).

Thus, our model is able to explain the different cell states observed experimentally in response to E2 manipulations. The breast cancer landscape we have computed here provides a useful visualization of the global behaviors of the breast cancer system with three different E2 sensitivity states.

3.4.2 A state transition model

Cell state transitions require the system to cross a barrier to move from one basin to another. The transitions are driven by intrinsic and extrinsic noise, with lower barriers corresponding to more probable transitions. The most probable routes for transitions among the four states on the breast cancer landscape were computed by finding the paths

that minimize the action (a measure of the difficulty of moving from one point to another, see methods) over all possible paths that start and end at the desired points. An example of minimum action paths (MAPs) on the breast cancer landscape is shown in Fig. 3.3A. Interestingly, the route taken from basin 1 to basin 2 is not the same as that from 2 to 1, as seen by the non-overlapping yellow and red curves in Fig. 3.3A. This divergence of MAPs is a consequence of the non-gradient component of the flow field, Eq. (7) [15, 16, 41].

The action along the MAP between two steady states in Fig. 3.3A can be used to estimate the transition probability between the two steady states [18]. To accomplish this, we again divide state space into four blocks (R_1-R_4 in Fig. 3.3B) corresponding to the four cancer-cell phenotypes. Each block has at most one attractor. For various E2 levels, the transition rates between pairs of state space blocks were computed by Monte Carlo simulations of the stochastic model (Fig. 3.8). In Fig. 3.3C we plot these transition rates as functions of the action of the MAP between the corresponding fixed points. As expected, the points all lie close to a single curve described by Eq. (9), with $\alpha = 80.48$, $\beta = 0.07197$, and $n = 0.9805$. Thus, for different values of E2 and any pair of fixed points we can compute the action and then use Eq. (9) to compute the transition probability, without recourse to additional Monte Carlo simulations. The comparisons between transition rates estimated from actions and from direct Monte Carlo simulations at different E2 levels are shown in Fig. 3.4D and E. Because the transition rates out of R_3 are very much greater than the transition rates into R_3 ($k_{13} >> k_{31}$, $k_{23} >> k_{32}$, $k_{43} >> k_{34}$), the third block is rarely populated and can be safely neglected. The transition rates

between R_1 and R_4 are much smaller than their transition rates with R_2 ($k_{41} << k_{21}$, $k_{14} << k_{24}$); hence, direct transitions between R_1 and R_4 can also be safely neglected.

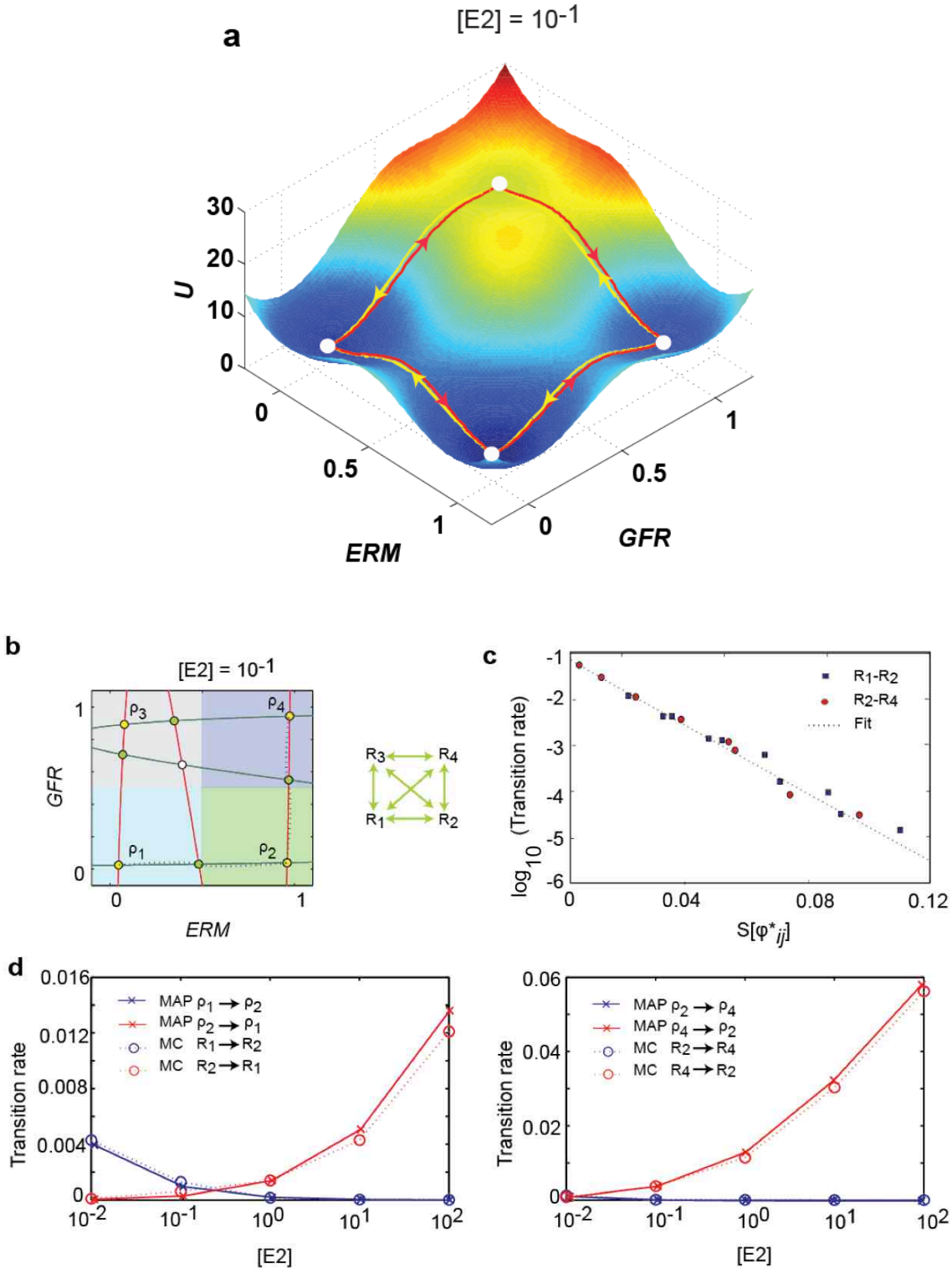

Figure 3.3 Minimum action paths (MAPs) characterize state transitions on the breast cancer landscape. (**A**) The breast cancer landscape $U = -\ln P_{ss}$ as a function of *ERM* (membrane ERα) and *GFR* (growth factor receptors), for [E2] = 10^{-1} and no selection pressure. White balls are put in basins. The red and yellow lines are the estimated MAPs connecting different basins. The arrows indicate the directions of the transitions. Notice that the red and yellow lines do not overlap. (**B**) The ERM-GFR phase plane (left panel, [E2] = 10^{-1} for illustration) is divided into four blocks (marked by different colors). Each block represents a state variable in the state transition model (R_1-R_4, right panel; green arrows represent reversible transitions). In each block there is at most one fixed-point attractor. The fixed-point attractors (ϱ_1-ϱ_4, light green dots) and first-order saddles (dark green dots) are located by finding the intersection points of the nullclines for ERM and GFR. The ERM nullcline (red curve) is the locus of points for which $ERM = H(W_{\mathrm{ERM}})$, and the GFR nullcline (green curve) is the locus of points for which $GFR = H(W_{\mathrm{GFR}})$. (**C**) Points represent transition rates, computed by direct Monte Carlo (MC) simulation, for transitions between states R_1 and R_2 (blue) and between states R_2 and R_4 (red). $S\left[\varphi_{ij}^{*}\right]$ is the value of the action along the MAP between the relevant fixed points in the states, evaluated for $T = 40$. The dashed line is the best fit of Eq. (9) to the data ($\alpha = 80.48$, $\beta = 0.07197$, and $n = 0.9805$). (**D**) and (**E**) compare the transition rates estimated by Eq. (9) with the transition rates computed by direct Monte Carlo simulations, as functions of E2.

Given the estimated transition rates, we built a deterministic model of phenotype transitions and simulated the growth of cancer cell populations under different E2 conditions. Figure 3.4A shows the steady-state proportion of each phenotype as a function of E2 level for the case of no selection pressure (PI = 0 for each phenotype). This distribution of phenotypes is consistent with the landscape plot in Fig. 3.2C. Notice that when E2 is LOW ([E2] = 1), although there is a small population of E2-hypersensitive cells (green curve), the majority of cells are still in the E2-sensitive state (blue curve). However, adding the effect of population selection significantly changes the story (Fig. 3.4B). As in Fig. 3.2D, the selective advantage of E2-hypersensitive cells in the LOW E2 environment substantially increases the proportion of E2-hypersensitive cells. The proportion of E2-supersensitive cells under TRACE E2 conditions ([E2] = 10^{-2}) is greatly enriched (Fig. 3.4B, right). Corresponding steady state probability distributions, $P_{ss}(x_1,x_2)$, in the state space of the cellular-level model are shown in Fig. 3.4C and D. Simulating the phenotype transition model at the population level provides an enormous reduction in computation compared to Monte Carlo simulations of the cellular level model and allows us to easily study the consequences of both sequential and intermittent treatments of breast cancer under a variety of conditions.

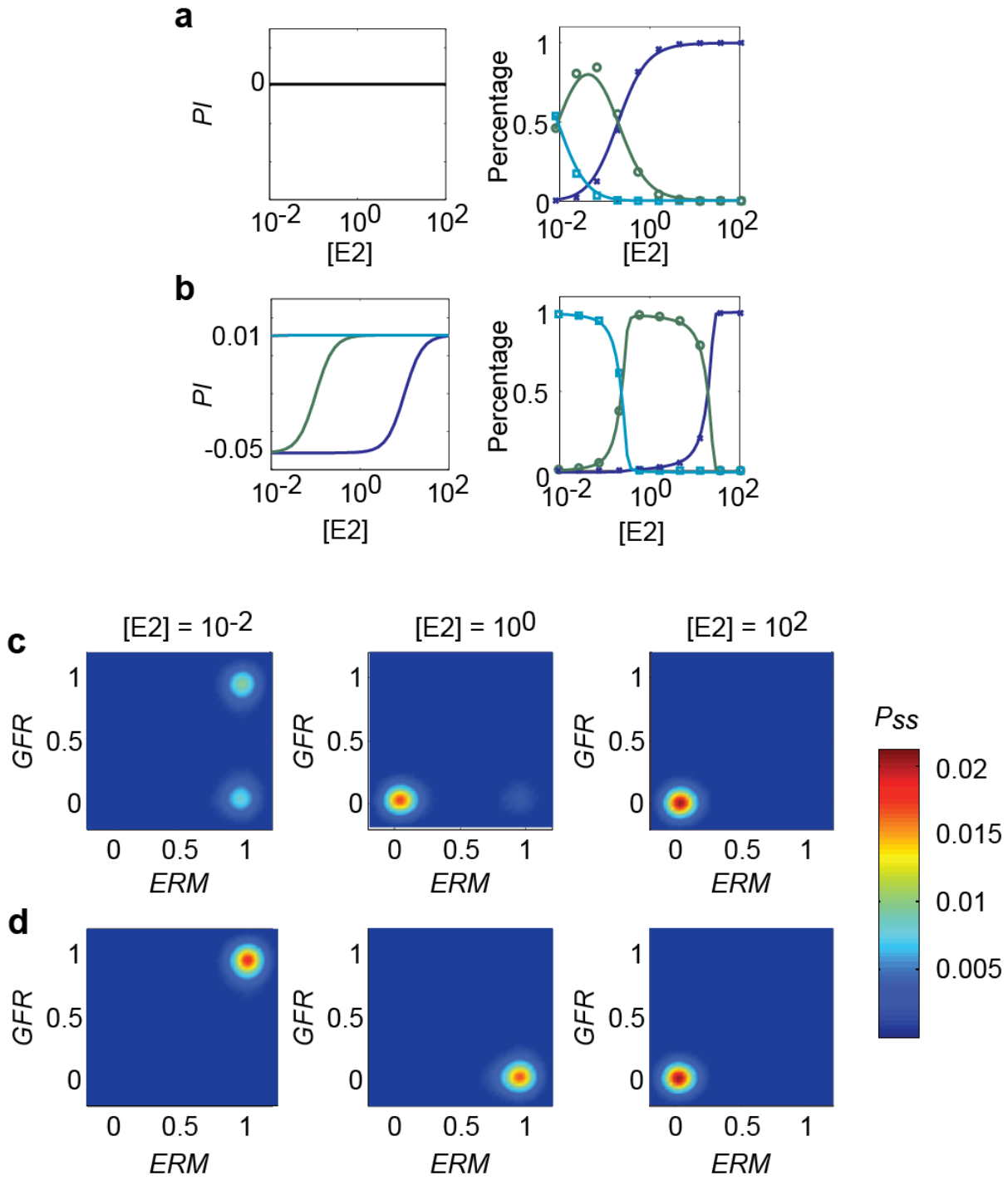

Figure 3.4 The state transition model approximates the dynamical behavior of the breast cancer landscape. (**A-B**) Right panels: the steady state proportions of cells in three of the E2 sensitivity states as a function of E2 level in the state-transition model

(solid lines) and cellular model (discrete makers) either without selection pressure (A) or with selection pressure (B). Left panels show the corresponding dose-response curves of proliferation index (PI) to E2 levels for cells in each state. Cyan, E2-sensitive state (R_1); green, E2-hypersensitive state (R_2); blue, E2-supersensitive state (R_4). The other E2-supersensitive state (R_3) is not populated to any appreciable extent. (**C-D**) The corresponding steady state probability distributions (P_{ss}) in the state space of the cellular level model are plotted as heat maps for [E2] = 10^{-2}, 10^{0} and 10^{2}, for the case without selection (C) and with selection (D). *ERM*, activity of membrane ERα; *GFR*, activity of growth factor receptors.

3.4.3 Sequential treatment of breast cancer

The role of sequential E2 deprivation in breast cancer cells has been reported in both clinical and pre-clinical settings [3, 9, 10]. For example, in pre-menopausal women, E2-dependent breast cancers often regress after surgical removal of ovaries, which lowers circulating E2 from 200 to 15 pg/ml. After an initial stage of regression, breast cancer often regrows. AIs, as second-line therapies, can induce additional tumor regression by further decreasing E2 to 5 pg/ml [10].

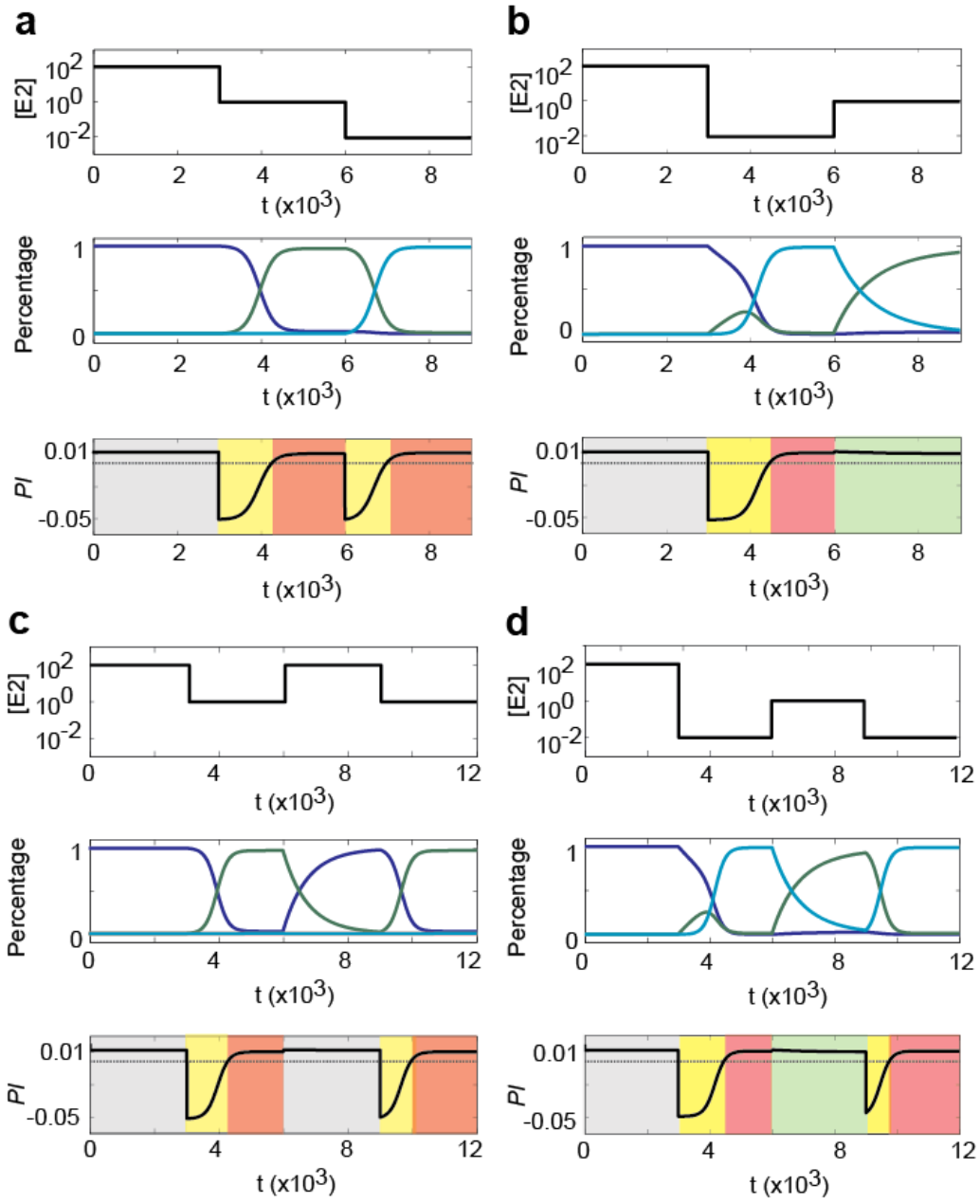

Figure 3.5 Sequential and intermittent treatments provide additional response windows to endocrine therapy. In sequential treatments, different E2 withdrawal sequences are used to mimic different endocrine treatment regimens: (**A**) reducing E2 from HIGH, to LOW, to TRACE level; (**B**) changing E2 from HIGH, to TRACE, to LOW level; In intermittent treatments: (**C**) two identical endocrine treatments are applied

with a break in between; or (**D**) two different endocrine therapies are applied with a break in between; as shown in the upper panels. *T*, time (arbitrary units). The resulting changes in proportions of cells in different E2 sensitivity states are shown in the middle panels. Cyan, E2-sensitive state (R_1); green, E2-hypersensitive state (R_2); blue, E2-supersensitive state (R_4). The lower panels indicate how the average proliferation index (PI) of the cell population changes during the course of the treatment. Yellow, responsive state; red, resistant state; green, cross-resistant state. The dotted horizontal line indicates no growth ($PI = 0$).

Creation of an additional 'response window' using a second-line endocrine therapy can be captured by our state transition model (Fig. 3.5A). Decreasing E2 in a step-wise fashion (Fig. 3.5A, top) results in sequential transitions of the cell population from the E2-sensitive to the E2-hypersensitive to the E2-supersensitive state (Fig. 3.5A, middle). At each transition, cells in the previously favored state begin to die off while some make the transition to the newly favored state and begin growing. Plotting the average population proliferation index (*PI*) versus time clearly shows the two response windows of negative average growth (Yellow regions, Fig. 3.5A, bottom). Notably, if the E2 steps are applied in the reverse order (Fig. 3.5B), the simulation shows no second response window, in accord with the phenomena of cross-resistance to endocrine therapies in breast cancer. For example, it is reported that using AIs or faslodex as a first-line therapy is not more effective than using tamoxifen, even though AIs and faslodex result in less E2ER than tamoxifen [3]. And AI-resistant breast cancers are usually cross-resistant to tamoxifen, whereas faslodex-resistant breast cancers are cross-resistant to both AIs and tamoxifen [3]. In Fig. 3.5B, the green region represents the cross-resistance of cells to endocrine treatment associated with LOW E2 (e.g., tamoxifen) when the cells have been pretreated with (and gained resistance to) endocrine treatment associated with TRACE levels of E2 (e.g., AIs). Thus, using AIs or faslodex as a first-line therapy in these patients is not recommended, since it can eliminate the opportunity for an additional drug response window.

3.4.4 Intermittent treatment of breast cancer

Similarly, intermittent E2 treatment to reverse acquired resistance and provide a second response window is simulated in Fig. 3.5C. Shifting between two different endocrine therapies can also produce a similar result (Fig. 3.5D). These simulation results provide a quantitative explanation for observations (widely reported in both pre-clinical and clinical observations [5-7]) that intermittent treatment is often better than continuous treatment to kill cancers. For example, re-challenging tamoxifen resistant breast cancer after a 'drug holiday' or a switch to a different type of therapy (such as chemotherapy), may give patients a second or even third response to tamoxifen [5].

Regarding intermittent treatment of cancer, people have long noticed that the response is sensitive to the duration of treatment and the interval between treatments. The state transition model can serve as a quantitative tool to find the optimum values for treatment duration, T_{treat}, and treatment breaks, T_{break}. Figure 3.6A shows the results for $T_{\text{treat}} = 3000$ and $T_{break} = 2000$, where cell population growth is reduced—but not stopped—by intermittent treatment. By contrast, intermittent treatment with $T_{\text{treat}} = 1000$ and $T_{\text{break}} = 2000$ (Fig. 3.6B) causes the total cell population to stop growing, thereby controlling—although not eliminating—the cancer. Comparing these two cases, we note that shorter treatment durations may be more beneficial than longer treatments, which is the experience of breast cancer oncologists [42].

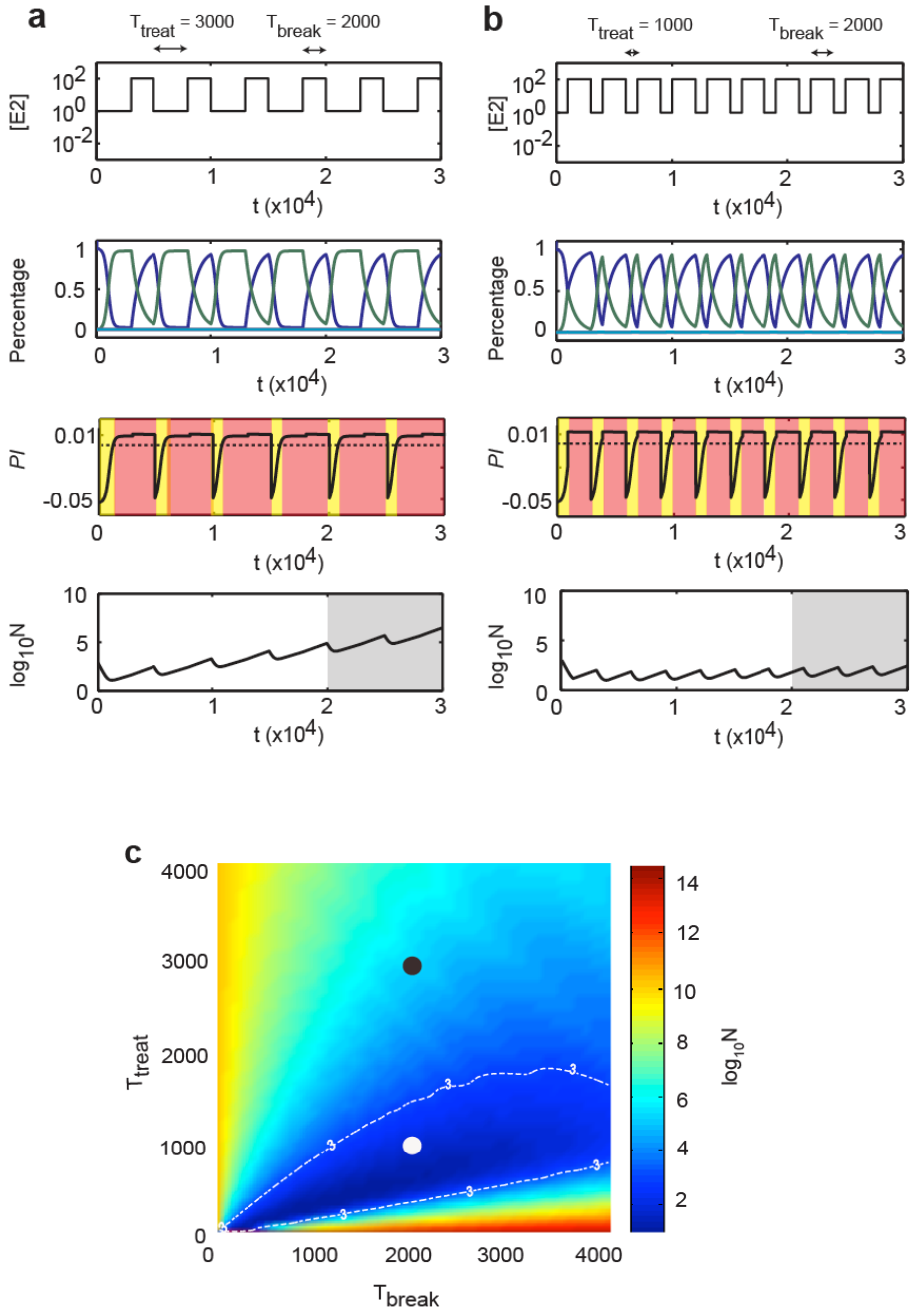

Figure 3.6 Different regimens of intermittent treatment show different prognoses. The endocrine treatment consists of periodically switching E2 level from HIGH to LOW and back to HIGH, with T_{treat} = duration at HIGH E2 level and T_{break} = duration at LOW E2 level (time in arbitrary units). As indicated in the top panels, two intermittent

treatment regimens are simulated: (**A**) $T_{treat} = 3000$, $T_{break} = 2000$; and (**B**) $T_{treat} = 1000$, $T_{break} = 2000$. Both treatments change the proportion of cells in different E2 sensitivity states (second panels). Cyan, E2-sensitive state (R_1); green, E2-hypersensitive state (R_2); blue, E2-supersensitive state (R_4). The average proliferation index (PI) of the cell population is shown in the third panel. Yellow, responsive state; red, resistant state. The dotted horizontal line indicates no growth ($PI = 0$). The total number of cells $N(t)$, is plotted in the fourth panel at logarithmic scale. The grey interval is used for the calculations in part C. (**C**) We plot, as a function of T_{treat} and T_{break}, the average value of cell number $\langle \log_{10} N \rangle$ over the interval $T \in [2\times10^4, 3\times10^4]$. The black and white dots indicate the cases in parts (A) and (B), respectively. Since we start from a population of 1000 breast cancer cells, any combination of T_{treat} and T_{break} that puts the system within the dotted white contour line, $\log_{10} N = 3$, will suppress cancer growth.

Using the model to explore the effects of the two key treatment parameters on the expansion of the cancer cell population, we plot in Fig. 3.6C the total number of cells after treatment as a function of T_{treat} and T_{break}. Since the simulation starts with 10^3 cells, any parameter values within the 10^3-contour (superimposed on Fig. 3.6C) will cause cancer progression to be arrested or reversed. These results point out the usefulness of a population-level, state-transition model grounded on a cellular-level, mechanistic model for optimizing cancer treatment protocols.

3.5 Discussion

As a heterogeneous population of cells, cancer can adaptively change in response to a varying environment. This plasticity can lead to acquired resistance and drug failure, a fundamental problem in cancer treatment. One widely accepted explanation for cancer plasticity is that cancer cells with advantageous mutations due to genome instability can be selected and enriched in a Darwinian type evolutionary process [43]. However, mutations are rare, random and irreversible, which makes this explanation unsuitable for the reversible resistance often observed in experiments and clinical observations. An appealing alternative explanation is the cancer stem cell model, which uses principles of developmental and stem cell biology to justify multiple cell states and phenotypes as non-genomic sources for Darwinian selection [12]. Growing evidence of non-genomic heterogeneity has been reported recently in different cancer types, including breast cancer [37]. This creates a need to investigate the mechanisms of phenotype transitions in cancer

cells, and to relate transitions at the cellular level with selection at the population level, in order to determine the efficacy of cancer treatments in the ongoing selection war.

Considering the three phenotypes of E2 sensitivity in breast cancer cells as an example of this sort of non-genomic heterogeneity, we modeled the crosstalk among the three major ERα signaling modes (E2ER, ERM, ERP) and the GFR pathway for cell survival and proliferation. The model, though simplistic, provides a qualitative match to the progressive, step-wise phenomenon of shifting E2 sensitivities and changing endocrine responsiveness in breast cancer cells under E2 manipulation.

However, the tremendous complexity of cancer must be kept in mind. In addition to the crosstalk mechanisms proposed in this study, there might be other currently-unknown links that have played key roles in making breast cancer cells to bifurcate into different states. Nevertheless, our model provides a plausible motif that could explain the underlying mechanism of observed experimental phenomenon. It would be appealing to expand this motif to a more realistic model when sufficient knowledge at molecular level is available. In addition, Cancer cells may have as many steady states as there are physiological states, including a spectrum of cell phenotypes from different differentiation stages [44]: cancer stem cells (CSCs), intermediate progenitor cells, and fully differentiated 'bulk' cells. Such physiological phenotypes and the transitions between them have been widely reported in breast cancer. The epithelial-mesenchymal plasticity of breast cancer also creates a broad spectrum of phenotypes, whereby epithelial primary cancers become mesenchymal-like and re-epithelialize into a solid tumor at secondary, metastatic sites [45]. In addition, the traditional classification of

breast cancers into simple, fixed categories (e.g., luminal A, luminal B, HER2+ and basal-like) has neglected the heterogeneous and dynamic properties in cancer. Phenotypic transitions among stem-like, basal and luminal subpopulations within a given breast cancer cell population have been reported in experiments [37]. Unfortunately, current knowledge of the underlying molecular mechanisms for these phenotypic transitions is very limited. Nevertheless, the sources of non-genomic heterogeneity in breast cancer cells are now under extensive study and will ultimately enable the creation of enhanced models with more (meta)-stable steady states corresponding to the various physiological states of breast cancer cells.

Mathematical modeling is useful to help understand the emergent behaviors of cancer physiology at different levels [46-51]. Numerous mathematical models address the mechanisms by which cancer cells develop resistance to treatment. Despite that most models attribute the source of Darwinian selection to rare mutations [52, 53], some have taken non-genetic heterogeneity into account by modeling spontaneous transitions between CSCs and 'bulk' cells at the population level [54, 55]. In this study, we adopted a multi-scale modeling strategy by first creating a biologically plausible, cell-level model of phenotypic transitions in breast cancer, and then deriving a state transition model from the cell-level model; thereby simplifying modeling of breast cancer behavior at the population level in response to endocrine therapies. This strategy enables a systematic understanding of how adaptations of breast cancer to a varying environment cooperate at both cellular and population levels to create resistance to endocrine therapies. Our modeling results indicate that selection pressure can change the shape of the breast cancer landscape (Fig. 3.2C and D) substantially and introduce new equilibrium state

distribution of the state-transition model (Fig. 3.4A and B). The transition approximation we propose provides a useful bridge between the molecular mechanisms of cellular phenotypic transitions and the phenomenological parameters that have been widely used to describe these transitions in population-based models.

We applied the state transition model to understand the effects of sequential and intermittent treatment that have proven to beneficial for breast cancer as well as other types of cancer [3, 5-7, 9, 56-58]. Many studies have focused on the benefits of these strategies in reducing side effects. Here we mainly focused on another major advantage, the potential of these strategies to reduce or reverse acquired resistance during treatment. The model provided a quantitative tool to understand and investigate the optimized endocrine treatment sequences and parameters. Based on the model predictions on the existences of an optimal sequence in sequential treatment and an optimal region of parameters in intermittent treatment, experiments can be designed to validate and find these optimal treatment strategies. While much remains to be done to make our models more comprehensive and realistic, the approach used in this study provides a potential path to investigate treatment strategies and improve treatment efficacy in breast and other cancers.

3.6 Acknowledgements

We thank Lei Zhang, Jin Wang, Hang Zhang and Xiaojun Tian for help and/or discussions. This work was supported in part by US National Institutes of Health grant

U54-CA149147 (to R.C., J.J.T. and W.T.B.), US National Science Foundation grant DMS-0969417 (to J.X.), and by a fellowship to C.C. provided by the Virginia Polytechnic Institute and State University graduate program in Genetics, Bioinformatics and Computational Biology.

3.7 References

1. Rimawi, M.F. and C.K. Osborne, *BREAST CANCER Blocking both driver and escape pathways improves outcomes*. Nature Reviews Clinical Oncology, 2012. **9**(3): p. 133-134.
2. Musgrove, E.A. and R.L. Sutherland, *Biological determinants of endocrine resistance in breast cancer*. Nat Rev Cancer, 2009. **9**(9): p. 631-43.
3. Normanno, N., et al., *Mechanisms of endocrine resistance and novel therapeutic strategies in breast cancer*. Endocr Relat Cancer, 2005. **12**(4): p. 721-47.
4. Ali, S. and R.C. Coombes, *Endocrine-responsive breast cancer and strategies for combating resistance*. Nat Rev Cancer, 2002. **2**(2): p. 101-12.
5. Stoll, B.A., *Rechallenging Breast-Cancer with Tamoxifen Therapy*. Clinical Oncology, 1983. **9**(4): p. 347-351.
6. McClelland, R.A., et al., *Enhanced epidermal growth factor receptor signaling in MCF7 breast cancer cells after long-term culture in the presence of the pure antiestrogen ICI 182,780 (Faslodex)*. Endocrinology, 2001. **142**(7): p. 2776-88.
7. Sabnis, G., et al., *Sensitivity to the aromatase inhibitor letrozole is prolonged after a "break" in treatment*. Mol Cancer Ther, 2010. **9**(1): p. 46-56.

8. Barrios, C., et al., *The sequential use of endocrine treatment for advanced breast cancer: where are we?* Annals of Oncology, 2012. **23**(6): p. 1378-1386.

9. Nicholson, R.I., et al., *Growth factor-driven mechanisms associated with resistance to estrogen deprivation in breast cancer: new opportunities for therapy*. Endocr Relat Cancer, 2004. **11**(4): p. 623-41.

10. Santen, R.J., et al., *Adaptive hypersensitivity to estrogen: mechanism for superiority of aromatase inhibitors over selective estrogen receptor modulators for breast cancer treatment and prevention*. Endocr Relat Cancer, 2003. **10**(2): p. 111-30.

11. Santen, R.J., et al., *Adaptive hypersensitivity to estrogen: Mechanism for sequential responses to hormonal therapy in breast cancer*. Clinical Cancer Research, 2004. **10**(1): p. 337S-345S.

12. Brock, A., H. Chang, and S. Huang, *OPINION Non-genetic heterogeneity - a mutation-independent driving force for the somatic evolution of tumours*. Nature Reviews Genetics, 2009. **10**(5): p. 336-342.

13. Masamura, S., et al., *Estrogen Deprivation Causes Estradiol Hypersensitivity in Human Breast-Cancer Cells*. Journal of Clinical Endocrinology & Metabolism, 1995. **80**(10): p. 2918-2925.

14. Waddington, C.H., *The strategy of the genes; a discussion of some aspects of theoretical biology*. 1957, London,: Allen & Unwin. ix, 262 p.

15. Wang, J., et al., *Quantifying the Waddington landscape and biological paths for development and differentiation*. Proc Natl Acad Sci U S A, 2011. **108**(20): p. 8257-62.

16. Wang, J., L. Xu, and E. Wang, *Potential landscape and flux framework of nonequilibrium networks: robustness, dissipation, and coherence of biochemical oscillations*. Proc Natl Acad Sci U S A, 2008. **105**(34): p. 12271-6.

17. Ao, P., et al., *Cancer as robust intrinsic state of endogenous molecular-cellular network shaped by evolution*. Medical Hypotheses, 2008. **70**(3): p. 678-684.

18. Wang, P., et al., *Global Epigenetic State Network Governs Cellular Pluripotent Reprogramming and Transdifferentiation*. arXiv:1209.4603 [q-bio.MN], 2012.

19. Zhou, J.X., et al., *Quasi-potential landscape in complex multi-stable systems*. Journal of the Royal Society Interface, 2012. **9**(77): p. 3539-3553.

20. Huang, S., I. Ernberg, and S. Kauffman, *Cancer attractors: a systems view of tumors from a gene network dynamics and developmental perspective*. Semin Cell Dev Biol, 2009. **20**(7): p. 869-76.

21. Zhu, X.M., et al., *Robustness, stability and efficiency of phage lambda genetic switch: dynamical structure analysis*. J Bioinform Comput Biol, 2004. **2**(4): p. 785-817.

22. Zhang, L., et al., *Noise drives sharpening of gene expression boundaries in the zebrafish hindbrain*. Molecular Systems Biology, 2012. **8**.

23. Osborne, C.K. and R. Schiff, *Mechanisms of Endocrine Resistance in Breast Cancer*. Annual Review of Medicine, Vol 62, 2011, 2011. **62**: p. 233-247.

24. Lannigan, D.A., *Estrogen receptor phosphorylation*. Steroids, 2003. **68**(1): p. 1-9.

25. Osborne, C.K., et al., *Crosstalk between estrogen receptor and growth factor receptor pathways as a cause for endocrine therapy resistance in breast cancer*. Clinical Cancer Research, 2005. **11**(2): p. 865S-870S.

26. Massarweh, S. and R. Schiff, *Resistance to endocrine therapy in breast cancer: exploiting estrogen receptor/growth factor signaling crosstalk*. Endocrine-Related Cancer, 2006. **13**: p. S15-S24.

27. Bates, N.P. and H.C. Hurst, *An intron 1 enhancer element mediates oestrogen-induced suppression of ERBB2 expression*. Oncogene, 1997. **15**(4): p. 473-81.

28. Chrysogelos, S.A., et al., *Mechanisms of Egf Receptor Regulation in Breast-Cancer Cells*. Breast Cancer Research and Treatment, 1994. **31**(2-3): p. 227-236.

29. Rao, J., et al., *Advances in the understanding of the structure and function of ER-alpha 36,a novel variant of human estrogen receptor-alpha*. Journal of Steroid Biochemistry and Molecular Biology, 2011. **127**(3-5): p. 231-237.

30. Zilli, M., et al., *Molecular mechanisms of endocrine resistance and their implication in the therapy of breast cancer*. Biochimica Et Biophysica Acta-Reviews on Cancer, 2009. **1795**(1): p. 62-81.

31. Zhou, Y., et al., *The NF kappa B pathway and endocrine-resistant breast cancer*. Endocrine-Related Cancer, 2005. **12**: p. S37-S46.

32. Tyson, J.J. and B. Novak, *Functional Motifs in Biochemical Reaction Networks*. Annual Review of Physical Chemistry, Vol 61, 2010. **61**: p. 219-240.

33. Wilson, H.R. and J.D. Cowan, *Excitatory and inhibitory interactions in localized populations of model neurons*. Biophys J, 1972. **12**(1): p. 1-24.

34. Mjolsness, E., D.H. Sharp, and J. Reinitz, *A Connectionist Model of Development*. Journal of Theoretical Biology, 1991. **152**(4): p. 429-453.

35. Chen, C., et al., *Modeling a survival signaling switch in MCF7 breast cancer cells*. unpublished.

36. Graham, R. and T. Tel, *Nonequilibrium Potential for Coexisting Attractors*. Physical Review A, 1986. **33**(2): p. 1322-1337.

37. Gupta, P.B., et al., *Stochastic State Transitions Give Rise to Phenotypic Equilibrium in Populations of Cancer Cells*. Cell, 2011. **146**(4): p. 633-644.

38. Kussell, E., et al., *Bacterial persistence: a model of survival in changing environments*. Genetics, 2005. **169**(4): p. 1807-14.

39. E, W., W.Q. Ren, and E. Vanden-Eijnden, *Minimum action method for the study of rare events*. Communications on Pure and Applied Mathematics, 2004. **57**(5): p. 637-656.

40. Freidlin, M. and M. Weber, *Random perturbations of dynamical systems and diffusion processes with conservation laws (vol 137, pg 595, 2007)*. Probability Theory and Related Fields, 2007. **137**(3-4): p. 595-596.

41. Wang, J., et al., *The potential landscape of genetic circuits imposes the arrow of time in stem cell differentiation*. Biophys J, 2010. **99**(1): p. 29-39.

42. Ward, J.H., *Duration of adjuvant endocrine therapy of breast cancer: how much is enough?* Curr Opin Obstet Gynecol, 2010. **22**(1): p. 51-5.

43. Greaves, M. and C.C. Maley, *Clonal evolution in cancer*. Nature, 2012. **481**(7381): p. 306-13.

44. Singh, A. and J. Settleman, *EMT, cancer stem cells and drug resistance: an emerging axis of evil in the war on cancer*. Oncogene, 2010. **29**(34): p. 4741-4751.

45. Tomaskovic-Crook, E., E.W. Thompson, and J.P. Thiery, *Epithelial to mesenchymal transition and breast cancer*. Breast Cancer Res, 2009. **11**(6): p. 213.

46. Tyson, J.J., et al., *Dynamic modelling of oestrogen signalling and cell fate in breast cancer cells*. Nat Rev Cancer, 2011. **11**(7): p. 523-32.

47. Sha, W., et al., *Hysteresis drives cell-cycle transitions in Xenopus laevis egg extracts*. Proc Natl Acad Sci U S A, 2003. **100**(3): p. 975-80.

48. Cui, J., et al., *Two Independent Positive Feedbacks and Bistability in the Bcl-2 Apoptotic Switch*. Plos One, 2008. **3**(1).

49. Chen, C., et al., *Modeling of the role of a Bax-activation switch in the mitochondrial apoptosis decision*. Biophys J, 2007. **92**(12): p. 4304-15.

50. Clarke, R., et al., *Endoplasmic reticulum stress, the unfolded protein response, and gene network modeling in antiestrogen resistant breast cancer*. Hormone Molecular Biology and Clinical Investigation, 2011. **5**(1): p. 35-44.

51. Byrne, H.M., *Dissecting cancer through mathematics: from the cell to the animal model*. Nat Rev Cancer, 2010. **10**(3): p. 221-30.

52. Komarova, N.L. and D. Wodarz, *Drug resistance in cancer: principles of emergence and prevention*. Proc Natl Acad Sci U S A, 2005. **102**(27): p. 9714-9.

53. Merlo, L.M.F., et al., *Cancer as an evolutionary and ecological process*. Nature Reviews Cancer, 2006. **6**(12): p. 924-935.

54. Sottoriva, A., et al., *Cancer stem cell tumor model reveals invasive morphology and increased phenotypical heterogeneity*. Cancer Res, 2010. **70**(1): p. 46-56.

55. Tomasetti, C. and D. Levy, *Role of symmetric and asymmetric division of stem cells in developing drug resistance*. Proceedings of the National Academy of Sciences of the United States of America, 2010. **107**(39): p. 16766-16771.

56. Labianca, R., et al., *Intermittent versus continuous chemotherapy in advanced colorectal cancer: a randomised 'GISCAD' trial*. Annals of Oncology, 2011. **22**(5): p. 1236-1242.

57. Das Thakur, M., et al., *Modelling vemurafenib resistance in melanoma reveals a strategy to forestall drug resistance*. Nature, 2013. **494**(7436): p. 251-255.

58. Lee, J.M., et al., *Combination therapy: intermittent sorafenib with bevacizumab yields activity and decreased toxicity*. British Journal of Cancer, 2010. **102**(3): p. 495-499.

3.8 Supporting materials

Transitions between endocrine therapy responsive and resistant states on the breast cancer landscape

Chun Chen[1], William T. Baumann[2], Jianhua Xing[3], Lingling Xu[4], Robert Clarke[5], John J. Tyson[3*]

[1]Graduate Program in Genetics, Bioinformatics and Computational Biology, [2]Department of Electrical & Computer Engineering, [3]Department of Biological Sciences, and [4]Department of Physics, Virginia Polytechnic Institute & State University, Blacksburg VA 24061, USA

[5]Lombardi Comprehensive Cancer Center, Georgetown University School of Medicine, Washington DC 20057, USA

[*] Corresponding author. Fax: +1 540 231 9307.

E-mail address: tyson@vt.edu.

Table 3.1 Model variables.

Variable	Description	Range	Receptor
x_1 (or *GFR*)	Growth Factor Receptor	[0, 1]	$[\mathrm{GFR}] = 10^{x1}$
x_2 (or *ERM*)	Membrane-associated ERα	[0, 1]	$[\mathrm{ERM}] = 10^{x2}$
x_3 (or *E2ER*)	E2-liganded ERα	[0, 1]	$[\mathrm{E2ER}] = 10^{x3}$

Table 3.2 Model Equations.

$$\frac{dGFR}{dt} = \gamma_{\mathrm{GFR}} \cdot \left(H\left(W_{\mathrm{GFR}}\right) - GFR \right) + \zeta_{\mathrm{GFR}}(t) \tag{1}$$

$$\frac{dERM}{dt} = \gamma_{\mathrm{ERM}} \cdot \left(H\left(W_{\mathrm{ERM}}\right) - ERM \right) + \zeta_{\mathrm{ERM}}(t) \tag{2}$$

$$E2ER = H\left(W_{\mathrm{E2ER}}\right) \tag{3}$$

$$H(W) = \frac{1}{1+e^{-W}} \tag{4}$$

$$W_{\mathrm{GFR}} = \omega_{\mathrm{GFR}} + \omega_{\mathrm{GFR,E2ER}} \cdot E2ER + \omega_{\mathrm{GFR,GFR}} \cdot GFR + \omega_{\mathrm{GFR,ERM}} \cdot ERM \tag{5}$$

$$W_{\mathrm{ERM}} = \omega_{\mathrm{ERM}} + \omega_{\mathrm{ERM,E2ER}} \cdot E2ER + \omega_{\mathrm{ERM,ERM}} \cdot ERM + \omega_{\mathrm{ERM,GFR}} \cdot GFR \tag{6}$$

$$W_{\mathrm{E2ER}} = \omega_{\mathrm{E2ER}} + \omega_{\mathrm{E2ER,E2}} \cdot E2 \tag{7}$$

Table 3.3 Model Parameter Values.

Parameter	Description	Value
γ_{GFR}	Rate of GFR reaching its steady	1
γ_{ERM}	Rate of ERM reaching its steady	1
ω_{GFR}	Basal inhibition of GFR	–2.56
$\omega_{GFR,E2ER}$	GFR inhibition by E2ER	–1.6
$\omega_{GFR,GFR}$	GFR self-activation	6.8
$\omega_{GFR,ERM}$	GFR activation by ERM	0.4
ω_{EPM}	Basal inhibition of ERM	–3.04
$\omega_{EPM,E2ER}$	ERM inhibition by E2ER	–1.6
$\omega_{ERM,ERM}$	ERM self-activation	6.64
$\omega_{ERM,GFR}$	ERM activation by GFR	0.4
ω_{E2ER}	Basal activation of E2ER	5
$\omega_{E2ER,E2}$	E2ER activation by E2	0.5
E2	E2 level on $\log_{10}$ scale, *E2* = $\log_{10}$[E2]	2 (HIGH) 0 (LOW) –2 (TRACE)

3.8.1 Solving the Fokker-Plank diffusion equation

3.8.1.1 Without population selection pressure

The noise terms in Eqs. (1) and (2) of Suppl. Table S2 create stochastic fluctuations in our two-dimensional state space (x_1 = *ERM;* x_2 = *GFR*). Let $P(x_1,x_2,t)$ be the probability density for finding the system at state (x_1,x_2) at time t. Then $P(x_1,x_2,t)$ is governed by the Fokker-Planck equation [1]:

$$\frac{\partial P(x_1,x_2,t)}{\partial t} + \nabla \cdot \mathbf{J}(x_1, x_2, t) = 0 \qquad (1.1)$$

where $\mathbf{J}(x_1,x_2,t)$ is the probability flux at state (x_1,x_2) at time t, given by

$$\mathbf{J} = P \cdot \mathbf{F} - D \cdot \nabla P, \qquad (1.2)$$

and the gradient operator is $\nabla = \hat{\boldsymbol{x}}_1 \frac{\partial}{\partial x_1} + \hat{\boldsymbol{x}}_2 \frac{\partial}{\partial x_2}$.

We used VCell software (V5.1, available at http://www.nrcam.uchc.edu/index.html) to solve the diffusion equation S1.1 using a finite difference method. The solution grid was a square region, $-0.2 \le x_1 \le 1.2$ and $-0.2 \le x_2 \le 1.2$. To conserve probability, Neumann (reflecting) boundary conditions were applied. We used 51 grid points in each dimension for all simulations. A time step of dt = 1 was chosen to avoid numeric instability. The model was simulated until t = 20000 to approach steady states. For example, when [E2] = 10^{-2}, the maximum difference of probability on any grids at t = 20000 and t=18000 is 1.17×10^{-9}; the total probability on the boundary grids is 1.81×10^{-3}; the maximum probability on the boundary grids is 9.06×10^{-5}; the maximum difference of probability on any grids by using dt = 1 and dt = 0.1 is 2.39×10^{-9}.

3.8.1.2 With population selection pressure

To study the effect of selection pressure on the distribution of cells in a population that may be expanding or shrinking, we rewrite Eq. (1.1) in terms of cell density $Y(x_1,x_2,t)$, where $Y(x_1,x_2,t)\mathrm{d}x_1\,\mathrm{d}x_2$ = number of cells found in the small rectangle $[x_1, x_1+\mathrm{d}x_1]\times[x_2, x_2+\mathrm{d}x_2]$ in state space at time t. By definition, $\iint \mathrm{Y}(\mathrm{x}_1,\mathrm{x}_2,\mathrm{t})\mathrm{dx}_1\mathrm{dx}_2 = \mathrm{N}(\mathrm{t}) =$ total number of cells at time t.

In terms of $Y(x_1,x_2,t)$, the Fokker-Planck equation becomes

$$\frac{\partial Y(x_1,x_2,t)}{\partial t} + \boldsymbol{\nabla}\cdot\mathbf{J}(x_1,x_2,t) = s(x_1,x_2;E2)\cdot Y(x_1,x_2,t) \qquad (1.3)$$

where $\mathbf{J}(x_1,x_2,t)$ is the flux of cells at state (x_1,x_2) at time t due to drift and noise terms, and $s(x_1,x_2)$ is the proliferation index of cells in state (x_1,x_2). The proliferation index, as a function of E2 level, depends on the functional block where the system point is located (see Fig. 3.2B in the main text). To simulate the case of no selection pressure, we set $s(x_1,x_2) = 0$ for all points in state space, and in this case $P = N_0Y$, where $N_0 = N(0)$ = constant total number of cells in the population. In places where $s(x_1,x_2) > 0$, cells have a selective advantage, and in places where $s(x_1,x_2) < 0$, they are at a disadvantage. Applying these modifications to the model built in VCell, we ran new simulations. The total population can grow larger or smaller than N_0, since cells can proliferate or die. In this case, to compute the potential landscape, $U(\mathbf{x}) = -\ln P_{ss}(\mathbf{x})$, we calculated $P_{ss} = P(\mathbf{x},t\to\infty)$ by normalizing the steady state density Y_{ss} by the total population: $P_{ss} = Y_{ss} / \sum Y_{ss}$.

3.8.2 Calculating the transition matrix of the state transition model

To convert the cellular-level dynamical system with multiple steady states into a state-transition model for convenient simulations of population of cells, we divided the two-dimensional state space of the cellular-level model into four blocks, representing four discrete 'states', or phenotypes (R_1, R_2, R_3 and R_4, as in Fig. 3.3B). Denoting by $\mathbf{v}$ the column vector of the number of cells in each of the four discrete states, we can write the state transition model as a vector ODE

$$\frac{d\mathbf{v}}{dt} = \mathbf{A} \cdot \mathbf{v} \tag{2.1}$$

where the state transition matrix is given by

$$\mathbf{A} = \begin{bmatrix} u_1 - (k_{21} + k_{31} + k_{41}) & k_{12} & k_{13} & k_{14} \\ k_{21} & u_2 - (k_{12} + k_{32} + k_{42}) & k_{23} & k_{24} \\ k_{31} & k_{32} & u_3 - (k_{13} + k_{23} + k_{43}) & k_{34} \\ k_{41} & k_{42} & k_{43} & u_4 - (k_{14} + k_{24} + k_{34}) \end{bmatrix}$$

Here k_{ij} denotes the proportion of cells that transit from state j to state i per unit time. The k_{ij}'s were calculated by the "minimum action path" method in the next section. Here, u_i indicates the proliferation rate of cells in state i. Similar to $s(x_1,x_2)$ in Suppl. Text 1, we assume that u_i is equal to the proliferation index PI_i in each state block ($i = 1,\ldots,4$, see Fig. 3.2B in the main text). For the case of no population selection pressure, $u_i = 0$ for all i. We solve Eq. (2.1) by the explicit Euler method:

$$\mathbf{v}_{t+\Delta t} \approx \mathbf{v}_t + \mathbf{A} \cdot \Delta t \cdot \mathbf{v}_t = (\mathbf{I} + \mathbf{A} \cdot \Delta t) \cdot \mathbf{v}_t = \mathbf{B} \cdot \mathbf{v}_t \tag{2.2}$$

So the state transition matrix **B** is defined by:

$$\mathbf{B} = \begin{bmatrix} \frac{1}{\Delta t} + u_1 - \left(k_{21} + k_{31} + k_{41}\right) & k_{12} & k_{13} & k_{14} \\ k_{21} & \frac{1}{\Delta t} + u_1 - \left(k_{12} + k_{32} + k_{42}\right) & k_{23} & k_{24} \\ k_{31} & k_{32} & \frac{1}{\Delta t} + u_1 - \left(k_{13} + k_{23} + k_{1,434}\right) & k_{34} \\ k_{41} & k_{42} & k_{43} & \frac{1}{\Delta t} + u_1 - \left(k_{14} + k_{24} + k_{34}\right) \end{bmatrix} \cdot \Delta t$$

In practice, we chose a small $\Delta t = 0.1$ to calculate **B**, and then update $\mathbf{v}_t$ according to Eq. (2.2).

3.8.3 Calculating the Minimum Action Path

Consider a random process $\mathbf{X}(t)$ in $\mathbf{R}^n$ defined by the following stochastic differential equation with a small positive parameter ε:

$$\dot{\mathbf{X}} = \mathbf{F}(\mathbf{X}) + \sqrt{\varepsilon}\,\dot{\mathbf{W}} \tag{3.1}$$

Here $\mathbf{W}(t)$ a Wiener process in $\mathbf{R}^n$ and $\mathbf{F}(\mathbf{X})$ is the vector form of the right hand side of Eqs. 1 and 2 in Table S2, without the noise terms. Wentzell–Freidlin theory [2] gives an estimate of the probability distribution of solutions $\mathbf{X}(t)$ over a given time interval $[0,T]$: for any small parameter δ and a smooth path $\boldsymbol{\phi}(t)$ over $[0,T]$,

$$P\{\rho(\mathbf{X}(t), \boldsymbol{\varphi}(t)) < \delta\} \approx exp\left(-\frac{1}{\varepsilon} \cdot S_T[\boldsymbol{\varphi}(t)]\right) \tag{3.2}$$

where ϱ is the distance between $\mathbf{X}(t)$ and $\boldsymbol{\phi}(t)$ in the continuous state space. The action functional S over a given path $\boldsymbol{\varphi}(t)$ $(t \in [0,T])$ is defined as:

$$S_T[\boldsymbol{\varphi}(t)] = \frac{1}{2}\int_0^T |\dot{\boldsymbol{\varphi}}(t) - \mathbf{F}(\boldsymbol{\varphi}(t))|^2 \mathrm{d}t \tag{3.3}$$

By minimizing the action functional $S_T[\boldsymbol{\phi}_{ij}]$ between any two states (state j at $t = 0$ and state i at $t = T$), we can compute the minimum action path (MAP), $\boldsymbol{\phi}_{ij}^*$, between these two states. The MAP becomes independent of T for T large enough, but not too large; we found that $T = 40$ is a convenient value. See Fig. 3.7. The probability that the system moves by another path is exponentially smaller in ε, i.e., the MAP is the most probable or 'characteristic' path connecting these two states over the time interval $[0,T]$. Following the methods in [3, 4], we found numerical solutions of $\boldsymbol{\phi}^*$ between different fixed-point attractors in the breast cancer landscape, with $T = 40$. These MAPs are plotted on the breast cancer landscape to indicate the most probable transition routes (Fig. 3.3A).

In this study, our aim is to use the biologically-based, multi-attractor model at the cellular level to create a state-transition model for efficient simulation of cell population dynamics. The two-dimensional state space of the cellular-level model was divided into four blocks, representing four discrete 'states', or phenotypes (Fig. 3.3B). To estimate k_{ij}, the transition probability from state j to i, we calculate the MAP going from the fixed-point attractor in state j to the fixed point attractor in state i in time $T = 40$. (If there is no fixed-point attractor located in a state block, e.g., when *E2* is too large or small, we use a 'characteristic' point for this state block as follows: (0, 0) for R_1, (1, 0) for R_2, (1, 0) for R_3, (1, 1) for R_4. We then estimate k_{ij} from the phenomenological relation

$$k_{ij} = \beta \cdot \exp\left\{-\alpha \cdot \left(S_T\left[\boldsymbol{\varphi}_{ij}^{*}\right]\right)^{n}\right\} \tag{3.4}$$

The parameters α, β and n in Eq. (3.4) are estimated from full Monte-Carlo simulations of a few representative transitions (Fig. 3.8 and Fig. 3.3C). In this study, for $T = 40$ and $D = 0.005$, the best-fit values are $\alpha = 80.48$, $\beta = 0.07197$, and $n = 0.9805$.

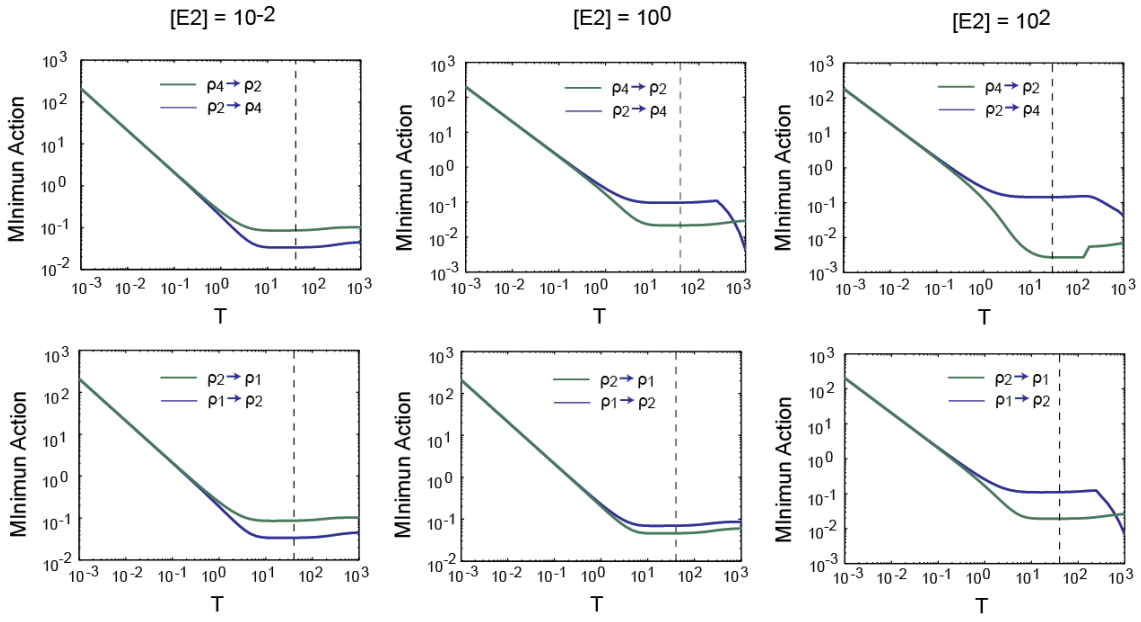

Figure 3.7 An appropriate T was chosen to calculate the minimum action. The minimum action of state transitions between different pairs of attractors (ϱ_1 and ϱ_2, ϱ_2 and ϱ_4) at different E2 levels were computed and plotted versus T within the range of [10^{-3}, 10^3]. Vertical dotted lines indicate T = 40, which is a reasonable choice in our calculation. Notice that the minimum action decreases initially when T is small; and when T is too large the minimum action will be unstable because of numerical errors. We used the method in [3,4] to compute the minimum actions.

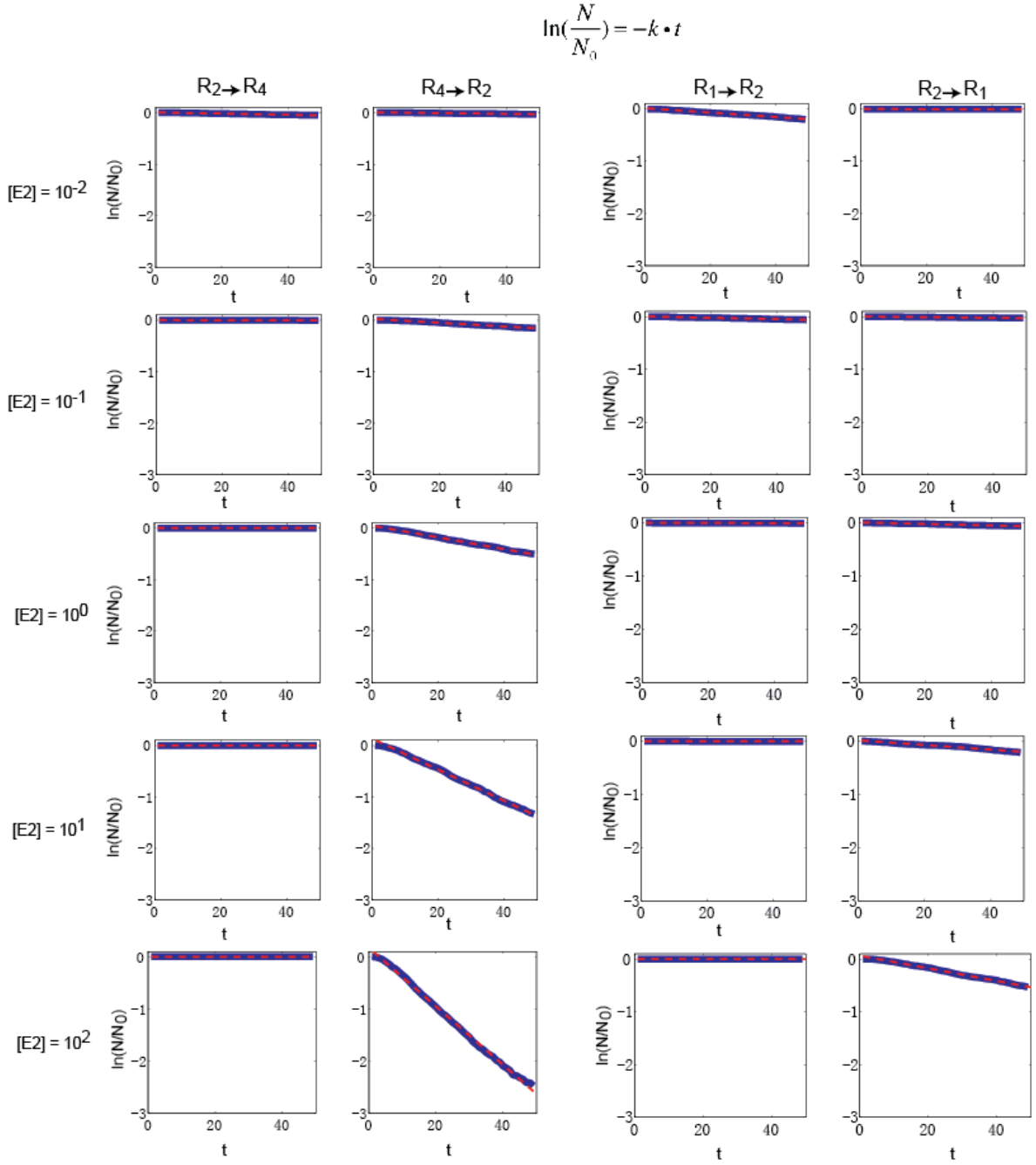

Figure 3.8 Transition rates are estimated from Monte Carlo simulation. The rate of transitions between different pairs of state blocks (R_1 and R_1, R_2 and R_4) at different E2 levels were computed from Monte Carlo simulation. In the upper equation: N_0, total number of cells simulated (N_0 = 10000); N, number of remaining cells without transition; k, the transition rate. In the lower panels: Blue solid line, proportion of remaining cells

without transition versus time based on the Monte Carlo simulation; Red dotted line, linear fit of the red curve according to the upper equation in the region of $t \in [5,50]$.

3.8.4 Supplementary references

1. Gardiner, C. W. (1985). *Handbook of stochastic methods (Vol. 3)*. Berlin: Springer.
2. Freidlin MI, Wentzell AD (1998) *Random perturbations of dynamical systems*: 2nd ed. Springer New York.
3. E W, Ren W, Vanden-Eijnden E (2004) Minimum action method for the study of rare events. *Communications on Pure and Applied Mathematics* 57: 637-656.
4. Zhang L, Radtke K, Zheng LK, Cai AQ, Schilling TF, et al. (2012) Noise drives sharpening of gene expression boundaries in the zebrafish hindbrain. *Molecular Systems Biology* 8:613.